A REVIEW OF QUASI-PERIODIC OSCILLATIONS IN LOW-MASS X-RAY BINARIES

WALTER H. G. LEWIN

Center for Space Research and Department of Physics, Massachusetts Institute of Technology, Room 37–627, Cambridge, MA 02139, U.S.A.

JAN VAN PARADIJS

Astronomical Institute 'Anton Pannekoek', University of Amsterdam, Roetersstraat 15, 1018 WB Amsterdam, The Netherlands

and

MICHIEL VAN DER KLIS

EXOSAT Observatory, Astrophysics Division, Space Science Department of ESA, ESTEC, Postbus 299, 2200 AG Noordwijk, The Netherlands

(Received 10 February, 1988)

Abstract. In this paper we present a review of the quasi-periodic oscillations (QPO) observed in the X-ray flux of low-mass X-ray binaries. In Section 1 a general background is given on galactic populations of accretion-driven X-ray sources. Section 2 contains a description of the methods that have been used to analyze these QPO. In Section 3 the QPO observations are described in some detail. Models for the QPO are considered in Section 4. In Section 5 the time lags observed between QPO at different photon energies, and their possible implications for X-ray spectral models, are discussed. Our conclusions are summarized in Section 6.

Table of Contents

Space Science Reviews **46** (1988) 273–377.

1. Introduction

We have tried to make this review of quasi-periodic oscillations in low-mass X-ray binaries complete up to December 1, 1987; preprints that reached us at a later date are not discussed. Before we start our review we give the reader some general background.

The bright galactic X-ray sources are close binary systems in which one of the components is a compact star which accretes matter transferred from its companion. In the large majority of cases the accreting compact object is probably a neutron star (in a few cases it may be a black hole; see McClintock, 1986). These X-ray sources can be divided into two broad classes: the high-mass X-ray binaries (HMXB) and the low-mass X-ray binaries (LMXB).

1.1. High-mass x-ray binaries (HMXB)

In these systems the companion is a young ($\lesssim 10^7$ yr), massive ($\gtrsim 10\,M_\odot$) star with an O- or B-type spectrum. The X-ray flux of most HMXB is pulsed; this signifies that the accreting neutron star rotates and has a strong magnetic field (not aligned with the rotation axis), that channels the inflowing matter onto the magnetic pole(s). The binary character of many HMXB shows up in periodic X-ray eclipses, and periodic Doppler shifts of the pulse-arrival times and lines in the optical spectrum. Studies of the orbital parameters of the neutron star and its companion have provided much of our present knowledge of neutron-star masses (see Rappaport and Joss, 1984, for a review). The X-ray spectra of HMBX are generally quite hard (see, e.g., White *et al.*, 1983; Rappaport and Joss, 1983). The optical properties of HMXB are dominated by the luminous early-type companion star. With respect to the mass transfer two sub-groups can be distinguished (Maraschi *et al.*, 1976). In the first sub-group the companion star has evolved away from the Main Sequence, and is (close to) filling its Roche lobe. Mass transfer occurs through a strong stellar wind and in some cases by incipient Roche-lobe overflow (e.g., Cen X-3 and SMC X-1, see Bonnet-Bidaud and Van der Klis 1979; Tjemkes *et al.*, 1986). The second sub-group is characterized by Be-type companions (for a recent review see Van den Heuvel and Rappaport, 1987), which underfill their Roche lobe; mass transfer in these systems is often transient (cf. Stella *et al.*, 1986), and is thought to be related to rapid rotation of the Be star (see Slettebak, 1987). For reviews of various other aspects of the HMXB we refer to Rappaport and Joss (1983, 1984), Van Paradijs (1983), and Van den Heuvel (1983).

1.2. Low-mass x-ray binaries (LMXB)

In these systems the companion is a low-mass ($\lesssim 1\,M_\odot$) star, which transfers mass by Roche-lobe overflow. The LMXB comprise, e.g., X-ray bursters, globular-cluster X-ray sources, soft X-ray transients, and bright galactic-bulge sources (for reviews see, e.g., Lewin and Joss, 1981, 1983; Ponman, 1982b; White *et al.*, 1984; Van Paradijs and Verbunt, 1984).

The X-ray spectra of LMXB are generally quite soft (kT values in exponential fits are typically ~ 5 keV; Jones, 1977; Parsignault and Grindlay, 1978). In many cases a positive correlation has been observed between variations in the hardness of the X-ray spectrum and the source intensity (Mason *et al.*, 1976; White *et al.*, 1976a, 1978; Parsignault and Grindlay, 1978; Holt, 1980; White *et al.*, 1980; Charles *et al.*, 1980; Ponman, 1982b; Sztajno *et al.*, 1983; Basinska *et al.*, 1984; Shibazaki and Mitsuda, 1984). However, at times the X-ray spectrum does not change much with source intensity (Branduardi *et al.*, 1980; Shibazaki and Mitsuda, 1984). EXOSAT observations, discussed in Section 3 of this review, have greatly contributed to our knowledge of these correlated spectral variations and intensity variations.

X-ray pulsations have been observed in three LMXB (GX 1 + 4: Lewin *et al.*, 1971; White *et al.*, 1976b; 4U 1626 – 67: Joss *et al.*, 1978; 1E2259 + 586: Fahlman and Gregory, 1983; we do not count Her X-1 as a LMXB). The optical counterparts of

LMXB are intrinsically faint objects, whose emission is dominated by the reprocessing of X-rays into lower-energy photons in the accretion disk around the compact star (for a review see, e.g., Van Paradijs, 1983). The galactic distribution of LMXB (in particular their presence in globular clusters) indicates that these systems are typically quite old ($\sim 10^9$ yr; for an estimate of the typical age of LMXB from their kinematic properties, see Cowley *et al.*, 1987).

Orbital periods are known for ~ 20 LMXB (Mason, 1986). They cover a large range from 11 min (4U 1820 – 30; Stella *et al.*, 1987) to 9.8 days (Cyg X-2; Cowley *et al.*, 1979). This implies that very different low-mass secondaries (white dwarfs, late-type Main-Sequence stars, evolved low-mass giant stars) can be present in LMXB, and probably different evolutionary histories can lead to the formation of a LMXB (Van den Heuvel, 1983; Verbunt, 1987; Van den Heuvel and Verbunt, 1988).

1.3. High-mass versus low-mass X-ray binaries

1.3.1. *General Remarks*

The division of compact galactic X-ray sources into two groups is the natural consequence of the fact that there appear to be two ways to produce a long-lived luminous galactic X-ray source, either through stellar-wind (from a high-mass companion star), or through Roche-lobe overflow (for a low-mass or high-mass star; Van den Heuvel, 1975). Companion stars with masses in the range between ~ 1 and $10\ M_\odot$ have too weak a stellar wind to sustain a strong X-ray source. On the other hand, Roche-lobe overflow, which causes mass transfer on a thermal time-scale, leads to such high mass transfer rates for these systems that the accreting compact star will ultimately become smothered, and cease to be observable as an X-ray source (Savonije, 1983b).

1.3.2. *Magnetic Field Decay*

X-ray pulsations and X-ray bursts have never been observed from the same source; these two phenomena appear to be mutually exclusive. This bimodal distribution of X-ray variability characteristics, which distinguishes the young HMXB (many X-ray pulsators) from the old LMXB (many X-ray bursters), can be understood as a result of a systematic decrease with time of the strength of the neutron-star magnetic field (for a recent review of the properties of the magnetic fields of accreting neutron stars, see Taam and Van den Heuvel, 1986). This fits in nicely with observations of the pulse period behaviour of radio sources which strongly suggest that the magnetic field of a neutron star decays on a time scale of $\sim 10^7$ yr (see, e.g., Lyne *et al.*, 1983). As we will discuss below in more detail, magnetospheric models (with neutron star magnetic fields of order 10^9 G) have been proposed for the quasi-periodic oscillations (QPO) in LMXB (Alpar and Shaham, 1985a). Since this proposal was made, independent evidence has become available that the magnetic dipole field decay does not continue indefinitely, but levels off when the magnetic field strength has decayed to a value in the range $\sim 10^{8.5-10}$ G (Kulkarni, 1986; Van den Heuvel *et al.*, 1986; Bhattacharya and Srinivasan, 1986; Wright and Low, 1986).

Whether or not, and how fast the observable magnetic fields of neutron stars decay is a matter of debate (see, e.g., Flowers and Ruderman, 1977; Kundt, 1981; Beskin *et al.*, 1983; Blandford *et al.*, 1983; Harvey *et al.*, 1986; Jones, 1987; Sang and Chanmugan, 1987). It is possible that the spin-down behaviour of radio pulsars, and the rarity of X-ray pulsations in the old LMXB, is not only due to magnetic-field decay but, at least in part, to the alignment of the field with the rotation axis (evidence for field alignment has been inferred from pulse-width and polarization data for radio pulsars; Candy and Blair, 1983, 1985). However, if alignment would be the major effect, the geometry of the (co-rotating) accretion flow within $\sim 10^8$ cm of the neutron star would be similar for the aligned and non-aligned sources. It is then hard to understand that the X-ray spectra of the pulsating sources are much harder than those of the non-pulsating ones, and that X-ray bursts never occur in pulsating sources (see Lewin and Joss, 1981, 1983). Magnetic dipole field co-alignment alone can probably not explain this spectral difference and the mutual avoidance of bursts and pulsations; in all likelihood there is also field decay at least during the first $\sim 10^8$ yr.

We note that the magnetic field evolution of accreting and non-accreting neutron stars may differ; the decay of the observable magnetic field may be caused by the accretion process itself (see Taam and Van den Heuvel, 1986; Blondin and Freese, 1986; Van den Heuvel *et al.*, 1987).

1.3.3. *Neutron Star Rotation Rates – Magnetospheres*

The decay of the magnetic field will not only affect the presence of X-ray pulsations, but also cause a systematic difference in the rotation rates of the neutron stars in HMXB and LMXB. During the periods that the neutron stars spin up (due to accretion torques), the rotation frequency of an accreting magnetized neutron star is expected to be at most of the order of the Kepler frequency of matter orbiting the neutron star at the inner edge of the accretion disk, at a radial distance, r_m, where the inflowing plasma attaches to the magnetic field lines. Inside this magnetospheric radius (Pringle and Rees, 1972; Davidson and Ostriker, 1973; Lamb *et al.*, 1973) the magnetic field, anchored in the neutron star, dominates the motion of the plasma, which then is forced to co-rotate. For small rotation frequencies the torques exerted by the accreting matter will spin the neutron star up. For rotation frequencies substantially larger than the above Kepler frequency centrifugal forces will inhibit accretion, and no strong X-ray source is observable; the neutron star then spins down (for a review, see e.g., Henrichs, 1983).

In the case of spherical accretion for a gas-pressure dominated case (however, for radiation-pressure dominated cases, see White and Stella, 1988), the magnetospheric radius is approximately given by

$$r_m \approx (2.9 \times 10^8 \text{ cm}) \mu_{30}^{4/7} m^{1/7} R_6^{-2/7} L_{37}^{-2/7} \approx (2.7 \times 10^8 \text{ cm}) \mu_{30}^{4/7} m^{-1/7} \dot{M}_{17}^{-2/7} , \tag{1.1}$$

where μ_{30} is the magnetic moment of the neutron star in units of 10^{30} G cm^3, m its mass in units of solar masses, R_6 its radius in units of 10^6 cm, L_{37} its X-ray luminosity in units of 10^{37} erg s^{-1}, and $\dot{M}_{17}$ is the mass accretion rate in units of 10^{17} g s^{-1}. For

$m = R_6 = 1$, the Kepler frequency, ν_K, at the magnetospheric radius depends on X-ray luminosity according to:

$$\nu_K = (0.37 \text{ Hz}) L_{37}^{3/7} \mu_{30}^{-6/7} . \tag{1.2}$$

In the more detailed model of Ghosh and Lamb (1979), that is often used to describe the interaction of the neutron-star magnetic field and an accretion disk, the numerical value of r_m is smaller by a factor ~ 2 compared to the value given in Equation (1.1). In this model, the spin-up or spin-down behaviour of the accreting neutron star is determined by the sum of a positive accretion torque, and a negative torque due to the interaction of the neutron-star magnetic field with the accretion disk outside the magnetospheric radius. The neutron star rotates at its equilibrium rate when the net accretion torque disappears. In the model of Ghosh and Lamb the equilibrium frequency is approximately given by

$$\nu_{eq} = (0.25 \text{ Hz}) L_{37}^{3/7} \mu_{30}^{-6/7} . \tag{1.3}$$

In the above expressions it is assumed that the structure of the accretion disk is dominated by gas pressure, which condition is fulfilled for the strong magnetic fields encountered in HMXB. White and Stella (1988) have pointed out that the magnetosphere around neutron stars with weak magnetic fields (such as expected in LMXB), is likely to be located in the inner region of the disk, which is radiation-pressure dominated. They argue that then the dependence of the magnetospheric radius on the mass accretion rate can be much stronger, or much weaker, than given by Equation (1.1), depending on the viscosity model that one assumes, and the detailed mechanism by which the magnetic field interacts with the disk.

For young neutron stars with magnetic fields of order 10^{12} G, and X-ray luminosities between 10^{36} and 10^{38} erg s^{-1}, the expected equilibrium rotation periods (Equation (1.3)) are in the range from 1 to 100 s, in fair agreement with the observed periods of X-ray pulsars. Using expression (1.3) we find for neutron stars with magnetic fields below $\sim 10^9$ G (i.e., near the apparent value after decay, see above) rotation periods below ~ 10 ms.

1.3.4. *LMXB and the Millisecond Radio Pulsars*

Smarr and Blandford (1976) suggested that the 59-ms binary radio pulsar PSR 1913 + 16 (Hulse and Taylor, 1975) is the end product of an X-ray binary mass-transfer phase during which the neutron star was spun up. In their historic paper they linked the evolution of X-ray binaries with the formation of fast-rotating radio pulsars. This idea of 'recycling' of radio pulsars was worked out in more detail by Van den Heuvel (1981), Radhakrishnan (1981) and Srinivasan (1982), Srinivasan and Van den Heuvel (1982), Alpar *et al.* (1982), and De Kool and Van Paradijs (1987). When the 6 ms binary radio pulsar PSR 1953 + 29 was discovered by Boriakoff *et al.* (1983), four groups independently showed that this object is probably the evolutionary product of a LMXB with an evolved low-mass giant companion whose accretion was terminated as a result

of exhaustion of the latter's envelope (Helfand *et al.*, 1983; Joss and Rappaport, 1983; Paczynski, 1983; Savonije, 1983a).

1.3.5. *Millisecond Pulsations in LMXB?*

Based on the expectation that LMXB harbour neutron stars that might be spinning with periods in the millisecond range, several searches for X-ray pulsations down to the millisecond range have been made (see Section 2.2 in Lewin and Joss, 1983; Leahy *et al.*, 1983). The discovery of PSR 1953 + 29 revitalized this search, and a number of groups proposed to use EXOSAT to search for millisecond X-ray pulsations.

Of course, the high rotation rates are only expected if the magnetic fields are relatively weak ($< 10^8$ G) but, if the fields are very weak, pulsations are also expected to be very weak as the accreted matter will then not be channeled to the magnetic poles. It is, therefore, possible that in many LMXB millisecond rotation rates of the neutron stars are present, but unobservable, at least in terms of X-ray pulsations. Co-alignement of the magnetic dipole axis would also inhibit the production of X-ray pulsations.

1.4. Some historical notes on QPO

Our first search with EXOSAT for millisecond coherent pulsations in LMXB was performed in September 1984 by a group involving the present authors; the analysis was performed by one of us (MvdK) and Fred Jansen of the Leiden Space Research Laboratory. We found no coherent X-ray pulsations, but we did find quasi-periodic oscillations (QPO) with a frequency of ~ 30 Hz which appeared as a broad peak ($\sim 25\%$ FWHM) in the power density spectra. The centroid frequency, ν, of the QPO was a linear function of the observed X-ray flux, I; it was ~ 20 Hz (50 ms) when the X-ray flux was near its lowest value, and it was as high as ~ 40 Hz (25 ms) when the flux was $\sim 30\%$ higher (see Figures 1.1 and 1.2). A power-law, of the form $\nu \propto I^{\alpha}$, fits the data equally well with $\alpha \sim 2$. The power density spectra also showed red noise*, below ~ 15 Hz, whose strength went hand in hand with that of the QPO (Van der Klis *et al.*, 1985a, b). Since we had used the 0.25 ms time-resolution mode of EXOSAT (with a duty cycle of only 12%) which nobody had used before for this purpose, we were worried at first that the QPO and the frequency dependence on the observed counting rate (i.e., the source flux) was an artifact of the analysis or the result of the on-board data formatting. It just so happened (luckily) that during the observations GX 5–1 became so bright that the counting rate reached a level where detector damage was feared. The counting rate was therefore artificially suppressed (by $\sim 30\%$) by off-set pointing. The QPO frequency was unaffected by this $\sim 30\%$ decrease in counting rate, and this showed convincingly that the new findings were real.

The results were discussed during an informal seminar on March 8, 1985 at the

* We use the term red noise to indicate broad-band power which increases toward lower frequencies, not necessarily as a power law. Where appropriate and possible, as discussed further on, we distinguish two components in the red noise: low-frequency noise (LFN), and very-low-frequency noise (VLFN); they have very different properties.

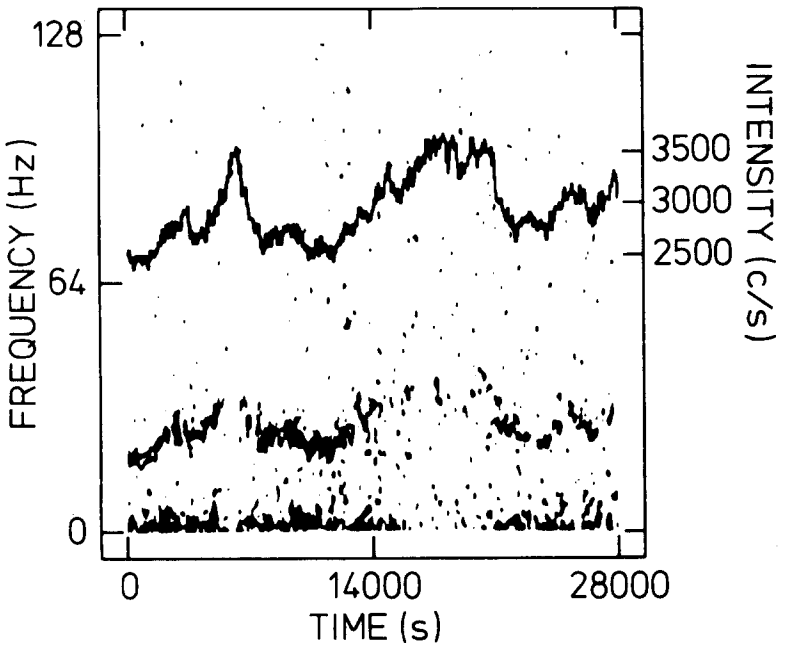

Fig. 1.1. Display of the temporal variation of power spectra from GX 5–1 (EXOSAT data). The frequency is in the vertical direction (left-hand scale). A vertical narrow slice is a grey-scale coded representation of a power spectrum; the darker the shade, the higher is the excess power. The variable broad QPO peak shows up as a dark ribbon between ~ 20 and ~ 40 Hz; the red noise is visible at the bottom. The intensity of GX 5–1 is also shown (upper dark line; use the right-hand scale). Both the QPO and the red noise become less visible at high source intensity. This is partly due to a decrease in their strength (fractional r.m.s. variation), and partly to a broadening in their profile. This diagram is similar to the 'dynamic spectra' used in solar radio astronomy (see, e.g., De Groot and Van Nieuwkoop, 1968); it was introduced into X-ray astronomy by Oda *et al.* (1972). This figure is from Van der Klis *et al.* (1985b).

Max-Planck-Institute for Extraterrestrial Physics in Garching, and as soon as the results were officially announced on March 13, 1985 (Van der Klis *et al.*, 1985a), a scenario to explain the results was proposed by Alpar and Shaham (1985a). Their scenario (see Section 4.2) was very similar to the one suggested by Warner (1983) to explain some of the (much slower) *optical* quasi-periodic oscillations observed in several cataclysmic variables (see Section 3.4 and Figure 3.32). Alpar and Shaham (1985a, b) derived from the observed dependence of the QPO frequency on the flux of GX 5–1 a neutron star rotation period of ~ 10 ms, and a neutron star magnetic dipole field strength of $\sim 10^{10}$ G. If 10 ms were the correct rotation rate, it was somewhat puzzling why this did not show up as coherent pulsations in the power density spectra. However, since the period as well as the magnetic field strength fit very well in the radio pulsar spin-up scenario described above, the model was greeted with enthusiasm.

It may be of historical interest to mention that in the early seventies, on the basis of a rocket observation, Angel *et al.* (1971) reported: "An analysis of the X-ray flux from Sco X-1 taken over a 4-minute period shows evidence for oscillations in the frequency range 1–10 Hz which persist for typically 1 minute."

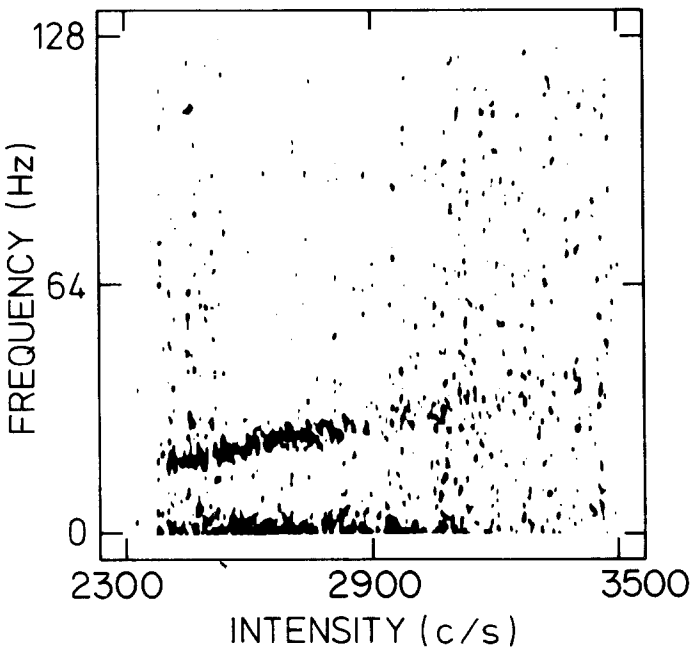

Fig. 1.2. Display of power spectra from GX 5–1 (see Fig. 1.1) as a function of source intensity. The latter was corrected for the detector transmission which was changed during the observation (see Section 1.4). Notice that the centroid frequency of the QPO is an approximately linear function of the source intensity; a power-law dependence also fits the data well (see Section 3.3.1, and Table I). This figure is from Van der Klis *et al.* (1985b).

Tawara *et al.* (1982) discovered quasi-periodic 2-Hz 'pulsations' in 2 of 64 long type-2 bursts from the Rapid Burster (see Figure 1.3). Since the pulsations were not coherent, they could exclude that they were directly the result of the neutron star rotation. There were several reasons why the QPO discovery in GX 5–1 received much more attention than the QPO discovery made a few years earlier by Tawara *et al.* (1982).

The Rapid Burster is a very peculiar source in its own right, exhibiting many strange properties, and the 2 Hz oscillations were 'just another' strange phenomenon. GX 5–1, on the other hand, is the prototype of the bright galactic bulge sources that had particularly distinguished themselves by their lack of observational diagnostic properties.

In GX 5–1 the oscillations were more than an order of magnitude faster, indicating a close connection with the compact object, and the QPO frequency was correlated with the source flux (suggesting a magnetospheric origin for the QPO), which provided a connection with millisecond radio pulsars. The fact that the strength of the red noise went hand in hand with that of the QPO may also have played a role.

Following the discovery of the intensity-dependent 20–40 Hz QPO in GX 5–1, a lot of observational and theoretical activity evolved. QPO with a frequency near ~ 6 Hz that were only very weakly dependent on intensity, and strongly intensity-dependent

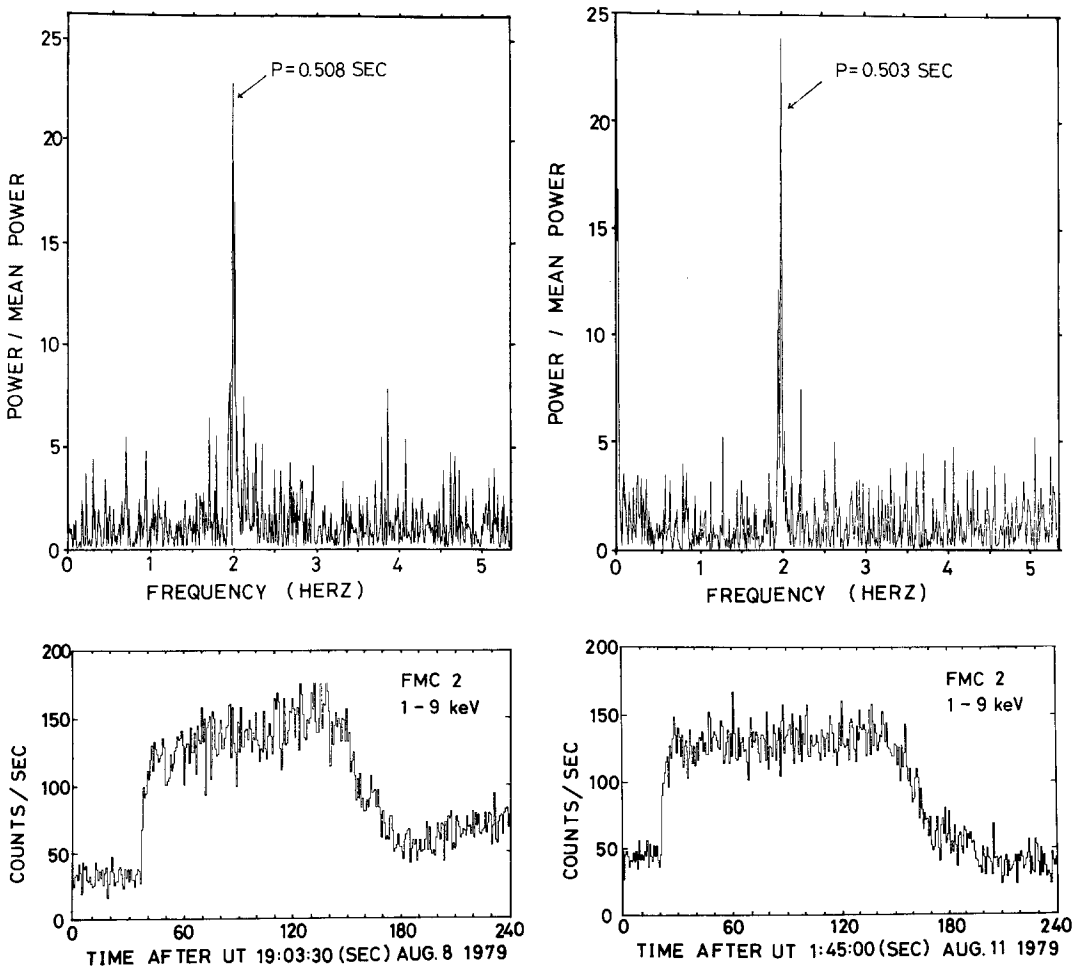

Fig. 1.3. Light curves (*bottom panels*) and power spectra (*upper panels*) of two type-2 bursts from the Rapid Burster in which ~2 Hz quasi-periodic oscillations were discovered by Tawara *et al.* (1982) using the *Hakucho* Observatory (see Sections 1.4 and 3.3.7).

10–20 Hz QPO, as well as 6–15 Hz QPO with an erratic frequency-intensity relation were found in Sco X-1 (Middleditch and Priedhorsky, 1985; Van der Klis *et al.*, 1985c). Intensity-dependent 25–55 Hz as well as ~5 Hz intensity-*independent* QPO were found in Cyg X-2 (Hasinger *et al.*, 1986; Norris and Wood, 1987). QPO detections in GX 17 + 2 (Stella *et al.*, 1987), GX 349 + 2 (Lewin *et al.*, 1986; Ponman *et al.*, 1988), and 1820–30 (Stella *et al.*, 1987) followed. The relation between QPO and the red-noise in Sco X-1 was very different from that in GX 5–1, and it was in strong disagreement with a prediction from the first model (F. Lamb, private communication) that evolved from the original idea of Alpar and Shaham (1985a). The QPO in Cyg X-2 had some similarities with those in GX 5–1 but also some very important differences.

Based on the analogy with Sco X-1, Stella (1986) proposed a classification of QPO based on their frequency and their frequency-intensity relation. He distinguished (i) low-frequency QPO ($\nu < 10$ Hz) with a weak (or no) frequency-intensity relation, (ii) high-frequency QPO ($\nu > 10$ Hz) with a strong positive correlation between QPO frequency and source intensity, and (iii) QPO with an 'erratic' frequency-intensity relation.

Another underlying 'organization' not entirely consistent with the above, revealed itself when correlations were found between the spectral states of the sources and the QPO characteristics. In GX 5–1, the 20–40 Hz QPO were only, and always, observed when the source was found in the so-called 'horizontal branch'* of the spectral hardness-intensity diagram (see Figure 3.4). Low-frequency noise (LFN) associated with the QPO, and an independent (i.e., not associated with the QPO) very-low-frequency noise (VLFN) component were also observed in GX 5–1. The LFN is easily visible in the EXOSAT data above the Poisson noise up to frequencies as high as the QPO frequencies. The excess power in the LFN (as a function of frequency), cannot be described by a power law. The VLFN rises steeply above the Poisson noise level, below ~ 0.1 Hz, with a power-law frequency dependence (with index generally between 1 and 2). In the 'normal branch' (see footnote above) no 20–40 Hz QPO and no LFN were detected but VLFN was observed (Van der Klis *et al.*, 1986, 1987a). In Cyg X-2 a similar pattern was observed with, in addition, ~ 6 Hz intensity-*independent* QPO in the 'normal branch'. In Sco X-1 a strong correlation was also found between QPO and the spectral state (Figure 3.17; Priedhorsky *et al.*, 1986); two-branched spectral behavior occurred with strongly intensity-dependent high-frequency QPO in one spectral branch and weakly intensity-dependent low-frequency QPO in the other. Both the morphology of the branches and the way in which the QPO frequency varied along them were quite different from that in GX 5–1 and Cyg X-2 (Van der Klis, 1986; Van der Klis *et al.*, 1987a).

1.5. A GLOBAL PHENOMENOLOGICAL PICTURE

Recently, Hasinger (1987b) proposed (based on an observation of Cyg X-2 which showed a sharp bend in the 'normal branch', suggesting a transition into yet another branch), that there are three branches: the horizontal branch, the normal branch, and the flaring branch (see footnote above), which form a Z-shaped pattern in the color-color diagram (Ostriker, 1977; see Figure 1.4). Further observations of Cyg X-2 (Hasinger *et al.*, 1987) and Sco X-1 (Hasinger *et al.*, 1988) confirmed this idea (see Hasinger, 1988). In the normal branch the low-frequency weakly intensity-dependent QPO occurred, while in the horizontal branch and in the flaring branch (in Sco X-1), strongly intensity-dependent high-frequency QPO occurred. LFN, described with a power law with an exponential high-frequency cut-off (the cut-off frequency is lower than the QPO frequency), was present only in the horizontal branch; VLFN was observed in all branches.

* The detailed shape of the spectral branches depends rather sensitively on the energy bands that one chooses (see Van der Klis *et al.*, 1987a; Hasinger, 1987a). For some choices the designation 'horizontal' can be misleading. Only Sco X-1 has shown QPO in the flaring branch.

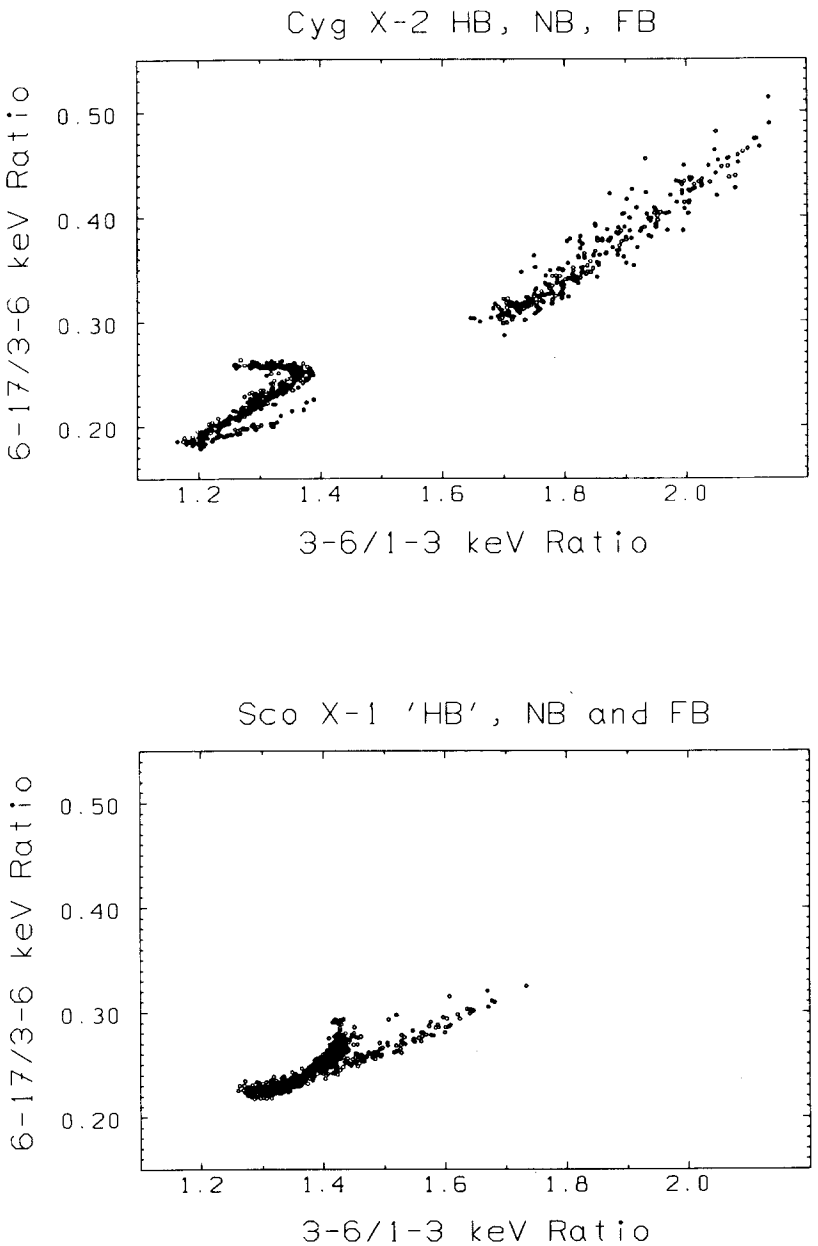

Fig. 1.4. 'Colour-colour' diagrams of Sco X-1 and Cyg X-2 (EXOSAT data). The vertical and horizontal scales of the two panels are identical. The Cyg X-2 data clearly form a Z-shaped curve which consists of the 'horizontal branch', the 'normal branch' and the 'flaring branch' (the latter is extending all the way to the upper right hand corner). The Sco X-1 data show the 'normal branch' and the 'flaring branch' and a hint of a 'horizontal branch'. Notice that the slope and the length of the normal branches is approximately the same, and that the slope of the flaring branches is similar. The similarity between these diagrams played an important role in Hasinger's recent classification (see Section 1.5). This figure is from Hasinger (1988).

The classification scheme thus distinguishes:

(i) high-frequency (20–55 Hz) horizontal-branch QPO associated with LFN,

(ii) low-frequency (5–8 Hz) normal-branch QPO not associated with the LFN, and

(iii) flaring-branch QPO that have only been seen in Sco X-1 (at frequencies between 6 and 20 Hz), not associated with LFN.

It is this last additional class that is the main difference of Hasinger's classification with that of Stella (1986) based on QPO properties only, and that resolves the confusion created by the flaring-branch QPO in Sco X-1. The 'erratic' QPO seen in Sco X-1 are in Hasinger's scheme described as erratic transitions between the normal branch and the flaring branch.

Of the ten sources with QPO, six seem to fit Hasinger's scheme; the Rapid Burster (Stella *et al.*, 1988a) does not fit, Cir X-1 (Tennant, 1987a, b; 1988a, b) may not fit (see Section 3.34), and there are two undecided cases (GX 349 + 2 and 1820 – 30; see Figure 6.1).

It is unclear what this phenomenological classification is telling us. No models/scenarios can (yet) adequately explain (let alone predict) this complex behavior. Nevertheless, we believe that Hasinger's classification is an important step.

2. Fourier Spectral Analysis

2.1. Introduction

All available information about QPO discussed in this review was obtained with the help of Fourier transforms. The reason for this is that we can almost never see QPO directly in the data: their relatively high frequencies ν and low fractional amplitudes r in combination with the limited count rates I attainable with present-generation X-ray detectors (a few 10^3 counts s^{-1} at most for the largest instruments) cause the Poisson noise of the data to exceed the amplitude of the oscillations: $\sqrt{I/\nu} \gtrsim rI/\nu$. By constructing Fourier transforms of the intensity variations in segments of high time resolution data whose length exceeds the QPO period $1/\nu$ by orders of magnitude, the QPO become observable in frequency space.

In this Section, we review the techniques that have been used to analyze these Fourier transforms, where it has generally been assumed that the following inequality holds:

$$\frac{rI}{\nu} \ll \sqrt{\frac{I}{\nu}} . \tag{2.1}$$

The QPO can then be considered as a small disturbance seen against the 'background' of a Poisson noise process corresponding to a constant average X-ray intensity (possibly modified by instrumental effects).

For the various types of red noise relevant in the context of QPO, Equation (2.1) does not necessarily hold. In practice, a Fourier spectral approach, in which the validity of Equation (2.1) is assumed, has in all cases also been used in the study of the red noise.

With this approach, the problems of detecting and characterizing the red noise are very similar to those for the QPO, and we will treat them together as much as possible.

The Fourier transform gives a decomposition of the signal into sine waves; it provides, in the form of complex numbers, both their amplitudes and their phases. In most applications, the phases are considered irrelevant and, therefore, nearly all of the work on QPO has been done using the squared modulus of the Fourier spectrum, the power spectrum. Only for the study of time lags between the signals in various X-ray spectral bands has the phase information contained in the Fourier spectra been used.

In the following, we will first consider the problem of the detection of (or, in the case of non-detection, the setting of upper limits to) QPO and other signals as features in a power spectrum, and the estimation of the significance of these features. We then turn to the determination of the properties of a power spectral feature and the interpretation of these properties in terms of the characteristics of the underlying signal. Finally, we discuss the use of the phase information in the Fourier transform for the construction of cross-spectra and cross-correlation functions in the context of measuring time lags (as a function of photon energy) in signals from QPO sources.

2.2. Power Spectrum Statistics

2.2.1. *The Distribution of the Powers*

The problem of detecting a signal in a power spectrum is determined by the probability distribution of the powers in the spectrum caused by the noise. Once we know this distribution, we can calculate the probability that a given power in the spectrum has attained its value by chance. If this probability is low, we are likely to have detected a true signal.

Consider a time series of duration T containing $N_{\rm ph}$ photons binned into N consecutive bins of duration T/N. The number of photons detected in bin k is denoted x_k ($k = 0, N-1$), so $N_{\rm ph} = \Sigma_{k=0}^{N-1} x_k$. We define the discrete Fourier transform of this time series as

$$a_j \equiv \sum_{k=0}^{N-1} x_k \, e^{2\pi i j k/N} \quad (j = 0, \tfrac{1}{2}N), \tag{2.2}$$

where $i \equiv \sqrt{-1}$ and a_j is the complex Fourier amplitude at the Fourier frequency $\nu_j \equiv j/T$. The zero-frequency term a_0 is just $N_{\rm ph}$; in practice one usually transforms the mean-subtracted time series $x_k - \bar{x}$ instead of x_k, so that $a_0 \equiv 0$. This does not affect the other a_j's. The highest accessible frequency $\nu_{N/2}$ is called the Nyquist frequency. In practice, the a_j's can conveniently be calculated with one of the various available implementations of the Cooley–Tukey or Sande–Tukey Fast Fourier Transform (FFT) algorithms (see, e.g., Press *et al.*, 1986).

Following Leahy *et al.* (1983), we further define the power spectrum as

$$P_j = 2 \, |a_j|^2 / N_{\rm ph} \, . \tag{2.3}$$

With this normalization it follows from Parseval's theorem (e.g., Press *et al.*, 1986) that

the total variance of any signal x_k is related to the summed power in the power spectrum as

$$\mathrm{Var}(x_k) \equiv \sum_{k=0}^{N-1} (x_k - \bar{x})^2 = \frac{N_{\mathrm{ph}}}{N} \sum_{j=1}^{N/2} P_j \tag{2.4}$$

(where, strictly speaking, $P_{N/2}$ should have half the value indicated by Equation (2.3)), so that the fractional root-mean-square (r.m.s.) variation in the x_k is

$$r \equiv \frac{\sqrt{\frac{1}{N}\mathrm{Var}(x_k)}}{\bar{x}} = \sqrt{\frac{\sum_{j=1}^{N/2} P_j}{N_{\mathrm{ph}}}} \,. \tag{2.5}$$

(r is often expressed in terms of a percentage, and is then also called the 'percentage r.m.s. variation'). A sinusoidal signal $x_k = A \sin(2\pi \nu_j t_k)$, where $t_k = kT/N$ will cause a spike at ν_j in the power spectrum with

$$P_j = \frac{1}{2} \frac{N^2}{N_{\mathrm{ph}}} A^2 \,. \tag{2.6}$$

The reason for choosing this apparently rather awkward normalization for the powers lies in the statistical properties of the noise power spectrum, to be described below.

In the case of a photon count signal, counting statistics will make the data x_k noisy. For a 'constant' count rate undistorted by instrumental effects (i.e., the chance to detect a photon is equal at every instant), the x_k will be distributed according to the Poisson distribution. This noise will cause the powers $P_{j,\,\mathrm{noise}}$ in the power spectrum to attain finite values, even in the absence of source variability. It will also cause the power spectrum to be noisy itself. It can be shown (e.g., Leahy *et al.*, 1983) that (with the exception of $P_{N/2}$) the distribution of the powers will be proportional to a χ^2 distribution with 2 degrees of freedom (d.o.f.). The whole sense of the normalization in Equation (2.3) used by Leahy *et al.* (1983) is to make the distribution of powers exactly equal to this distribution. So, with Definitions 2.2 and 2.3 the probability for a given $P_{j,\,\mathrm{noise}}$ to exceed, say, $P_{\mathrm{threshold}}$ is given by

$$\mathrm{Prob}(P_{j,\,\mathrm{noise}} > P_{\mathrm{threshold}}) = Q(P_{\mathrm{threshold}} \,|\, 2) \quad (j = 1, \tfrac{1}{2}N - 1) \,, \tag{2.7}$$

where the integral probability of the χ^2 distribution is defined as

$$Q(\chi^2 \,|\, v) \equiv \left[2^{v/2}\Gamma\left(\frac{v}{2}\right)\right]^{-1} \int_{\chi^2}^{\infty} t^{v/2-1} e^{-t/2} \,\mathrm{d}t \,, \tag{2.8}$$

where v is the number of d.o.f.

Independent of the count rate, for any Poisson noise signal, the mean value of the powers will be 2 and the variance 4. Two more or less equivalent methods have been used in the study of QPO sources to decrease this large variance. One has been to rebin

the power spectrum, summing together M consecutive bins; the other to divide the data up into M equal segments, transform these segments individually and then sum the resulting M power spectra, each normalized according to Equation (2.3), where $N_{\rm ph}$ is now the number of photons *in one transform*. Both methods of power spectrum compression, of course, degrade the frequency resolution.

As the time required to calculate the Fourier transform of N data points using an FFT algorithm is proportional to $N \log N$, there is a computational advantage to the second method; the time saving factor is about $1 + \log M/\log N$. In many cases, considerable additional time savings result from the smaller array sizes that have to be handled by the computer. For a variable source, a further advantage of the second method is that cutting up the data into smaller segments allows one to study variations in the power spectra as a function of, e.g., source intensity by selectively averaging power spectra obtained within certain source intensity intervals (Van der Klis *et al.*, 1985b), and that is allows the construction of 2-dimensional images (see, e.g., Figure 1.1) showing the time evolution of the power spectrum. This technique has proven particularly useful in the detection of transient QPO phenomena. The first method, on the other hand, has the advantage of producing a power spectrum that extends to lower frequencies (the lowest measurable frequency being $1/T$).

Because of the additive properties of the χ^2 distribution, the powers in the summed spectrum obtained by either of the two methods will be distributed according to a χ^2 distribution with $2M$ d.o.f., with mean $2M$ and variance $4M$. Most observers *average*, rather than sum, their power spectra, and we will follow this practice here. In this way, Equations (2.4–2.6) remain valid when $N_{\rm ph}$ and N are interpreted as the values for one transform. The result of the averaging is a spectrum with a mean of 2 and a standard deviation of $2/\sqrt{M}$, as compared to a standard deviation of 2 for one single spectrum; for large M, the spectrum becomes much less noisy. The power distribution is compressed similarly, and analogously to Equation (2.7), the probability for a given power $P_{j,\,\rm noise}$ in the averaged spectrum to exceed a $P_{\rm threshold}$ is given by

$$\text{Prob}(P_{j,\,\rm noise} > P_{\rm threshold}) = Q(MP_{\rm threshold} \mid 2M)\,, \tag{2.9}$$

where $Q(\chi^2 \mid v)$ is again given by Equation (2.8). For large M, this distribution tends asymptotically to a normal distribution with a mean of 2 and standard deviation $2/\sqrt{M}$:

$$\lim_{M \to \infty} \text{Prob}(P_{j,\,\rm noise} > P_{\rm threshold}) = Q_{\rm Gauss}\left(\frac{P_{\rm threshold} - 2}{2/\sqrt{M}}\right), \tag{2.10}$$

where the integral probability of the normal distribution is

$$Q_{\rm Gauss}(x) \equiv \frac{1}{\sqrt{2\pi}} \int_x^\infty e^{-t^2/2}\, dt\,. \tag{2.11}$$

With Equations (2.9) and (2.10), the problem of detecting a small signal in the power spectrum is reduced to an exercise in χ^2 or Gaussian statistics.

2.2.2. *Detection and Upper Limits*

In defining criteria for the detection of a broad feature in the power spectrum, it is possible to generalize the formalism described by Leahy *et al.* (1983) for the detection of a narrow peak (i.e., coherent oscillations). In this formalism, it is assumed that Equation (2.1) holds, so that the total power spectrum is the sum of the noise spectrum described above and a signal spectrum

$$P_j = P_{j,\,\mathrm{noise}} + P_{j,\,\mathrm{signal}} \,. \tag{2.12}$$

One defines a $(1 - \varepsilon)$ confidence detection level P_{detect} that has only a small probability ε of being exceeded by at least one of the powers $P_{j,\,\mathrm{noise}}$ in the frequency range of interest. Each of the frequency bins in this range constitutes a 'trial' in which P_{detect} could be exceeded. Therefore, if there are N_{trial} bins in this range, P_{detect} should be chosen such that the probability for one individual noise power to exceed P_{detect} is $\varepsilon/N_{\mathrm{trial}}$. With Equation (2.9), this implies that P_{detect} is given by

$$\frac{\varepsilon}{N_{\mathrm{trial}}} = Q(MP_{\mathrm{detect}} \,|\, 2M) \,. \tag{2.13}$$

If there is a particular frequency ν_j where the power P_j exceeds P_{detect} (and if the noise is correctly described as purely Poissonian counting noise) then with a probability $(1 - \varepsilon)$ we have detected a signal with a power (see Equation (2.12)) $P_{j,\,\mathrm{signal}} \geq P_j - P_{\mathrm{detect}}$.

If P_{detect} is *not* exceeded, then we can derive a $(1 - \delta)$ confidence upper limit P_{UL} to any $P_{j,\,\mathrm{signal}}$ as follows. Define a power level P_{exceed} that has the *large* probability $(1 - \delta)$ to be exceeded by a given individual $P_{j,\,\mathrm{noise}}$ due to the statistical fluctuations. So, on average, the number of $P_{j,\,\mathrm{noise}}$'s in the range of interest that will exceed P_{exceed} is $(1 - \delta)N_{\mathrm{trial}}$. Again using Equation (2.9), we see that P_{exceed} is given by

$$1 - \delta = Q(MP_{\mathrm{exceed}} \,|\, 2M) \,. \tag{2.14}$$

If at any frequency ν_j there were an (undetected) signal $P_{j,\,\mathrm{signal}}$ in the data, then the total power at this frequency would again be given by Equation (2.12). As, with a probability $(1 - \delta)$, we have $P_{j,\,\mathrm{noise}} > P_{\mathrm{exceed}}$, we can state with the same confidence that

$$P_{j,\,\mathrm{signal}} < P_j - P_{\mathrm{exceed}} \quad (1 - \delta \text{ confidence level}) \,. \tag{2.15}$$

Without looking at the data any further, we can make use of the fact that $P_j < P_{\mathrm{detect}}$ for all j in the interval of interest, so that $P_{j,\,\mathrm{signal}} < P_{\mathrm{detect}} - P_{\mathrm{exceed}}$. This is the 'two-confidence level' $(1 - \varepsilon,\, 1 - \delta)$ upper limit described by Leahy *et al.* (1983); it is the worst case upper limit one can always anticipate to be able to set from a given observation if there is no detection. When the data are available, it is better to replace P_j in Equation (2.15) with P_{max}, the actually observed highest power in the range of interest, rather than with P_{detect}. As P_{max} will always be less than P_{detect}, this will lead to the somewhat tighter $(1 - \delta)$ confidence upper limit

$$P_{\mathrm{UL}} = P_{\mathrm{max}} - P_{\mathrm{exceed}} \,. \tag{2.16}$$

It is straightforward to extend this formalism to the detection of, and the setting of upper limits to, a broad feature in the power spectrum with a width of W frequency bins, by working with the averaged power of W adjacent bins: all one needs to do is to replace M in Equations (2.13) and (2.14) with WM. If there is no *a priori* knowledge of the value of W, one will want to try several different values; this will lead to different values for P_{detect} and P_{exceed} for different subsets of trials. Similarly, it may be judged necessary to use overlapping sets of W bins. In both of these cases, the trials will not all be independent. By counting all trials in N_{trial} in Equation (2.13), and by selecting the largest P_{UL} among those obtained for the different subsets, one will at least err on the conservative side, obtaining higher detection levels and upper limits. Note, that contrary to the case for coherent oscillations, no improvement in sensitivity occurs when, for the same data set, the individual transforms are made longer (N larger) and their number M is reduced. The reason for this is, loosely speaking, that by increasing N the variance in the noise is distributed over more frequency bins, while the power due to coherent oscillations remains concentrated in one bin; the power in a broad feature is distributed out in exactly the same way as that due to the noise.

In practice, the formal method described above has not been used by many (prospective) QPO observers (an exception is the paper by Mereghetti and Grindlay, 1987). A more typical approach has been to average many power spectra and to make use of Equation (2.10) to perform standard functional χ^2-minimization fits to features picked out by eye in plots of the power spectra. The confidence level is then estimated in the usual way from the shape of the χ^2 hypersurface in parameter space (Avni, 1976; Lampton *et al.*, 1976). Clear disadvantages of this approach are that, without extensive simulations, it is difficult to estimate the probability that a certain combination of fit parameters could have been obtained from statistical fluctuations. It is also impossible to say, *a posteriori*, how many trials in centroid frequency and width of the feature are implicit to the procedure (see, e.g., Lewin *et al.*, 1987). An advantage might be that the method is somewhat more sensitive to the 'correct' functional shape of a QPO or red noise signal (as predicted, for example, from the known properties of a brighter source).

In the Gaussian approximation (Equation (2.10)), the summed power of a feature with a width $\Delta\nu$ in the averaged power spectrum will have a statistical uncertainty of $(2/M)\sqrt{T_{\text{obs}}\Delta\nu}$ where T_{obs} is the total observing time. Using Equation (2.5) and substituting $N_{\text{ph}} = IT_{\text{obs}}/M$, where I is the count rate, it is easy to derive that in terms of 'sigmas' the confidence level n_σ at which a feature corresponding to a signal with a fractional r.m.s. variation of r will be detected is

$$n_\sigma = \frac{1}{2} Ir^2 \sqrt{\frac{T_{\text{obs}}}{\Delta\nu}} \,. \tag{2.17}$$

From this expression it is seen that the observing time needed to detect a feature is strongly dependent on the intensity of the source, and *extremely* sensitive to its r.m.s. variation (see also Section 6). Provided (as before) that a sufficient number of power spectra is summed so that the Gaussian approximation (Equation (2.10)) is valid,

Equation (2.17) can also be applied to a narrow peak in the power spectrum (coherent oscillations). Then the width of the feature $\Delta\nu$ must be replaced by the width M/T_{obs} of a frequency bin in the power spectrum.

2.2.3. *Deadtime Effects*

Instrumental effects summarized under the name 'deadtime' can modify the simple properties (see Equation (2.9)) of the noise distribution of the powers, and thus influence the detection levels and upper limits that can be obtained. (They can also modify the power spectrum of a QPO or red-noise signal; this problem will be adressed in Section 2.3.2.)

After the detection of a photon, the detector with its associated electronics and logic needs a certain time interval to recover before it can detect the next photon. Photons arriving during this time interval are completely ignored. Usually the output from the detector system is in the form of consecutive 'samples' with a short duration τ. The value of a sample is the number of photons detected during this time interval τ. Depending on how the deadtime process interacts with the sampling process, one can distinguish various types of deadtime, for example, one characterized by a 'dead' interval that is constant and does not depend on the sampling process, and a type where the dead interval lasts until a given predetermined instant with respect to the sampling cycle.

As an example of the latter type, we consider the simple case that this instant is the end of the sample in which the photon arrives, so that only one photon per sample (the first one) can be detected; all photons arriving within the same sample after the first one are ignored. If the incident counting signal is Poisson noise at an average rate λ, then the probability p that at least one photon will arrive during a given sample is given by the Poisson distribution as $p = 1 - e^{-\tau\lambda}$, where τ is the duration of one sample. The observed count rate will be $\mu = p/\tau$, so that the factor by which the deadtime attenuates the intensity is

$$f(\lambda) \equiv \frac{\mu}{\lambda} = \frac{1 - e^{-\tau\lambda}}{\tau\lambda} \,. \tag{2.18}$$

If the samples are binned up into bins containing N_{sample} samples each, then the number of counts per bin x_k is the number of times that the probability p is realized among N_{sample} independent tries, so that (by definition) the x_k follow the binomial rather than the Poisson distribution, with mean pN_{sample} and variance per bin $p(1-p)N_{\text{sample}}$. With expression (2.4) for the total variance of the x_k and noting that $N_{\text{ph}} = \Sigma\, x_k = pNN_{\text{sample}}$, it is readily derived that the average noise power will be $\langle P_{j,\,\text{noise}} \rangle = 2e^{-\tau\lambda}$, so that, as compared to the case of zero deadtime, the 'Poisson level' of the power spectrum will be depressed by a factor

$$\frac{\langle P_{j,\,\text{noise}} \rangle}{2} = e^{-\tau\lambda} = 1 - \mu\tau \,. \tag{2.19}$$

A further complication arises, when not all photons that take part in the sampling

process are taken into account in the analysis. This occurs, for example, when only photons within a given energy band are considered. Denoting the incident rate of the photons which we wish to consider as λ_c and that of the other, remaining photons as λ_o, so that $\lambda = \lambda_c + \lambda_o$, and in obvious notation, $\mu = \mu_c + \mu_o$, we may note that Equation (2.18) gives the probability for *any* photon that it will be the first in its sample and, therefore, be detected, so that the same deadtime intensity attenuation factor applies for any subset of incident photons:

$$\frac{\mu_c}{\lambda_c} = \frac{\mu_o}{\lambda_o} = \frac{\mu}{\lambda} = f(\lambda)\,. \tag{2.20}$$

The probability that in a given sample a ('considered') photon will be detected is $p_c = \mu_c \tau$, so that the distribution of the binned data x_k will again be binomial and the average noise power level will be given by

$$\frac{\langle P_{j,\,\mathrm{noise},\,c}\rangle}{2} = 1 - \mu_c \tau = 1 - \frac{1 - e^{-\tau\lambda}}{\lambda}\,\lambda_c\,. \tag{2.21}$$

It is interesting to note that to calculate the incident count rate of considered photons one needs to known the total rate (λ or μ) in addition to μ_c, whereas the 'Poisson level' of the power spectrum can be evaluated from only the observed count rate of the considered photons μ_c.

In practice, the sampling process is often much more complex than assumed in the above example. In particular, most types of deadtime introduce correlations between the samples, and thereby, between the x_k, which means that the noise power spectrum will no longer be flat. The most complete analysis of these problems in the context of the EXOSAT Medium Energy (ME) instrument was given by Tennant (1987a; see also Andrews, 1984; Andrews and Stella, 1984). In the EXOSAT ME a nearly negligible constant detector deadtime of ~ 5.5 μs combines, but only in the case of the photon-energy resolved data modes (see Section 3.1), with a complicated sampling process. The main feature in which this process differs from the above example is, that the 'dead' interval starting with the detection of a photon in a given sample lasts until a predetermined instant in the next sample. This means that the chance to detect a photon in a given sample depends on what happened in the previous sample: the samples are correlated.

By distinguishing between the probability p_S to detect a photon in a given sample if one was detected in the previous one, and the probability p_L applying if the previous sample is empty, Tennant (1987a) shows that (for $N_{\mathrm{sample}} = 1$; i.e., one sample per bin) the noise power spectrum will be of the form

$$P_{j,\,\mathrm{noise}} = P_0(1 + \alpha_1 \cos(2\pi j/N) + \alpha_2 \cos(4\pi j/N) + \cdots)\,, \tag{2.22}$$

where P_0 is the constant power level that would have obtained without correlations between the samples, and the α_i form a rapidly decreasing sequence determined by the values of p_S and p_L.

In practice, the observers' way of dealing with all these complexities has often been to choose the number of power spectra to be added (M) large, to empirically determine the standard deviation σ_j of the M values of P_j in the individual power spectra, and, invoking the central limit theorem, to assume that their mean value is normally distributed with standard deviation $\sigma_j/\sqrt{M}$. The disadvantage of this approach is that an extra free parameter is introduced: the Poisson level of the power spectrum as modified by deadtime effects. Therefore, this technique is completely insensitive to white noise that is intrinsic to the source. The advantage, of course, is that no detailed knowledge of the sampling process is required.

2.2.4. *Doppler Effects*

Orbital motion of the X-ray source will cause the observed frequency of the signals produced by the source to show periodic shifts of a magnitude given by $\delta\nu(t)/\nu = v_{\mathrm{rad}}(t)/c$, where v_{rad} is the radial velocity and c the light velocity. As the orbital velocities in X-ray binaries are usually of the order of a few 100 km s^{-1} at most, these frequency shifts are quite small and can be neglected for QPO signals, which typically produce a peak in the power spectrum with a width that is of the same order as its centroid frequency.

However, in the case of coherent pulsations, orbital frequency shifts can be of importance. If the observing time per transform $T \equiv T_{\mathrm{obs}}/M$ exceeds the orbital period P_{orb}, then the power spectrum of a pulsar will show a pattern of side lobes around the central peak at the nominal pulse frequency. The separation between the side lobes is the orbital frequency. The side lobes remove power from the central peak, which, therefore, becomes more difficult to detect above the noise. If, on the other hand, T is much shorter than P_{orb}, then a single, broadened peak will be observed. The centroid frequency of this peak will shift according to the orbital phase corresponding to each power spectrum, while the width of the peak in each individual power spectrum is determined by the change in radial velocity during the time T, i.e., by the radial acceleration.

Assuming a circular orbit, the radial velocity is given by $v_{\mathrm{rad}}(t) = K \sin(2\pi t/P_{\mathrm{orb}})$, where K is the radial velocity amplitude and P_{orb} the orbital period, and consequently the radial acceleration is $a_{\mathrm{rad}}(t) = 2\pi K/P_{\mathrm{orb}} \cos(2\pi t/P_{\mathrm{orb}})$. One usually demands that the frequency change occurring during one individual transform is always less than the width of a frequency bin in the power spectrum, which implies:

$$T < \sqrt{\frac{cP_{\mathrm{orb}}}{2\pi K \nu_{\mathrm{puls}}}}\,, \tag{2.23}$$

where ν_{puls} is the pulse frequency. There are several reasons why this condition is not sufficient to prevent a sometimes severe decrease in the sensitivity to pulsations. First, even when Equation (2.23) is satisfied, power will be removed from the central peak due to the small frequency- and phase-shifts still present within each individual transform (see Section 2.3.1 for analogous problems occurring even in the case of a constant

observed pulse frequency). Second, in the course of one orbital period, the pulse frequency will vary over a range $2K\nu_{\rm puls}/c$; this will cause the peak in the successive power spectra to shift over $2K\nu_{\rm puls}T/c$ bins. Third, by cutting up the observation into small sections and transforming these individually, the frequency bins in the power spectrum become wider so that the sensitivity gain potentially present in the coherence of the pulsations is lost (see also Section 2.2.2). It is sometimes attempted to overcome these three types of sensitivity decrease all at once by correcting the data for different assumed binary orbits (e.g., Middleditch and Priedhorsky, 1986); this technique is most often applied if one or more of the orbital parameters (in particular, the orbital period) are known. While a large increase in sensitivity occurs for the correct choice of orbital parameters, the fact that the analysis must be repeated for several different sets of orbital parameters to have a chance to succeed means that the number of trials ($N_{\rm trial}$ in Equation (2.13)) increases drastically.

2.3. The Signal Underlying the Power Spectrum

2.3.1. *Fractional r.m.s. Variation*

Once features have been detected in the power spectrum, the next problem is to interprete them in terms of the underlying signal in the time series. Even in the case of a purely sinusoidal signal, there are several complications that make the calculation of the sine amplitude from the spike in the power spectrum deviate from that suggested by the simple expression (2.6).

One of these complications is caused by the fact that the time series and, therefore, the Fourier spectrum are discretely sampled. The frequency $\nu_{\rm sine}$ of the sinusoid does not need to be equal to any one of the Fourier frequencies ν_j, but may be at an intermediate frequency. This causes some of the power in the signal to be spread out over the entire spectrum, and decreases the power in the central peak $P_{j,\,\rm sine}$ at the Fourier frequency $\nu_{j,\,\rm sine}$ that is closest to $\nu_{\rm sine}$. The phase that the sinusoid has with respect to the discrete time samples x_k also influences the shape of the final spectrum. The average factor (averaged over all possible phases and frequencies) by which $P_{j,\,\rm sine}$ decreases due to these effects was calculated by Leahy *et al.* (1983) to be approximately equal to 0.773.

Another complication is that in our application, the x_k are data *binned* into equally spaced bins rather than equally spaced, infinitely narrow discrete samples of the signal. The binning causes the signal to be averaged out somewhat, an effect that gets worse when the frequency of the signal increases. Due to this effect the amplitude of the sinusoid will be lower by a factor $\sin(\pi\nu_{\rm sine}T/N)/(\pi\nu_{\rm sine}T/N)$ (Leahy *et al.*, 1983). Combining these factors, the expectation value of the power caused by a sinusoidal signal of arbitrary phase and of frequency $\nu_{\rm sine}$ at the Fourier frequency $\nu_{j,\,\rm sine}$ nearest to $\nu_{\rm sine}$ is

$$\langle P_{j,\,\rm sine}\rangle = \langle P_j\rangle - \langle P_{j,\,\rm noise}\rangle = 0.773 \times \frac{1}{2}\,\frac{N^2}{N_{\rm ph}}\,A^2\left(\frac{\sin(\pi j_{\rm sine}/N)}{\pi j_{\rm sine}/N}\right)^2. \qquad (2.24)$$

Here $P_{j,\,\rm noise}$ is given by Equation (2.9) and A is the amplitude of the sinusoid.

As a non-negligible fraction of the total power in the signal may appear at the other Fourier frequencies, it may even in the case of a sinusoidal signal be better to work in terms of the *total* summed power rather than the power at just one Fourier frequency. This is certainly the case for an intrinsically broad feature such as a QPO peak.

It has become standard practice to express the summed 'excess' power

$$P_{\text{excess}} = \sum (P_j - P_{j,\,\text{noise}}) = \sum P_{j,\,\text{signal}}\,, \tag{2.25}$$

in terms of the fractional r.m.s. variation defined according to Equation (2.5) that the x_k would have had due to the signal in the absence of noise. Various authors have taken different approaches to applying the two correction factors described above. The factor 0.773 describes how much the power is lower at one particular Fourier frequency; this power is not lost, but appears at other Fourier frequencies. Therefore, this correction should not be applied when expressing a total summed power into an r.m.s. variation. The effect of binning the data up will still be that the observed amplitude of the signal, and consequently its summed power, decreases, so that a correction for this is in order.

A common approach to analyzing the power spectrum has been to express the power as a function of the frequency $P(\nu) = P_{\text{noise}}(\nu) + P_{\text{signal}}(\nu)$ defined such that $P(\nu_j) \equiv P_j$. To calculate the excess power in a power spectral feature one then integrates the function describing the signal power spectrum. Noting that $\int P(\nu)\,\mathrm{d}\nu = T^{-1}\,\Sigma\,P_j$, we have $P_{\text{excess}} = T \int P_{\text{signal}}(\nu)\,\mathrm{d}\nu$, and we can write, applying the binning correction and using Equation (2.5) for the fractional r.m.s. variation:

$$r \approx \frac{\pi \bar{j}/N}{\sin(\pi \bar{j}/N)} \sqrt{\frac{\Sigma\,P_{j,\,\text{signal}}}{N_{\text{ph}}}} = \frac{\pi \bar{\nu} \tau_{\text{bin}}}{\sin(\pi \bar{\nu} \tau_{\text{bin}})} \sqrt{\frac{\int P_{\text{signal}}(\nu)\,\mathrm{d}\nu}{\mathrm{I}}}\,, \tag{2.26}$$

where $I = N_{\text{ph}}/T$ is the count rate, $\bar{\nu}$ the average frequency of the feature considered and $\bar{j}$ the corresponding Fourier number, $\tau_{\text{bin}} = T/N$ the duration of a time bin, and where the sum and the integral run over all frequencies where the signal causes a non-negligible power.

2.3.2. *Deadtime Effects; Channel Cross-Talk*

Provided that the variations in the signal of interest are slow with respect to the deadtime process (see Section 2.2.3), the way in which deadtime changes the signal is completely described by the instrument-dependent relation between λ and μ, the incident and observed count rates. An example of such a relation is given in Equation (2.18); any relation, either theoretical or empirical, can be used.

Expressing the relation as the deadtime attenuation factor $f(\lambda) = \mu/\lambda$, one finds that a small change $\delta\lambda$ in the incident rate causes a change $\delta\mu$ in the observed rate given by

$$\frac{\delta\mu}{\mu} = \left(1 + \frac{\lambda}{f}\frac{\mathrm{d}f}{\mathrm{d}\lambda}\right)\frac{\delta\lambda}{\lambda}\,. \tag{2.27}$$

From this expression we can derive the relation between the observed fractional r.m.s.

variation r and the incident one, R:

$$\frac{R}{r} = \frac{|\delta\lambda|/\lambda}{|\delta\mu|/\mu} = \left(\left|1 + \frac{\lambda}{f}\frac{\mathrm{d}f}{\mathrm{d}\lambda}\right|\right)^{-1} . \tag{2.28}$$

Once again, the situation is more complex when only a subset of the sampled photons is considered. With the notation of Section 2.2.3 and using Equation (2.20), we have

$$\frac{\delta\mu_c}{\mu_c} = \frac{\delta\lambda_c}{\lambda_c} + \frac{\lambda}{f}\frac{\mathrm{d}f}{\mathrm{d}\lambda}\frac{\delta\lambda}{\lambda} . \tag{2.29}$$

Note that for $\delta\lambda_c \equiv 0$ it is not necessarily true that $\delta\mu_c$ is equal to zero as well; variations can be induced in the considered band, via deadtime effects, by variations wholly *outside* this band. This 'communication' between different bands via deadtime effects is known as 'channel cross-talk'. If, as is usually the case, with increasing λ the deadtime increases ($f(\lambda)$ decreases) then an increase in the total count rate will cause the observed rate to drop in those bands where the incident rate does not change: the induced effect has a negative amplitude. In the power spectrum these negative-amplitude variations of course show up as a positive feature, introducing an ambiguity in the final result. When evaluating the strength of a power spectral feature in several bands, one must, therefore, using the deadtime attenuation function, carefully check from the power spectrum of the *total* sampled flux whether a feature observed in a particular band could not be exclusively due to channel cross talk, and in any case correct any measured signal in the considered band for this effect.

The ambiguity can often be resolved by calculating the power spectra of the summed flux in two or more bands in addition to those of the flux in the individual bands, and using the fact that $\Sigma\, \delta\mu_i = \delta\mu$, where $\delta\mu_i$ is the amplitude of variation in band i and $\delta\mu$ that in the summed flux. The individual power spectra will allow determination of the $|\delta\mu_i|$ and the spectrum of the summed flux that of $|\delta\mu|$. If this last quantity is less than $\Sigma\,|\delta\mu_i|$, then at least one of the $\delta\mu_i$ must be negative. Alternatively, cross-spectral techniques (see Section 2.4) can be used; a negative-amplitude signal will stand out because it has a 180° phase difference with the total signal.

2.3.3. *The Shape of the Power Spectrum*

The integrated power observed in a feature in the power spectrum measures the variance of the underlying signal. In principle, the detailed shape of the feature contains a large amount of additional information about the signal. Empirically, the observed power spectrum has usually been described with a function

$$P(\nu) = A_{\mathrm{WH}} + P_{\mathrm{RN}}(\nu) + P_{\mathrm{QPO}}(\nu) , \tag{2.30}$$

where the fit parameter A_{WH} is usually assumed to be completely due to the ('white') Poisson noise and $P_{\mathrm{RN}}(\nu)$ and $P_{\mathrm{QPO}}(\nu)$ describe the shape of the red noise and the QPO, respectively.

For the QPO peak, both Lorentzian

$$P_{\mathrm{Lor}}(\nu) = C_{\mathrm{Lor}} \frac{\Gamma/2\pi}{(\nu - \nu_c)^2 + (\Gamma/2)^2} \tag{2.31a}$$

and Gaussian

$$P_{\mathrm{Gauss}}(\nu) = C_{\mathrm{Gauss}} \frac{1}{\sigma\sqrt{2\pi}} \exp\left[-\frac{1}{2}\left(\frac{\nu - \nu_c}{\sigma}\right)^2\right] \tag{2.31b}$$

fit functions have been used. For the LFN component of the red noise (see Section 3.3.1), the above functions, with $\nu_c \equiv 0$, as well as exponential

$$P_{\mathrm{exp}}(\nu) = B_{\mathrm{exp}}\, \eta\, e^{-\eta\nu} \tag{2.31c}$$

and power law functions with an exponential roll-over

$$P_{\mathrm{pl.ex}}(\nu) = B_{\mathrm{pl.ex}}\, \nu^{-\gamma} e^{-\eta\nu} \tag{2.31d}$$

have been used; the VLFN (Section 3.3.1) has always been described with a simple power law

$$P_{\mathrm{pl}}(\nu) = B_{\mathrm{pl}}\, \nu^{-\gamma}. \tag{2.31e}$$

In these expressions, C_{Lor} and C_{Gauss} are the integrated power in the QPO peak ($\nu = -\infty$ to $+\infty$), and B_{exp} that in the LFN component ($\nu = 0$ to ∞); the integrals of $P_{\mathrm{pl.ex}}(\nu)$ and $P_{\mathrm{pl}}(\nu)$ often diverge near $\nu = 0$. The centroid frequency of the QPO peak is denoted ν_c; the full width at half maximum of the Lorentzian peak is Γ and the standard deviation of the Gaussian peak is σ. The quantity γ in Equation (2.31e) is often called the 'power-law slope'; in the exponentials in Equations (2.31c) and (2.31d) often the e-folding frequency $1/\eta$ is quoted rather than the steepness η itself.

We note here, that very steep red noise, with a power-law slope γ exceeding 2 cannot be adequately estimated using a Fourier transform. This is because of 'low-frequency leakage', a spill-over of power from low-frequency bins into adjacent higher-frequency bins that is, in turn, caused by the fact the frequency response of the Fourier transform at every frequency has a finite width (Deeter, 1984).

Interpreting these empirical functions in terms of the underlying signal one needs a model for the signal. Mathematically completely random models are perfectly able to explain the observed power spectra. An example for QPO is a second-order auto-regressive process

$$x_k = a x_{k-1} + b x_{k-2} + v_k, \tag{2.32}$$

where v_k is a random noise process. For the right choice of the constants a and b, this process will produce an oscillatory signal that causes a broad peak in the power spectrum without the involvement of any underlying 'clock' (e.g., Robinson and Nather, 1979). Other possible models for a broad peak in the power spectrum include (i) the

superposition of a number of coherent oscillations with a close, unresolved frequency spacing, and (ii) an infinitely extended frequency-modulated oscillation. No physical models have been proposed as yet that can profitably be described in any of these ways.

Much more popular have been the oscillating shot models (Lamb *et al.*, 1985; Lamb, 1986; Alpar, 1986, 1987; Shibazaki and Lamb, 1987; Elsner *et al.*, 1987; Shibazaki *et al.*, 1988a, b). In these models, the QPO signal is a superposition of random shots, each of which contains a deterministic oscillating component but of which onset time, oscillation phase, etc., are randomly distributed parameters,

In a formalism introduced by Lamb *et al.* (1985) and motivated by the magnetospheric accretion-modulated beat-frequency model (see Section 4.2), the signal $I(t)$ is described in terms of shots $F_i(t)$ with onset times t_i as

$$I(t) = I_0 + \sum_i F_i(t - t_i) . \tag{2.33}$$

With the simplifying assumptions that $F_i(t)$ can be written as the product of an envelope function $G(t)$ and a modulation function that is a harmonic series with a basic frequency ν_B that is constant in time (e.g., the 'beat' frequency):

$$F_i(t) = G(t)\left[A_i + \sum_{n=1}^{\infty} B_{n,i} \cos(n(2\pi\nu_B t + \phi_i) + \alpha_{n,i})\right], \tag{2.34}$$

where the A_i, $B_{n,i}$, ϕ_i, $\alpha_{n,i}$, and t_i (Equation (2.33)) are randomly distributed uncorrelated variables (the t_i and ϕ_i being in addition uniformly distributed), the expectation value for the signal power spectrum becomes

$$\langle P_{\text{signal}}(\nu)\rangle = \frac{\langle N_{\text{shots}}\rangle \langle A^2\rangle}{\langle I\rangle} g(\nu) + \frac{1}{4}\frac{\langle N_{\text{shots}}\rangle}{\langle I\rangle} \sum_{n=1}^{\infty} \langle B_n^2\rangle [g(\nu - n\nu_B) + g(\nu + n\nu_B)] , \tag{2.35}$$

where N_{shots} is the number of simultaneous shots, the angled brackets denote ensemble averages and $g(\nu)$ is the power spectrum of $G(t)$ normalized such that $\int_{-\infty}^{+\infty} g(\nu)\, d\nu \equiv 1$. The first term on the right-hand side of Equation (2.35) describes the red noise, the second the QPO. Noting that g(ν) is symmetric around $\nu = 0$ and ignoring the binning correction, we have with Equation (2.26) for the fractional r.m.s. variation in red noise and QPO, respectively:

$$r_{\text{RN}} = \sqrt{\frac{\langle N_{\text{shots}}\rangle \langle A^2\rangle}{2\langle I\rangle^2}} \quad \text{and} \quad r_{\text{QPO}} = \sqrt{\frac{\langle N_{\text{shots}}\rangle}{4\langle I\rangle^2} \sum_{n=1}^{\infty} \langle B_n\rangle^2} . \tag{2.36}$$

In this description, the shape of the red noise and that of the wings of the QPO peak are predicted to be identical. If the modulation function is sinusoidal ($B_{n,i} \equiv 0$ for $n \neq 1$) and the shot is required to be positive at all times, then $B_{1,i} < A_i$ for each i and the power in the QPO is predicted to be less than half the power in the red noise (see Section 4.2). If $G(t)$ is an exponential function $e^{-t/\tau_{\text{decay}}}$ for $t > 0$ then $g(\nu)$ is a Lorentzian with full

width at half maximum $\Gamma = (\pi\tau_{\text{decay}})^{-1}$. By allowing harmonics of the basic frequency, various envelope functions, and by introducing biases and correlations into the distributions of the random parameters, a large variety of power spectral shapes can be modeled (see in particular, Alpar, 1986; Shibazaki and Lamb, 1987; Elsner *et al.*, 1987; see also Figure 4.1).

2.4. Cross spectrum and cross-correlation function

2.4.1. *General Description*

The complex Fourier amplitudes a_j defined in Equation (2.2) can be written as $a_j = |a_j|\, e^{i\phi_j}$. ϕ_j is the phase of the best-fit sinusoid with frequency ν_j to the data, and $|a_j|$ its amplitude. As ϕ_j is measured with respect to the usually arbitrary start time of the data, it is not in general a useful quantity. When the transforms of two simultaneous data sets (for example the X-ray intensity in two X-ray energy bands) are considered, say, $a_{1j} = |a_{1j}|\, e^{i\phi_{1j}}$ and $a_{2j} = |a_{2j}|\, e^{i\phi_{2j}}$, then, if a significant signal is detected in each data set at frequency ν_j, the phase difference $\Delta\phi_j = \phi_{1j} - \phi_{2j}$ is of interest: it measures the time lag $\Delta t_j = \Delta\phi_j/2\pi\nu_j$ of the signal in one data set with respect to that in the other as caused by, for example, Comptonization (see Section 5).

The $\Delta\phi_j$ are readily calculated by multiplying a_{1j} with the complex conjugate of a_{2j}:

$$C_j = a_{1j}a_{2j}^* = |a_{1j}|\,|a_{2j}|\, e^{i(\phi_{1j} - \phi_{2j})}\,; \tag{2.37}$$

$C_j (j = 0, N/2)$ is called the cross-spectrum.

Another approach to QPO time lag analysis has been to make use of the cross-correlation function (CCF) of the two time series $x_{1,k}$ and $x_{2,k}$, defined as

$$F_j = \sum_{k=0}^{N-1} x_{1,k+j}x_{2,k} \quad (j = 0, N-1)\,. \tag{2.38}$$

With a periodic boundary condition on the data ($x_{i,k} \equiv x_{i,k+N}$) it can be shown that the CCF is the inverse Fourier transform of the cross-spectrum, so that CCF and cross-spectrum contain the same information.

In the case of the CCF, the time lag Δt is derived by fitting a function $F(t)$ (defined such that $F(t_k) = F_k$) to it that describes the shape of a CCF of a typical QPO signal (see, e.g., Figure 3.10) in terms of an asymmetrically damped sinusoid (Hasinger, 1987a):

$$F(t) = A\, e^{-|t-\Delta t|/\tau_{\text{decay}}}[1 + B\cos(2\pi\nu_c(t - \Delta t))]\,. \tag{2.39}$$

In this function the damping time τ_{decay} has two different values depending on whether $t - \Delta t > 0$ or < 0; ν_c is the QPO frequency. A disadvantage of this CCF approach is that Δt is an average over all frequencies; it is then not possible to infer which frequencies contribute to the time lag, so that it is difficult to disentangle any time lag in the QPO from possible other time shifts in the data. This is illustrated by the fact that Δt appears twice in Equation (2.39), once in the cosine function describing the QPO, and once more in the (exponential) envelope function that can be identified with the red

noise. The advantage of the cross-spectrum over the CCF is that it allows a direct determination of the dependence of time lag on frequency (Van der Klis *et al.*, 1987c).

The values of $\Delta\phi_j$ for random uncorrelated noise are uniformly distributed between 0 and 2π; therefore, plots of time-lag or phase-lag spectra (Δt_j or $\Delta\phi_j$ as function of ν_j) that contain frequency ranges where noise dominates the spectrum tend to have a very scattered appearance (e.g., Figure 3.14). One solution to this is to display amplitude and phase together, so that the frequency ranges where the signal dominates can immediately be identified. By representing the complex cross Fourier amplitudes C_j as vectors with their real part along the positive Y-axis, and their imaginary part along the positive X-axis, and by attaching these vectors at the appropriate position to a frequency axis that is drawn diagonally over the X,Y plane, one obtains a 'three-dimensional' display (e.g., Figure 3.11, see also Bracewell, 1965) where the angle that a vector makes with the Y-axis is identical to its $\Delta\phi_j$. The random $\Delta\phi_j$'s in the noise are no longer a problem as the associated $|C_j|$'s are small (or can be made small by 'background substraction').

2.4.2. *Deadtime and Channel Cross-Talk*

Deadtime effects can severely distort the cross spectrum. At an instant that the intensity in a given band is higher than the time-average due to a statistical fluctuation, it will tend to be lower in the others, as the detection of a photon in one band makes the detection of photons in the others less likely (see Section 2.2.3). This induces a $\Delta\phi_j$ of 180° for all frequencies ν_j where the noise dominates. It is an advantage of the CCF over the cross-spectrum, that, because the statistical fluctuations are uncorrelated from one bin to the next, only the value of F_j for time zero is affected by this deadtime effect. In the cross-spectrum all points are affected. The empirical correction procedure that has usually been adopted for the cross-spectrum is to calculate an average noise vector C_{noise} from a region of the spectrum free of source variability, and to subtract this C_{noise} from every C_j; for the CCF, to just ignore the point at $t = 0$.

Channel cross-talk (see Section 2.3.2.) between the signals caused by the actual source variability in the various bands can, of course, also cause spurious phase shifts between the bands. The amplitude of the cross-talk induced signal is given by Equation (2.29); its phase shift with the true signal will be 180°. If there are no intrinsic phase shifts between the signals then the observed shifts will be either 0 or 180°. However, if there are intrinsic phase shifts then these will combine with those induced by the channel cross-talk. If the deadtime attenuation function is known, a correction for this effect can be made by using the expressions given in Section 2.3.2.

3. Observations

3.1. General remarks on EXOSAT

Since virtually all observations reviewed here have been made with the Medium Energy (ME) detector array (Turner *et al.*, 1981) on board EXOSAT (Taylor *et al.*, 1981), we will start this chapter with some general remarks on this instrument. For more details

we refer the reader to the EXOSAT Express which is regularly issued by the EXOSAT observatory.

The ME array had a total effective area of $\sim 1600\ \mathrm{cm}^2$. It was divided into eight separate identical detector units, each of which consisted of two proportional counters (front and rear) filled with mixtures of Ar and CO_2, and Xe and CO_2, respectively. The Ar detectors were sensitive to X-rays in the energy range between ~ 1 and ~ 15 keV, with a spectral resolution ($E/\Delta E$) ranging between ~ 2 and ~ 10. The Xe detectors covered the energy range between ~ 5 and ~ 50 keV, with a spectral resolution of ~ 5. The ME detectors had a square field of view, with a full width at half-maximum (FWHM) of ~ 50 arc min. The eight detector units were arranged in four quadrants (two detector per quadrant). The quadrants formed two 'half arrays'. The half arrays could be offset mechanically; one half array could monitor the source, and the other the background. The two half arrays could also be co-aligned. Typical values for the background counting rate were $\sim 80\ \mathrm{s}^{-1}$ (all Ar detectors combined), and $\sim 600\ \mathrm{s}^{-1}$ (all Xe detectors combined). For comparison, bright galactic bulge sources yielded typical counting rates in the Ar detectors of $\sim 800\ \mathrm{s}^{-1}$ (e.g., GX 17 + 2) and $\sim 3000\ \mathrm{s}^{-1}$ (e.g., GX 5–1).

The detector signals were processed by the on-board computer (OBC), which could be configured in a large variety of 'OBC programs'. For observations of QPO, the main OBC programs of interest were the high-time resolution modes (HTR3 and HTR5) and the spectral modes (HER2, HER3, HER4, HER5, HER6, HER7, and HTR4). In the high-time resolution modes the events were accumulated in equal time bins without energy resolution (one energy channel only). It was possible to select either the Ar or the Xe detectors or both, but no further control existed over the energy range. For the highest time resolution of 0.25 ms, data gaps existed up to 88% (using HTR3) of the total observing time (i.e., data are then only recorded $\sim 12\%$ of the time). This problem was solved with the introduction of the HTR5 program. The deadtime of these modes (see Sections 2.2.3 and 2.3.2) when data were recorded, was small; typically $< 1\%$.

In some spectral modes the spectral resolution was traded off against time resolution. In most of these modes, X-ray spectra were recorded at a rate that was too slow for the detection of QPO. However, simultaneously with the X-ray spectra the spectral modes generated integrated count rates with a higher time resolution. These count rates were integrated over a spectral range that could be freely chosen. Special cases were the HTR4, HER6, and HER7 modes that allow to record integrated count rates simultaneously only in, respectively, 1, 2, and 4 freely selectable spectral ranges. The highest time resolution that could be obtained in the case of four energy channels was ~ 4 ms. In all spectral modes considerable dead time (typically a few tens of % for bright sources) existed; it was caused by the onboard data processing.

In a typical observation one would have 4 energy channels and a time resolution of 4 ms. Simultaneously with the fast-timing observations, detailed spectral information could be obtained using the HER5 OBC program (8, 32, or 64 energy channels with a time resolution ranging from 0.1 to 8 s). In addition, spectral data with low time resolution were also available simultaneously from the gas scintillation proportional counters (the so-called GSPC; Peacock *et al.*, 1981).

3.2. Low-frequency QPO in LMXB

Before we discuss the observations of the high-frequency QPO in the bright LMXB, we want to mention that low-frequency QPO (periods of ~ 10–10^3 s) have also been reported from several X-ray binaries. The QPO spectrum can be softer as well as harder than the mean source spectrum. The fractional modulations in the flux (thus the strength of the QPO) can be large (typically $\sim 50\%$). We list here some obvious cases in sequence of increasing frequency from ~ 1 mHz to ~ 2 Hz (1626–67: Joss *et al.*, 1978; Li *et al.*, 1980, see Figure 3.1; GX 5–1: Ponman, 1982b; Cyg X-3: Van der Klis and Jansen, 1985; GX 349 + 2: Matsuoka, 1985; 1820–30: Stella *et al.*, 1984; GX 339 – 4: Maejima *et al.*, 1984). Perhaps the 1.5-hr (~ 0.2 mHz) oscillations observed by Langmeier *et al.* (1985) in GX 17 + 2 are also quasi-periodic; this would then extend the range of long-period QPO in LMXB up to periods of $\sim 5 \times 10^3$ s. In most cases these reports concern transient phenomena which last up to a few tens of periods. In some cases there is concern as to the evaluation of the significance of the features in the presence of strong stochastic variability. We believe that most of these QPO have a different origin than those that are the subject of this review. This is almost certainly the case for quasi-periodicities reported on time scales of *days*, as reported for GX 5–1 (Ponman, 1982b).

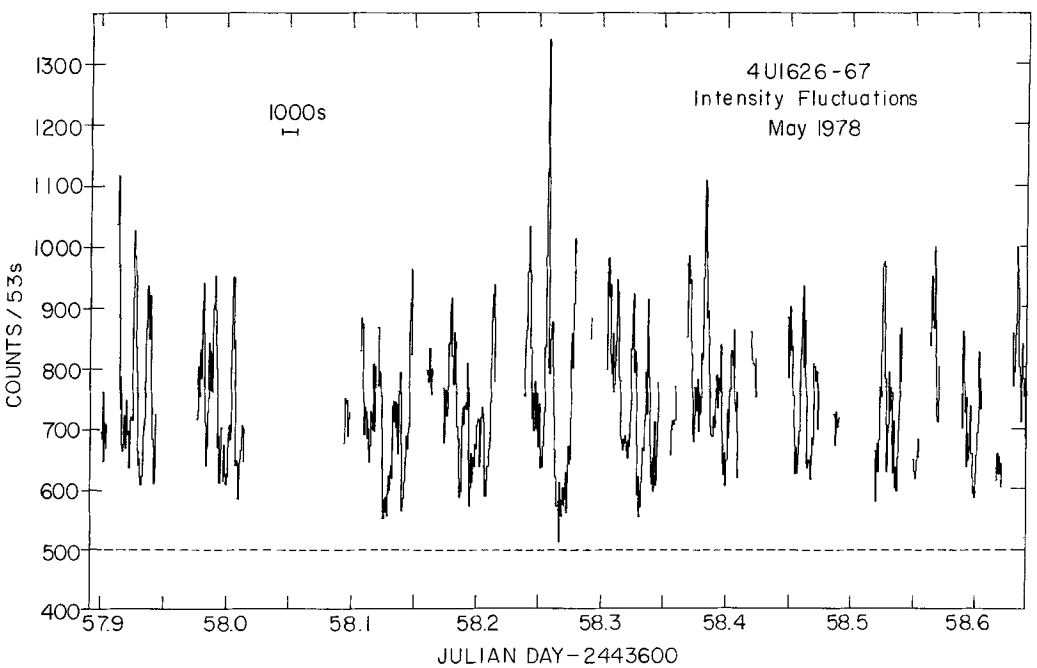

Fig. 3.1. A light curve (counts per 53 s) of ~ 18 h of SAS-3 data from the 7.7-s LMXB 4U 1626 – 67. The large flares have a characteristic recurrence time of $\sim 10^3$ s (see Section 3.2). Gaps in the data correspond to times when the source was occulted by the Earth, the satellite was in the South Atlantic Anomaly, or data were lost in transmission. The dashed line indicates the background level. This figure is from Li *et al.* (1980).

The dividing line between them is almost certainly not at a particular frequency. Our choice, to not further discuss in this review the observations listed above, is therefore somewhat arbitrary.

3.3. HIGH-FREQUENCY QPO IN LMXB

In this section we will be discussing in detail the QPO observations for each source individually. We also give some general background on each source in terms of its X-ray, optical and radio characteristics. The order in which we discuss the sources was chosen mainly for didactic reasons; much of the development in our thinking on QPO has been based on observations of the sources GX 5–1, Cyg X-2, and Sco X-1. For this reason, these sources are discussed first; the other sources are discussed in order of their right ascension.

In Table I we give an observational summary; the sources are listed in order of their right ascension (column 1). We list the spectral states (column 2, see footnote a), the QPO frequency (column 3), the FWHM of the QPO peak in the power spectrum (column 4), the ratio of the FWHM and the QPO frequency (column 5), the r.m.s. variation of the QPO (column 6), the best fit to the red noise (column 7, see footnote b), the slope of the red noise spectrum (column 8, see footnote c), the r.m.s. variation of the red noise (column 9, see footnote d), the frequency range used to derive the strength of the red noise (column 10, see footnotes d and e), the ratio of the r.m.s. variations of the red noise and the QPO (column 11, see footnote d), the dependence of QPO frequency on the source intensity in terms of a power-law fit (column 12, see Section 4.1, and footnote f), upper limits to the strength of the coherent pulsations (column 13; see also Section 2.2.2), the frequency ranges for which the upper limits hold (column 14), the corresponding confidence level of the upper limits (column 15), and references (column 16).

3.3.1. *GX 5–1 (4U 1758 – 25)*

GX 5–1 is the brightest source in the galactic center region, with a long-term average brightness of $\sim 10^3$ μJy (see, e.g., Forman *et al.*, 1978; Warwick *et al.*, 1981). No optical counterpart has been found, which is almost certainly the result of the high interstellar extinction ($A_V > 10$ mag), as inferred from the low-energy cut off in the X-ray spectrum (e.g., Mason *et al.*, 1976; Hertz and Grindlay, 1984) using the relation between A_V and the interstellar hydrogen column density (Gorenstein, 1975; Ryter *et al.*, 1975). There may be a weak variable radio source connected with GX 5–1 (Braes *et al.*, 1972; Geldzahler, 1983; Grindlay and Seaquist, 1986).

Observations of GX 5–1 with Uhuru, Ariel V, and COS-B show that its X-ray flux is variable on time scales ranging between seconds (Forman *et al.*, 1976) and days (Ponman, 1982b; Van der Klis and Rappaport, 1983), but no periodicity has been found in this period range (some evidence for quasi-periodic oscillations on a time scale of ~ 2 days has been reported by Ponman, 1982b). The hardness of the X-ray spectrum is often correlated with the source intensity on time scales of hours to a day (Mason *et al.*, 1976; Ponman, 1982b); in addition, the source has also shown intensity variations

TABLE I

Summary of results on QPO, red noise, and coherent pulsations

Source	Spectral state[a]	QPO				Red noise			
		Freq. (Hz)	FWHM (Hz)	FWHM / Freq.	r.m.s. (%)	Fit[b]	Slope[c]	r.m.s.[d] (%)	Freq. range[d,e] (Hz)
(1)	(2)	(3)	(4)	(5)	(6)	(7)	(8)	(9)	(10)
Cir X-1	?	1.42 ± 0.03	0.03–0.06	0.07	1.8–4	PL	$\sim 1-2.3$		
1516 – 56	?	5.7–18			~ 4				
	?	138–195	191–185	1–1.4	9				
Sco X-1	NB	5.8 – 7.9	1.0–3.2	0.28 ± 0.13	4.2–6.6	PL	1.4–2	1.5–2.1	0.016–1
1617 – 15	IF	6.9 – 17.7	3.5–7.1	0.47 ± 0.15	6.6–9.8	PL	1.4–2	1.2–2.7	0.016–1
	FB	11–22	1.6–32.3	0.69 ± 0.47	5.2–10.4	PL	1.4–2	1.5–2.6	0.016–1
	NB	6	2	0.33	5			2.7	0.0025–0.122
	FB	1.8–25[g]			3			5.5	0.0025–0.122
	NB	6–7			~ 6			2.1	0.016–5
	FB	10–20			~ 8.5				
GX 340 + 0	NB	5.6 ± 0.3	2.7 ± 0.9	0.48 ± 0.46	1.8 ± 0.2	PL	1.2–1.6	0.9–1.5	0.004–0.1
1642 – 45	HB							2.0–3.2	0.5–10
GX 349 + 2	NB?	11 ± 1.5?	$7.5(+9, -5)$	0.2–1.5	2 ± 1	PL	1.54 ± 0.04	1.1–2.6	0.008–0.5
1702 – 36						PL	1.67 ± 0.05	1.3–3.1	0.008–0.5
	NB?	5.3 ± 0.4	10.1 ± 1.4	1.9 ± 0.3	2.0–3.2	Lor	0.3–0.5	0.8–1.2	Fit
					< 0.7	PL	1.4 ± 0.1	2.2 ± 0.1	0.063–10
Rapid Burster									
1730 – 335									
Bursts	?	2	~ 0.1	~ 0.05	~ 30				
Bursts	?	2.2–5.0	0.05–1.0	0.10 ± 0.07	2.6–20.6	PL	> 2	< 1.7–6.2	0.06–1
Pers. Em.	?	2–4	0.03–0.3		< 8–35			< 6–26	0.03–1
Pers. Em.	?	0.4–1							
GX 3 + 1	NB	8 ± 1	8 ± 4	1 ± 0.5	3.5 ± 0.9	PL	1.29 ± 0.03	3.1	0.01–32
1744 – 26					< 2.7	PL	1.22 ± 0.04	2.3	0.01–32
GX 5 – 1	HB	20–36	4.2–12.6	0.21–0.40	4.2–6.5	Exp	0.2–0.4	4.3–6.3	Fit
1758 – 25						PL	1.7		< 0.1
	HB	5.6 ± 0.35	4.8	0.9	1–2				
GX 17 + 2	NB	7.2 ± 0.5	2.2–6.8	0.3–1.0	1.4–2.8	PL	0.7–1.9	1.2–2.7	0.03–64
1813 – 14	HB	23.7–28.1	3.0–6.5	0.12–0.27	1.9–2.7	PL	0.4–0.7	5.9–14.7	0.03–64
	HB[h]	2.4 ± 0.4?	4.3 ± 1.1	1.8 ± 0.5	4				
1820 – 30	NB?	16.1 ± 28.2	13–25	0.47–1.55	5.9–7.8	Lor	22.8 ± 5.2	< 2.6–4.4	0.4–128
	NB?	7.8 ± 0.9	10.9 ± 1.9	1.4 ± 0.3	2				
Cyg X-2	HB	18–55	12–20	0.4 ± 0.2	2.9–5	Exp	0.12–0.16	4.6–6.0	Fit
2142 + 38	NB	5.6 ± 0.2	1–3	0.2–0.5	1.5–3	Exp		0.5–8	0.4–50
	NB	5.6				PL	~ 1.5		
	NB	5.5 ± 0.8	3.7 ± 1.5	~ 0.7	2.5				

[a] 'HB' stands for Horizontal Branch, 'NB' for Normal Branch, 'IF' for Interflaring state, 'FB' for Flaring Branch.
[b] 'Exp' stands for Exponential (Equation (2.31c)), 'PL' for Power Law (Equation (2.31e)), and 'Lor' for Lorentzian (Equation (2.31a)).
[c] The numbers in this column represent the 'slope' of the red noise in the power spectra. We list η for an Exponential fit (see Equation (2.31c)), γ for a Power-Law fit (see Equation (2.31e)), and the width (FWHM), Γ, for a Lorentzian fit (see Equation (2.31a)).
[d] The r.m.s. variation in the red noise was sometimes obtained by direct summation of the excess power (above the Poisson noise level and the QPO signal, if present) over a given frequency range (see column 10), and sometimes from the parameters of the functional fit to the red noise. For detailed information we refer to the original papers.

r.m.s. red noise[d] / r.m.s. QPO	α[f]	Coherent pulsation: Upper limit (%)	Coherent pulsation: Freq. range (Hz)	Coherent pulsation: Confid. level (%)	References
(11)	(12)	(13)	(14)	(15)	(16)
					Tennant (1988a) Tennant (1987b)
0.39 ± 0.07 0.21 ± 0.05 0.24 ± 0.09					Van der Klis *et al.* (1987b)
0.55	-0.52 ± 0.06	0.8	<250	90	Middleditch and Priedhorsky (1986)
1.99		0.5	<125		
0.35	-0.87 ± 0.15 $+3.15 \pm 0.2$				Priedhorsky *et al.* (1986)
0.67		0.5–0.7	0.03–500	99	Van Paradijs *et al.* (1988)
0.85 ± 0.4					Lewin *et al.* (1986)
0.4 ± 0.2 >3					Ponman *et al.* (1988)
					Tawara *et al.* (1982)
0.3 ± 0.2 <0.2	-0.75 ± 0.09				Stella *et al.* (1988a)
0.9 ± 0.2					Lewin *et al.* (1987)
1.04 ± 0.05	~ 2	0.4–0.6 0.6–2.5	50–256 400–2000	99	Van der Klis *et al.* (1985b) Mitsuda *et al.* (1988)
0.9 ± 0.2 2.7 ± 0.5	~ 2 4.0 ± 0.8	0.5 1.9	0.125–256 256–2048	99.9 99.9	Stella *et al.* (1987)
					Langmeier *et al.* (1985) Langmeier (1988)
<0.33–0.75		1.5 2.8	0.25–512 512–2048	99.9	Stella *et al.* (1987b) Mitsuda *et al.* (1988)
1.4 ± 0.5 0.3–2	1.7 ± 0.2	0.3–0.5	<100	90	Hasinger *et al.* (1986) Norris and Wood (1987) Hasinger (1987a) Mitsuda *et al.* (1988)

[e] The word 'Fit' indicates that the r.m.s. variation of the red noise was obtained from the parameters of the red noise fitting function (see column 7).
[f] α expresses the QPO frequency (ν) dependence on the source intensity (I) according to $\nu \propto I^{\alpha}$ (see Section 4.1).
[g] Excess power over a broad frequency range.
[h] Near the transition to the NB.

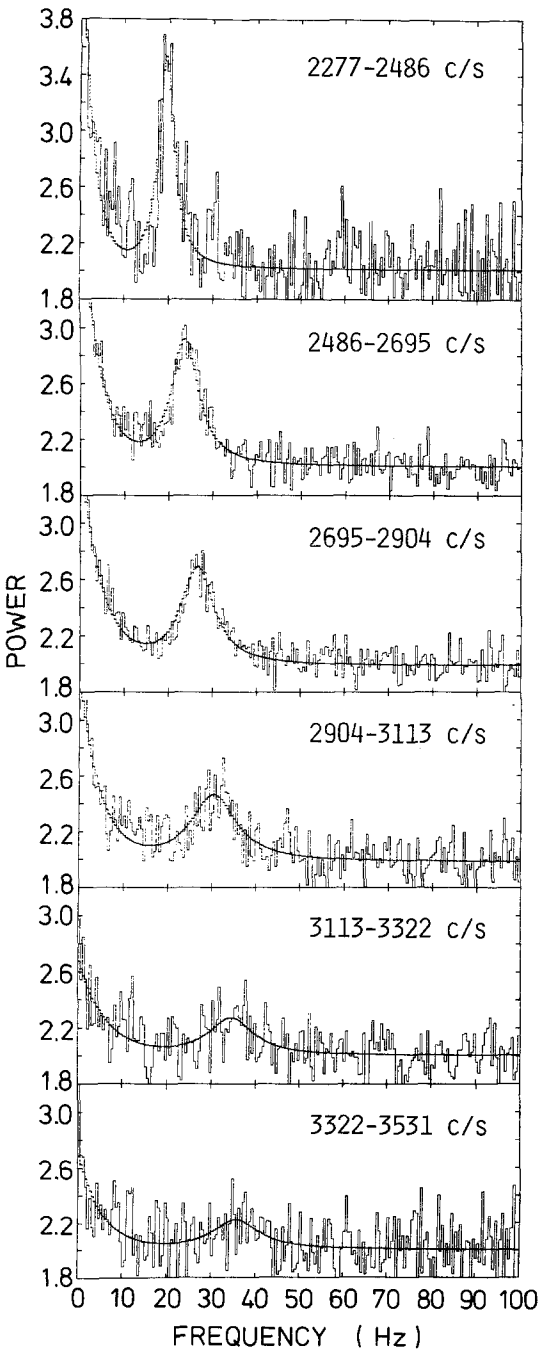

Fig. 3.2. Linear display of average power spectra from GX 5–1 in six different source-intensity intervals. The intensity intervals are indicated in each panel. The lines drawn through the data indicate fits to the data described by a function which is the sum of a constant (Poisson noise), a line with a Lorentzian profile (the QPO peak), and an exponentially rising red noise component (see Section 2.3.3). This figure is from Van der Klis *et al.* (1985b).

without significant changes in spectral hardness ('horizontal-branch'; Shibazaki and Mitsuda, 1984).

EXOSAT observations of GX 5–1, made in September 1984, with a time resolution of 0.25 ms, revealed the presence of intensity-dependent QPO (Van der Klis *et al.*, 1985a, b), whose centroid frequency shifted up and down together with the source intensity, which ranged between ~ 700 and ~ 1100 μJy (see Figures 1.1, 1.2, and 3.2). The power spectrum also showed red noise, detectable above the Poisson noise level up to the QPO frequency. However, no coherent pulsations were seen with a 99% confidence upper limit to the pulsed fraction of 1% in the frequency range 50–400 Hz (the value of 0.3% quoted in Van der Klis *et al.*, 1985b is incorrect). A follow-up EXOSAT observation in April 1985 confirmed the presence of the QPO, and lowered the upper limit to coherent pulsations to 0.4–0.6% (in the range 50–256 Hz; see also Section 1.4).

The centroid frequency and the FWHM of the peak varied between ~ 20 and ~ 36 Hz, and from ~ 4 to ~ 12 Hz, respectively. The centroid frequency, ν, was a linear function of the source intensity, I (Figure 1.2); a power law fit to the function $\nu \propto I^{\alpha}$ (see Section 4.1), also gave a good fit, with $\alpha \sim 2$. The strength of the QPO, expressed as the percentage r.m.s. variation (see Section 2.3.1) ranged between $4.2 \pm 1.0\%$ and $6.5 \pm 0.4\%$. The red noise was well described by an exponential function, but not by a power law (i.e., this is the LFN component); the slope of the red noise, which is represented by the parameter η (see Equation (2.31c)), was also correlated with the source intensity; η varied between 0.2 and 0.4. The r.m.s. percentage variation of the red noise (obtained from the constants in the functional fit to the shape of the power spectrum, see Equation (2.31c)) varied between 4.3 ± 0.4 and $6.3 \pm 0.2\%$. The variations of the strenght of the QPO and of the red noise went hand in hand (see Figure 3.3); their ratio was constant to within the accuracy of its determination.

Analysis of archival *Einstein* Observatory MPC data confirmed the presence of QPO and red noise in the flux variations of GX 5–1 during one of several observations (Elsner *et al.*, 1986). The source intensity was then ~ 500 μJy. The QPO had a centroid frequency of 15.8 Hz; the r.m.s. percentage variations in the QPO and the red noise (as obtained from the parameters in a fit to the data of a modulated shot model) were both roughly 7%. During the other observations the sensitivity of the QPO search was insufficient to detect QPO and red noise at these levels. No coherent pulsations were detected (2σ upper limit to the amplitude of $\sim 4\%$, in the frequency range 2.4–4000 Hz).

A search for QPO and coherent pulsations in the soft (0.2–2.0 keV) X-ray flux of GX 5–1 using archival *Einstein* Observatory *HRI* data was made by Mereghetti and Grindlay (1987). No evidence was found for a broad peak in the power density spectrum (95% confidence limit of $\sim 10\%$), neither were coherent pulsations detected (2σ upper limits to the pulsation amplitude of ~ 20 to $\sim 30\%$).

EXOSAT observations, following the discovery of QPO in GX 5–1, and analysis of already existing archival EXOSAT data show that the properties of the QPO and the red noise of GX 5–1 are strongly correlated with the bi-modal spectral behaviour of the source (Van der Klis *et al.*, 1987a). One of the spectral states is characterized by an

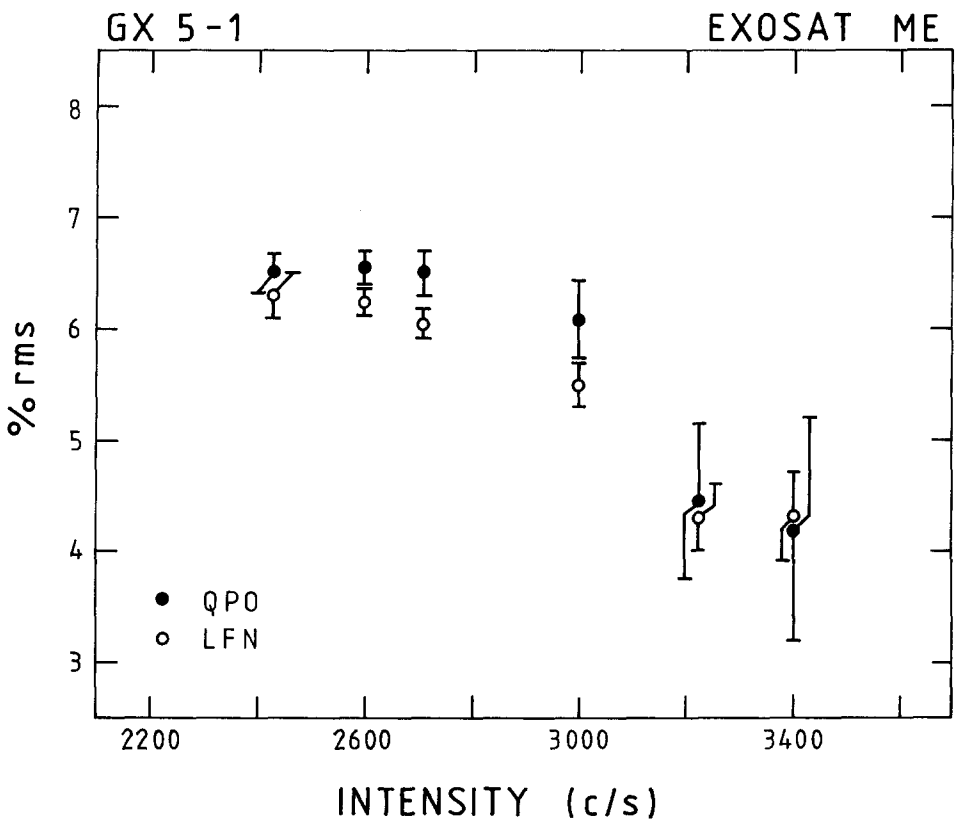

Fig. 3.3. The excess power (in terms of r.m.s. variation; see Section 2.3.1) of the QPO (dots) and of the red noise (circles) versus the intensity of GX 5–1. Notice that the two go hand in hand. This figure is from Van der Klis *et al.* (1986a).

approximately linear correlation between the hardness of the X-ray spectrum and the source intensity (the 'normal branch' in a spectral hardness-intensity diagram; occasionally confusion may arise with the 'flaring branch', see Section 1.5). This spectral behaviour has been observed in many LMXB (see Section 1). In the other spectral state the X-ray spectrum is relatively hard, and its hardness varies little with source intensity; in the spectral hardness-intensity diagram the source is then represented by a point on the 'horizontal branch' (see Branduardi *et al.*, 1980; Shibazaki and Mitsuda, 1984). During all four of the seven EXOSAT observations that GX 5–1 was in the horizontal branch (HB) spectral state it showed the 20–40 Hz QPO, and the associated LFN (visible below ~ 60 Hz). During the other three observations, when GX 5–1 was in the normal branch (NB) state, no QPO between 6 and 60 Hz were detected, neither was red noise above 1 Hz (see Figure 3.4). There was, however, an indication for weak QPO near 5 Hz (the presence of QPO with a frequency of 5.5 ± 0.3 Hz has recently been confirmed by *Ginga* observations, Mitsuda *et al.*, 1988). A comparison of two typical power density spectra, obtained during the two spectral states, is shown in Figure 3.5.

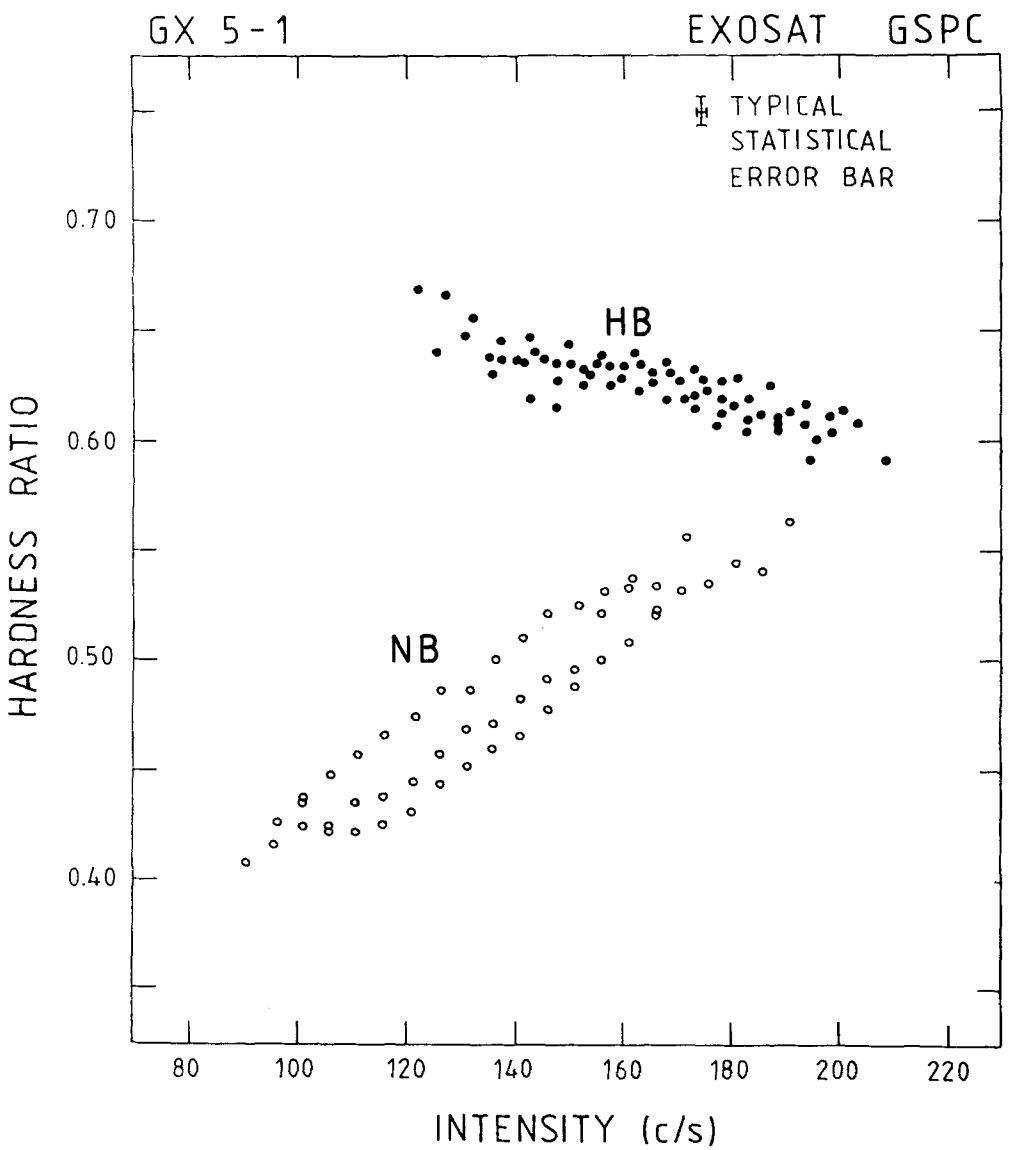

Fig. 3.4. Spectral hardness (ratio of the 6–10 and 3–6 keV count rate) versus intensity (3–10 keV) diagram for some GX 5–1 data from the EXOSAT GSPC detectors (see Section 3.1). The solid dots in the 'horizontal branch' (HB) represent data when strong ~ 20–40 Hz QPO were observed; the power spectra from the data represented by the open circles on the 'normal branch' (NB) showed no significant QPO (see Figure 3.5). This figure is from Van der Klis *et al.* (1987a).

Apart from the lack of the QPO in the NB power spectrum, the absence of red noise in the frequency range between ~0.1 and 10 Hz is striking. In both power density spectra a break occurs between 0.03 and 0.3 Hz, below which frequency the power rises rapidly. This 'very low frequency noise' (VLFN) below ~0.1 Hz can be represented by a power law with exponent $\gamma = 1.7$ (see Equation (2.31e)). The dependence of the

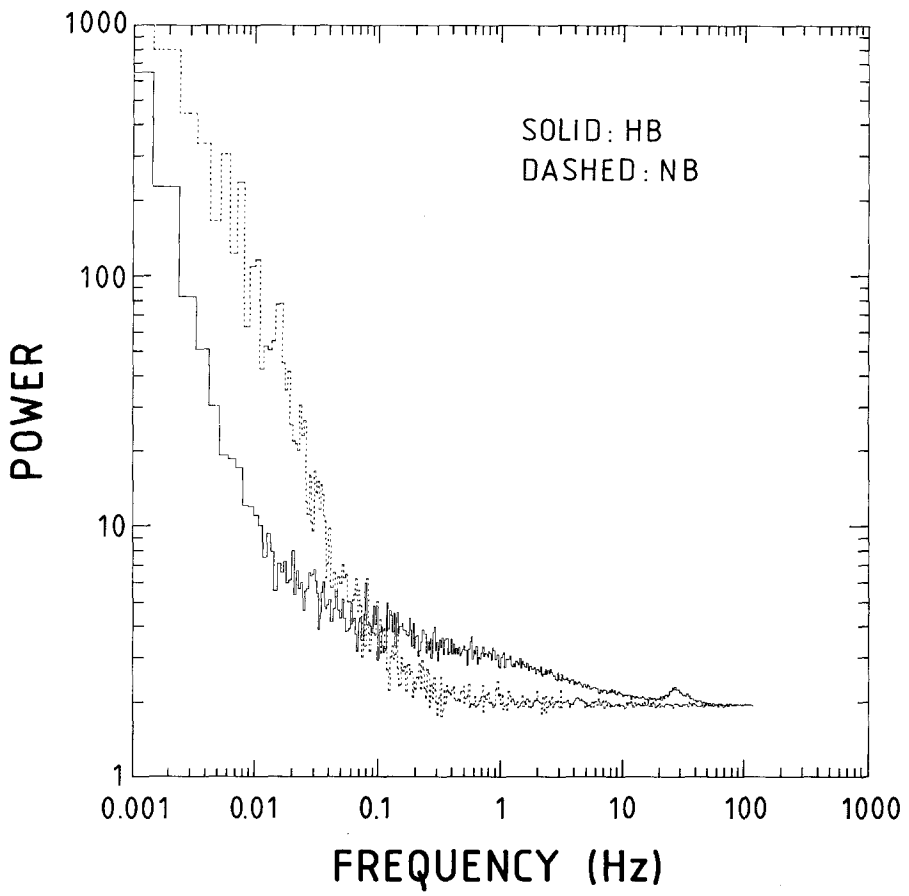

Fig. 3.5. Power spectra of GX 5–1 data when the source was in the 'horizontal branch' (HB; solid lines), and in 'normal branch' (NB; dashed lines) state. Notice that the HB data show (i) the QPO peak (near ~ 30 Hz), (ii) a low-frequency noise (LFN) component (below ~ 10 Hz), and (iii) a very low-frequency noise (VLFN) component (below ~ 0.1 Hz). No QPO peak, and no LFN component are present in the NB data, but a VLFN component is clearly visible below ~ 0.3 Hz (see Section 3.3.1). This figure is from Van der Klis *et al.* (1987a).

strength of this VLFN on source intensity is very different from that of the strength of the QPO and the red noise (see Figure 3.6). Whereas the latter decrease with increasing source intensity by more than a factor 2.5, the fractional strength of the VLFN (in both the NB and the HB spectral state) remains approximately constant.

Observations (in 4 channels) of GX 5–1, carried out in September 1985, showed that the strength of the 20–40 Hz QPO (GX 5–1 was then in the HB state) increases strongly with X-ray energy (Van der Klis 1986a; see Figure 3.7). The strength of the LFN changed with X-ray energy in a remarkably similar way. The strength of the VLFN, however, showed no significant energy dependence.

A cross-correlation analysis of 12.5 h of EXOSAT data on GX 5–1 showed that the high-energy X-rays (6–16 keV) lagged the low-energy (1–6 keV) ones (Van der Klis,

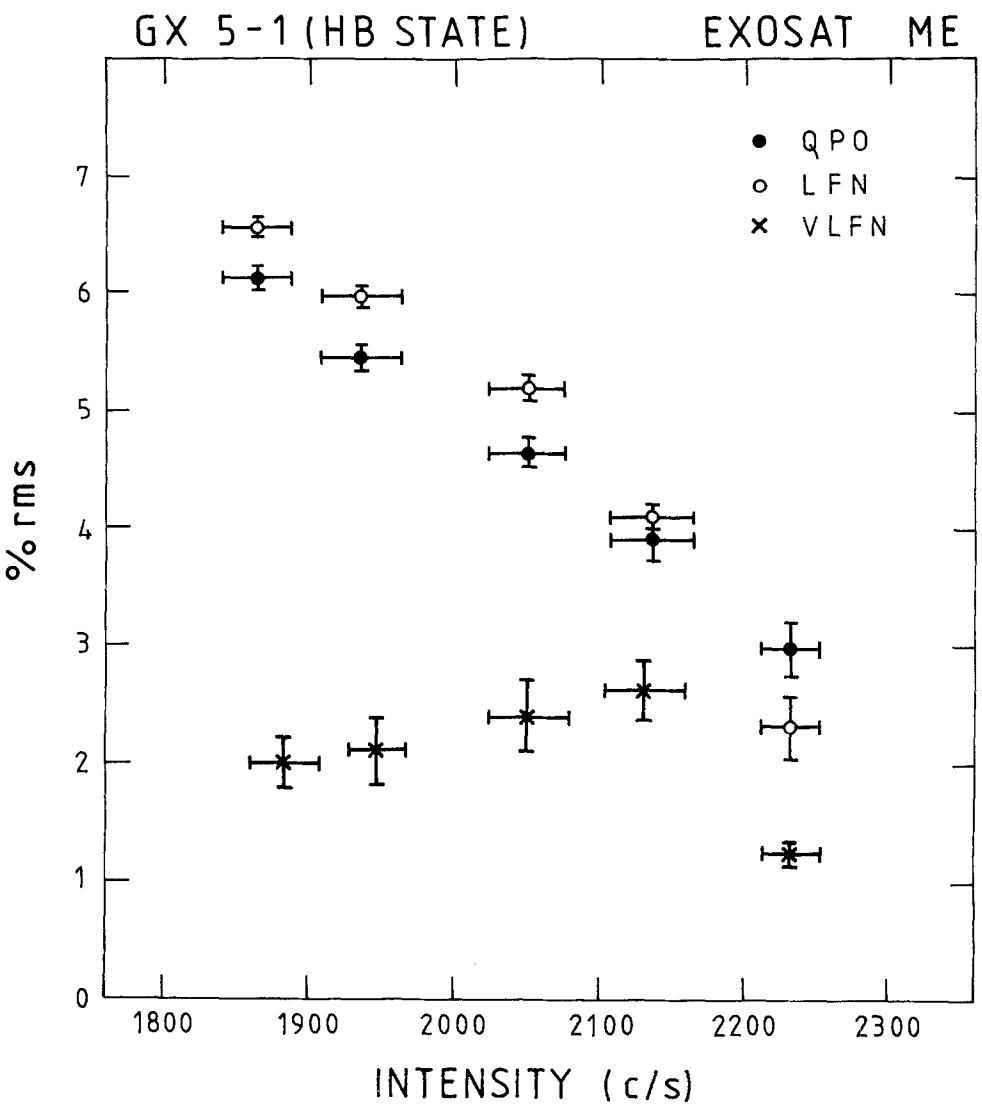

Fig. 3.6. The 'strength' in terms of the fractional r.m.s. variation (in %) of the ~20–40 Hz QPO (solid dots), the LFN (open circles), and the VLFN (crosses) components in GX 5–1 as a function of source intensity (not corrected for deadtime) when the source was in the HB state (EXOSAT ME data; see Section 3.1). The strength of the QPO and the LFN depend strongly on the source intensity, and they track each other fairly well (see also Figure 3.3). There is no obvious relation between the strength of the VLFN (which varies between ~1.5 and ~2.5%) and the source intensity. The data in this figure were obtained during a different observation with different dead-time and from a different energy channel than those in Figure 3.3. This figure is from Van der Klis *et al.* (1987a).

1986b). A subsequent cross-spectral analysis of the same data (Van der Klis *et al.*, 1987c; Van der Klis, 1988) showed that below ~10 Hz (LFN) the low-energy X-rays lag the high-energy ones, whereas in the frequency range where the QPO occur, the opposite is the case. The average values of the time lags in the LFN frequency range,

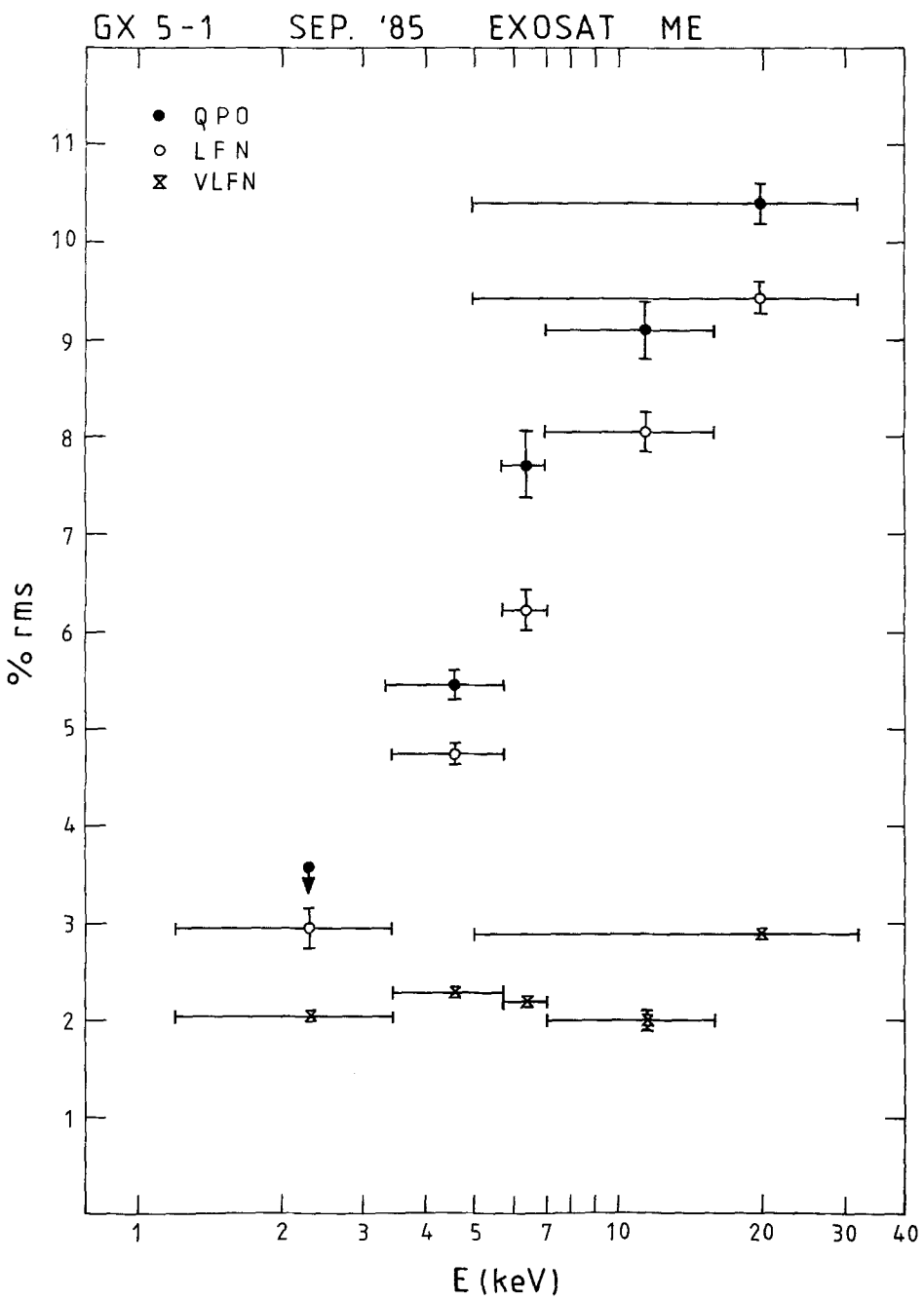

Fig. 3.7. The 'strength' in terms of the fractional r.m.s. variation (in %) of the ~20–40 Hz QPO (solid dots), the LFN (open circles), and the VLFN (crosses) components in GX 5–1 as a function of X-ray energy when the source was in the HB state (EXOSAT ME data; see Section 3.1). The strength of the QPO and that of the LFN increases (from ~3 to ~10%) between X-ray energies of ~2 and ~20 keV; the strength of the VLFN component (~2–3%) shows no energy dependence. This figure is from Van der Klis (1986a).

and in the QPO frequency range, are 2.3 ± 0.7 ms (soft lag) and 0.44 ± 0.17 ms (hard lag), respectively (see also Section 5). Mitsuda *et al.* (1988) have recently reported a hard lag of 80 ± 30 ms based on a CCF analysis of *Ginga* data.

3.3.2. *Cyg X-2 (4U 2142 + 38)*

Cyg X-2 may have been detected (Giacconi *et al.*, 1967a) during the very first X-ray observation, in which Sco X-1 was discovered (Giacconi *et al.*, 1962). Spectroscopic studies of the optical counterpart (Giacconi *et al.*, 1967b; Kristian *et al.*, 1967) led to early suggestions (Lynds, 1967; see, however, Kraft and Miller, 1967) that Cyg X-2 is a binary system, analogous to cataclysmic variables, and indicated that it is a member of the galactic halo population (Burbidge *et al.*, 1967). From a detailed study of the optical radial velocity variations Cowley *et al.* (1979) found that the orbital period of Cyg X-2 is 9.8 days, and that the system is indeed a halo object, at a distance of ~ 8 kpc. Initial reports of coherent X-ray variability at this period (Marshall and Watson, 1979; Ilovaisky *et al.*, 1979) have not been confirmed in other observations (e.g., Holt *et al.*, 1979). On rare occasions Cyg X-2 shows flaring events which may (or may not) be type 1 X-ray bursts (Kahn and Grindlay, 1984). Cyg X-2 has been detected as a radio source (Hjellming and Blankenship, 1973).

From *Copernicus* observations of Cyg X-2 Branduardi *et al.* (1980) found the first evidence for a horizontal-branch spectral state of LMXB, in addition to the well-known state in which the spectral hardness is positively correlated with intensity (normal branch). Based on this result it was suggested that Cyg X-2 is an accreting white dwarf (Branduardi *et al.*, 1980); its luminosity should then be at most a few times 10^{36} erg s^{-1}, and its distance smaller than 300 pc. An accurate distance determination, based on a study of the relation between reddening and distance, allowed McClintock *et al.* (1984) to reject this model.

QPO were first detected from Cyg X-2 in July 1984 during a 14-h EXOSAT observation at 7.8 ms time resolution in one energy channel (Hasinger *et al.*, 1985, 1986). The power spectra, made separately for four intensity-selected data sets showed LFN below ~ 15 Hz, and a broad QPO peak with centroid frequency shifting from 28.3 ± 0.6 to 45.3 ± 2.0 Hz as the source intensity increased. The FWHM of the peak was possibly variable (6–10 Hz), reaching a maximum at intermediate intensities. The LFN was fit with an exponential function (see Equation (2.31c)); the *e*-folding frequency (average value 7.1 ± 0.4 Hz) did not change significantly with source intensity. The r.m.s. fractional variation of the QPO (average value $4.2 \pm 0.5\%$) did not vary significantly, whereas that in the LFN increased gradually from 4.6 ± 0.2 to $6.0 \pm 0.8\%$ over the observed intensity range. No coherent pulsations were detected (1% upper limit in the 4–20 ms period range). The relation between QPO frequency and source intensity could be described as a power law with exponent $\alpha = 1.7 \pm 0.2$ (see Section 4.1), similar to the value (~ 2) found for GX 5–1 by Van der Klis *et al.* (1985a) (see Section 3.3.1). From a decomposition of the X-ray spectrum into a black-body and a thermal component Hasinger *et al.* (1986) found for the black-body flux a corresponding value of $\alpha = 0.56 \pm 0.06$, i.e., close to the value of $\frac{3}{7}$ expected for gas-pressure dominated

magnetospheric Kepler frequencies (Bath, 1973; Section 4.1; see White and Stella, 1988, for radiation dominated cases). Subsequent EXOSAT observations showed that the QPO frequency correlates better with the flux in this black-body component than with the total flux (Hasinger, 1987a; this was also observed in Sco X-1, see Van der Klis *et al.*, 1987b). To put this result in perspective it should, however, be noted that the interpretation of the X-ray spectra of LMXB in terms of two-component models is highly uncertain at present (see Section 5.2 for a brief discussion of this topic, and references).

Subsequent analysis of five EXOSAT observations in September, 1983 showed the presence of QPO during one of them, with centroid frequency 28 ± 0.4 Hz, FWHM 2.7 ± 0.5 Hz, and $2.7 \pm 0.2\%$ r.m.s. variation (Chiappetti *et al.*, 1986; Stella *et al.*, 1986). These data also suggest a possible second peak in the power spectrum at 60 ± 3 Hz, which could be the second harmonic of the 28.3 Hz peak. A second peak in a power spectrum of Cyg X-2, at a frequency ratio 1.85 ± 0.03, has also been reported by Hasinger (1987a).

From an analysis of 8 hours of archival HEAO-1 data at 5 ms resolution, Norris and Wood (1987) found intermittent QPO at a stationary frequency of 5.6 Hz; any frequency variations were less than 4%, and not correlated with source intensity. The FWHM of the QPO peak varied between ~ 1 and ~ 3 Hz, unrelated to the QPO frequency. The strength of the red noise varied substantially (at times it could be seen up to ~ 40 Hz; at other times it was almost undetectable), without an obvious relation to the QPO properties. The r.m.s. variations in the QPO and the red noise ranged between 1 and 3%, and between ~ 1 and $\sim 8\%$, respectively. Using an inter-calibration of the HEAO-1 and EXOSAT data Norris and Wood (1987) concluded that these 5.6 Hz QPO did not follow the relation between QPO frequency and source intensity found earlier by Hasinger *et al.* (1986). No coherent pulsations were detected in the HEAO-1 data (90% confidence limit of 0.3%); however, Norris and Wood found evidence in the power spectrum for a broad feature near 52 Hz, which they suggest may be a frequency-broadened pulsar signal. [Hasinger (1987b) pointed out that possibly during part of these observations Cyg X-2 was on the horizontal branch in the hardness-intensity diagram, which could explain the high-frequency QPO.] Norris and Wood (1987) conclude that these 5.6 Hz QPO represent a distinct phenomenon from the higher-frequency QPO found by Hasinger *et al.* (1986; see above).

Elsner *et al.* (1986) found low-frequency structure in a power spectrum obtained from 50 min of archival *Einstein* Observatory data which, however, they could not identify unambiguously as either QPO or red noise. Interpreting this structure as QPO they found a centroid frequency of 9.2 ($+3.6$, -4.2 Hz).

Subsequent EXOSAT observations (Hasinger, 1987a; Hasinger *et al.*, 1988) showed that the 5.6 Hz QPO found by Norris and Wood (1987) is a stable feature, which is always, and only, present when Cyg X-2 is in the intermediate part of the normal branch in the spectral hardness vs intensity diagram (see Figure 3.8). In all cases that it was observed, its frequency was consistent with a value of 5.6 Hz. This stability in frequency, over a time-scale of years, in spite of the rapid variations in its occurrence (related to

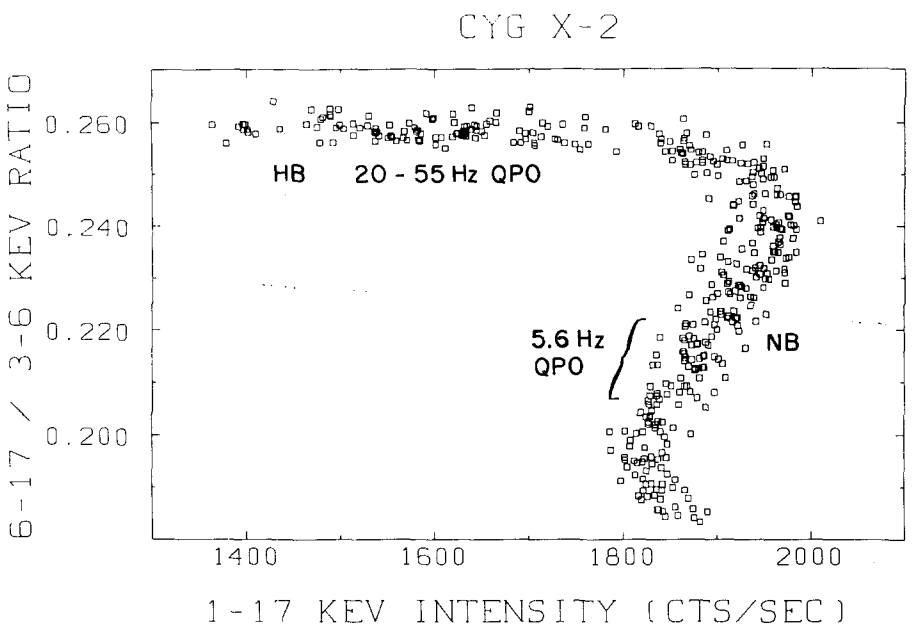

Fig. 3.8. Spectral hardness (ratio of 6–17 and 3–6 keV count rates) versus source intensity (1–17 keV countrate) diagram for EXOSAT data from Cyg X-2. Each point represents a 200 s observation. The figure illustrates globally when $\sim$ 20–55 Hz QPO, when $\sim$ 6 Hz, and when no QPO are observed. Notice that the high-frequency QPO are only observed in the horizontal branch (HB) state, and that the 6-Hz QPO are exclusively observed in the normal branch (NB) state, but only when the spectral hardness ratio is within certain limits. The 6-Hz QPO has a maximum strength when the spectral hardness is near the middle of the NB, and it is only observed over an $\sim\frac{1}{3}$ range (FWHM) of the NB (Hasinger, private communication; see bracket). The NB data in this figure are from two different observations; the two normal branches happen to precisely overlap (there is another NB observation, not shown here, which does not overlap with these data). This figure is adapted from Hasinger *et al.* (1986).

spectral hardness), is a very striking feature of these normal-branch QPO. The 5.6 Hz QPO in Cyg X-2 have a relatively soft X-ray spectrum. Their r.m.s. variations are typically $\sim$4% near 1 keV, and drop below 2.3% above 4.5 keV; for the horizontal-branch QPO typical numbers are $\sim$4% at 1 keV, and $\sim$10% at 10 keV (Hasinger, 1987a). Cyg X-2 also exhibits a 'flaring branch', like Sco X-1 (see Figure 1.4).

Hasinger (1987b) showed that also the red noise behaviour of Cyg X-2 is strongly correlated with the spectral state, in the same way as was found for GX 5–1 (Van der Klis *et al.*, 1987a). This is illustrated in Figure 3.9, which shows typical power spectra for Cyg X-2, during a horizontal-branch and a normal-branch state. When Cyg X-2 is in the normal branch the red noise is relatively weak, and can be described by a power law (see Equation (2.31e)) which extends to very low frequencies (exponent $\gamma \sim 1.5$). When Cyg X-2 is on the horizontal branch this power-law component is also present, but in addition there is a component, which extends to $\sim$ 50 Hz, and can be represented by a power law with exponent $\gamma \sim 0.3$ and a exponential high-frequency cut off (see

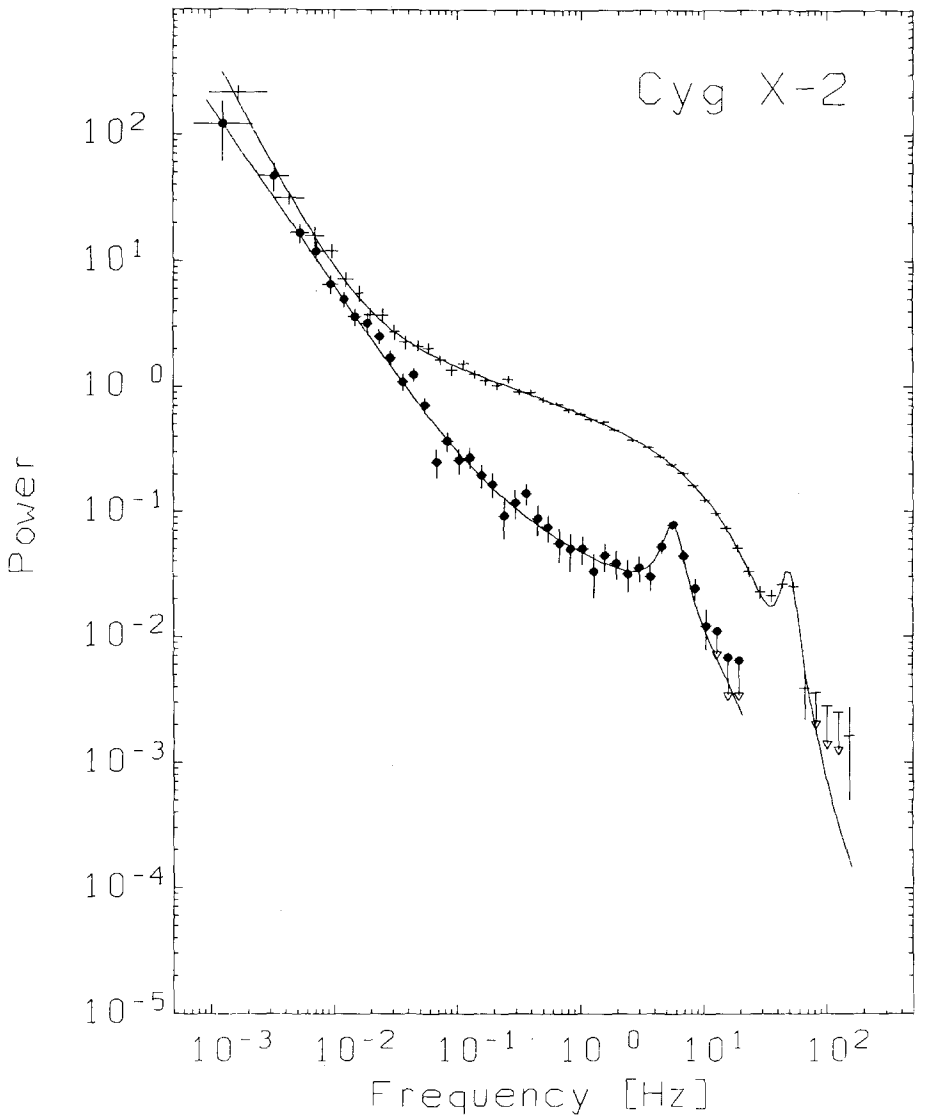

Fig. 3.9. Power spectra of Cyg X-2 (EXOSAT data). The upper curve is from horizontal-branch (HB) data, the lower from normal-branch (NB) data. The constant Poisson white-noise level has been subtracted. Notice the high-frequency QPO (near ~ 40 Hz), the LFN, and the VLFN component in the HB data. In the NB data ~ 6-Hz QPO is present, and a VLFN component, but no LFN component (see also Figure 3.5). This figure is from Hasinger (1987b).

Equation (2.31d)). The strength of this component (which can be identified with the LFN component), increases strongly with photon energy, as is the case for the corresponding high-frequency QPO. The $\gamma \sim 1.5$ power-law component can be identified with the VLFN component which is always present in the power spectrum of GX 5–1 (see Section 3.3.1).

From a cross-correlation analysis of energy-resolved high-time resolution EXOSAT data of Cyg X-2 Hasinger (1987a) found the first evidence in LMXB for delays (of order milliseconds) of high-energy photons, as compared to low-energy photons (see Figure 3.10). For the horizontal branch data this 'hard' time lag is anti-correlated with

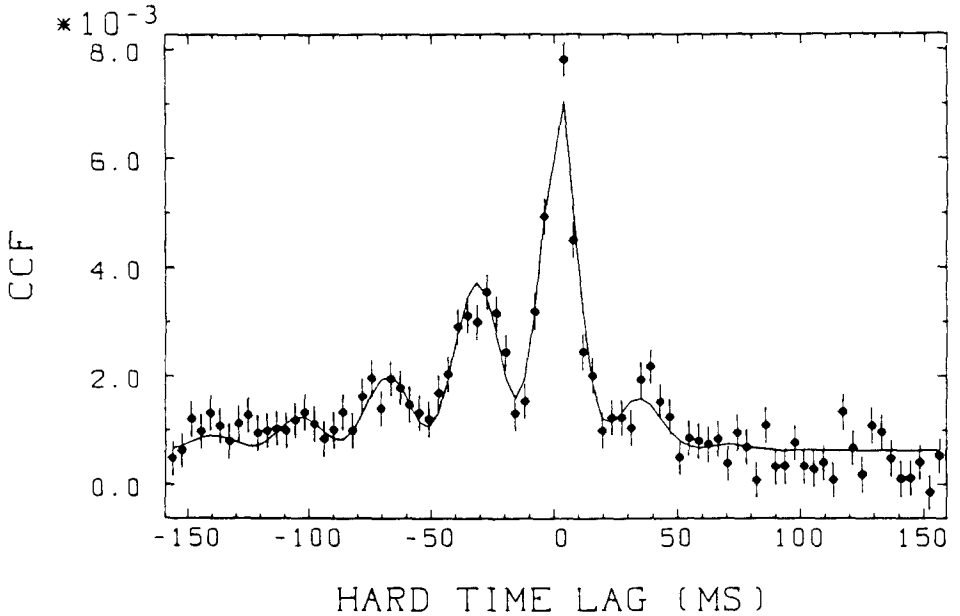

Fig. 3.10. Cross-correlation function (CCF) between high-energy (4.5–17 keV) and low-energy (1–4.5 keV) EXOSAT data from Cyg X-2 in the HB state. The data points are separated by 3.91 ms. The CCF shows sinusoidal ondulations which are due to the QPO. The CCF is asymmetric, indicating that the rapid fluctuations are different in the 2 energy channels. The asymmetry near-zero time lag indicates that the high-energy photons are delayed (the 'hard' time lag is positive) relative to the low-energy ones by several milliseconds. This figure is from Hasinger (1987a).

the QPO frequency. Hasinger (1987a) suggested that these delays are the result of Comptonization of photons in a cloud of high-energy electrons around the neutron star (see Section 5 for a discussion of this model). From an analysis of these data with a Fourier cross-spectral technique (see Section 2.4) it was found (see Figures 3.11 and 3.12) that the delay of the high-energy photons is caused by variations in the QPO frequency range (Van der Klis *et al.*, 1987c). In the frequency range of the LFN the sign of the time-delay is opposite; here the low-energy photons are lagging the high-energy photons. The average time lag in the QPO frequency range, which varies between ~ 4 ms and < 1 ms, is anti-correlated with the QPO centroid frequency (see Figure 3.13), confirming Hasinger's (1987a) above-mentioned result.

Observations made with *Ginga* found time lags in Cyg X-2 data up to ~ 70 ms (see Figure 3.14 and Section 5.1; Mitsuda *et al.*, 1988).

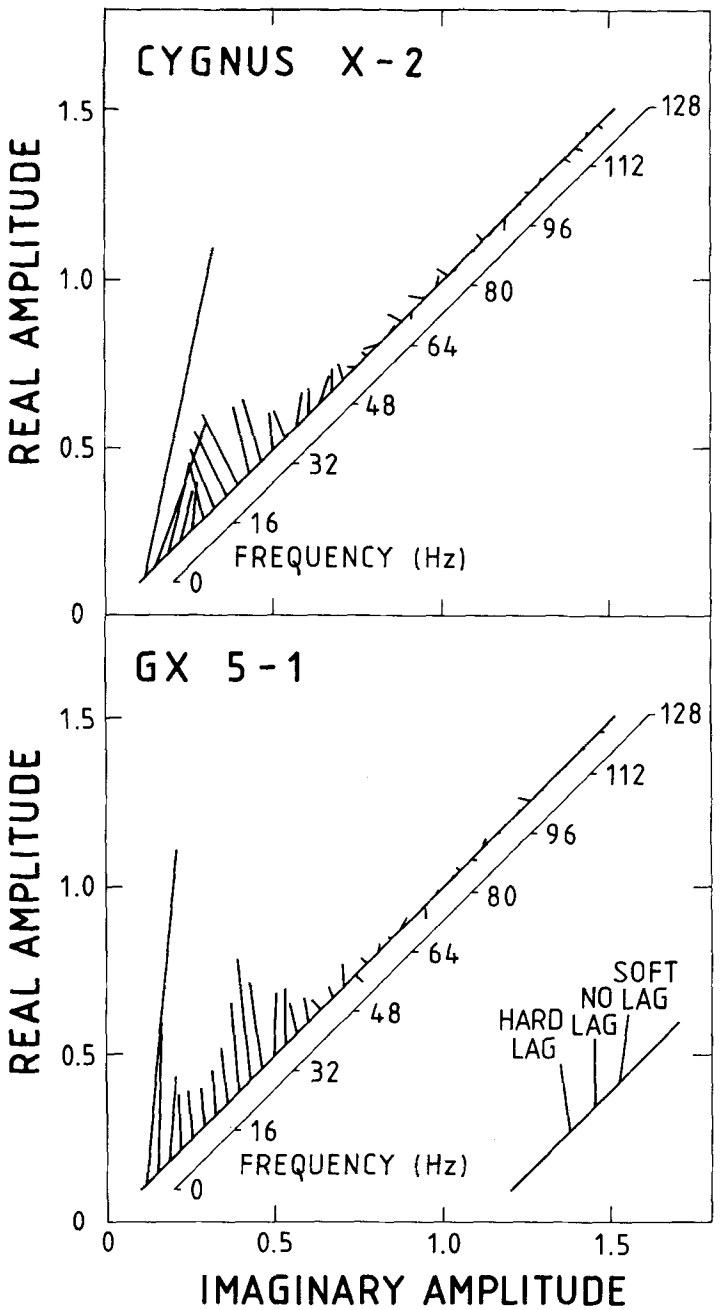

Fig. 3.11. Time-averaged complex cross-spectra of the intensity variations in Cyg X-2 (*upper panel*) and GX 5–1 (*lower panel*), when they were in the HB state (for details on cross-spectra see Section 2.4). The long diagonal line is the frequency axis; the short lines, indicated every 3.125 Hz along the frequency axis are vectors that represent the complex Fourier amplitudes. Vectors leaning towards the left with respect to the vertical axis indicate a 'hard' time lag (i.e., the high-energy photons of ~ 5–18 keV are delayed relative to the low-energy ones of ~ 1–5 keV); those leaning towards the right indicate a 'soft' lag. Hard lags are observed in the QPO (most notably in Cyg X-2 near ~ 15–20 Hz), and soft lags in the red noise (the LFN component). This figure is from Van der Klis *et al.* (1987c).

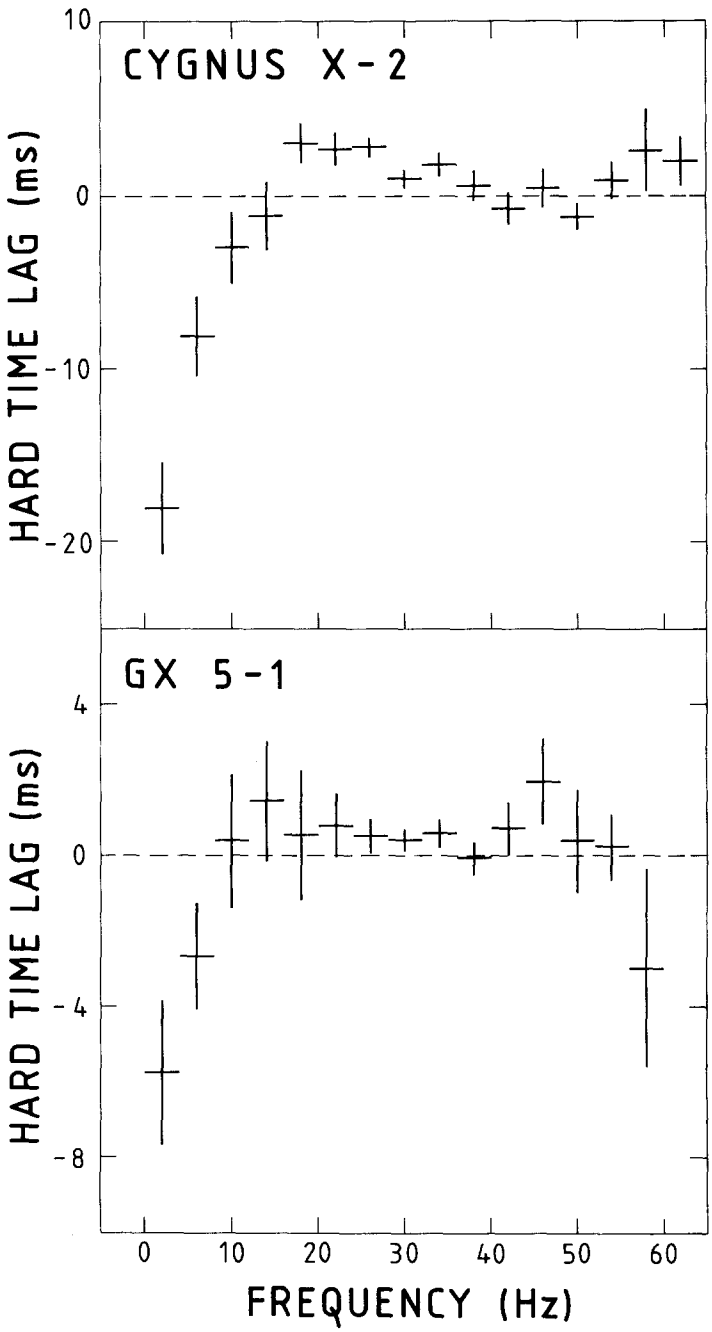

Fig. 3.12. Hard time lags for Cyg X-2 (*upper panel*), and GX 5–1 (*lower panel*) as a function of frequency; negative 'hard' time lags are 'soft' lags (for details see the caption of Figure 3.11). Soft lags occur in the red noise (LFN component) range below ~ 10 Hz; hard lags (up to several milliseconds) are observed in the QPO frequency range. This figure is from Van der Klis *et al.* (1987c).

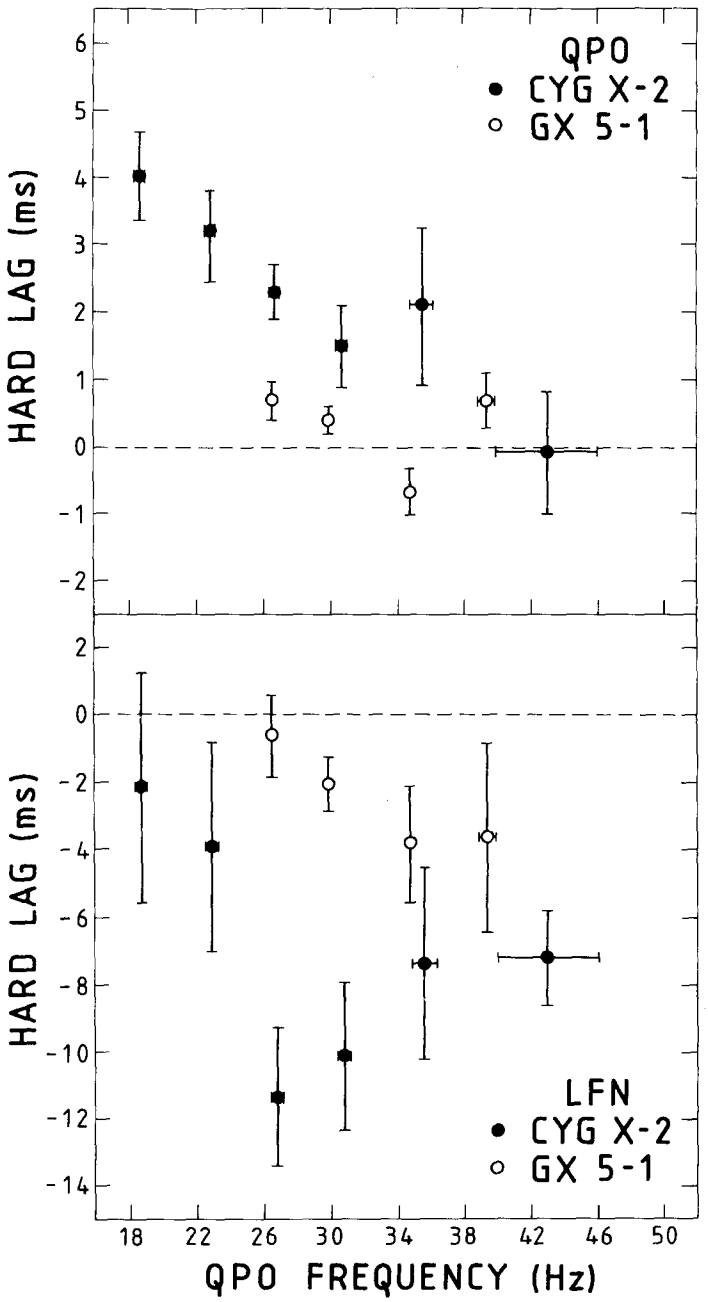

Fig. 3.13. Dependence of the hard time lags for Cyg X-2 (solid dots) and GX 5–1 (open circles) in the HB state on QPO frequency (for details see the caption of Figures 3.11 and 3.12). The time lag in the LFN component (*lower panel*) was measured between 1 and 10 Hz; that for the QPO (*upper panel*) in a frequency interval around the center of the peak with a width equal to the FWHM of the peak. The horizontal and vertical bars represent 1-σ errors. For Cyg X-2, the hard time lag decreases with increasing QPO frequency. All hard time lags at frequencies in the LFN domain are negative, independent of the frequency of the QPO. This figure is from Van der Klis *et al.* (1987c).

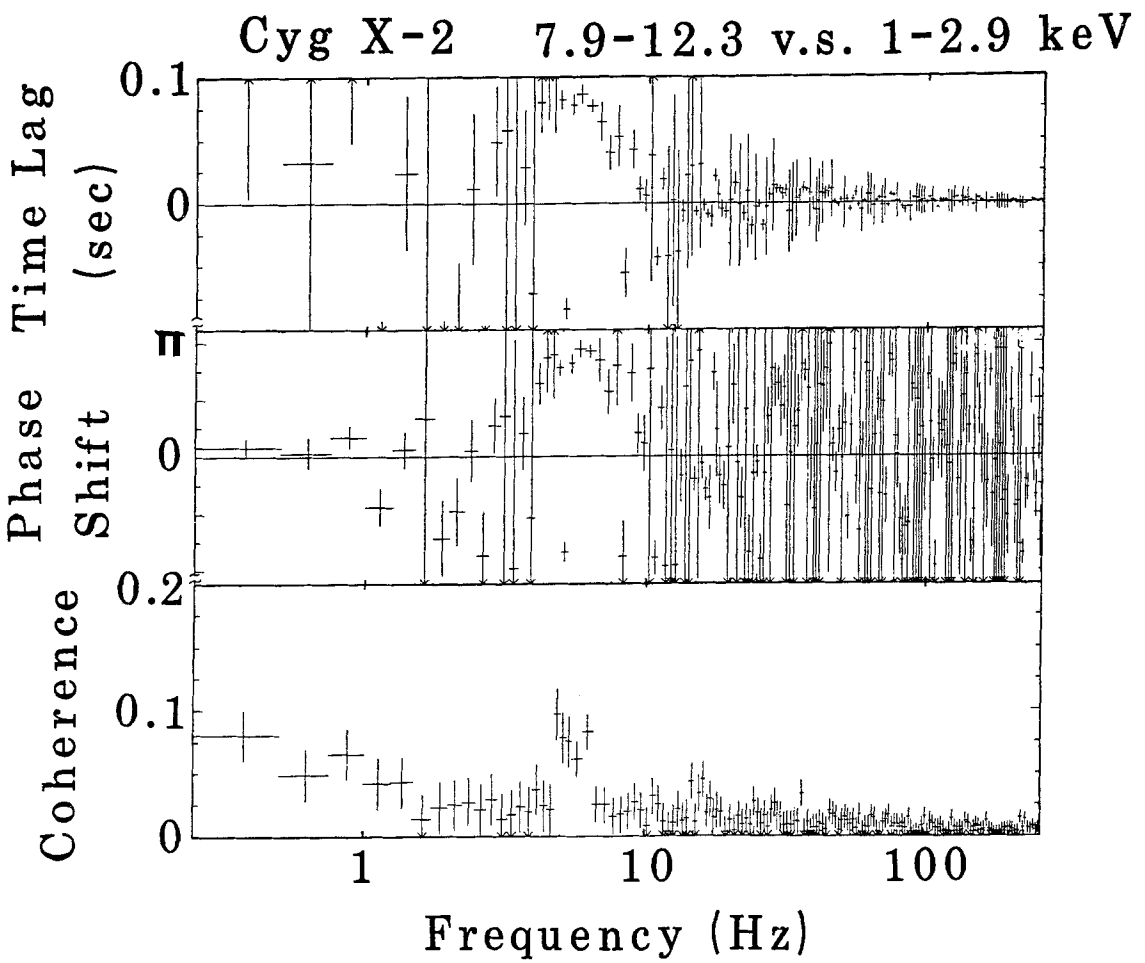

Fig. 3.14. Cross-spectrum (for some details on cross-spectra see Section 2.4, and the caption of Figure 3.11) for *Ginga* data from Cyg X-2 in the normal branch (~6 Hz QPO) between 7.9–12.3 and 1–2.9 keV energy bands. Zero-time lag is defined for the energy band 1–2.9 keV. The upper panel shows the time lags in seconds. Notice that in the frequency domain near ~5.5 Hz 'hard' lags up to ~80 ms are observed. The time lag has a systematic uncertainty of $\pm n$ oscillations (n is an integer). Thus, the negative time lag of ~75 ms near 6 Hz (~170 ms) can also be a positive lag of ~95 ms (similarly, the ~50 ms negative lag at ~7 Hz can be a positive lag of ~90 ms). The middle panel shows the phase shifts in radians defined as the time lag ($\times 2\pi$) multiplied by the Fourier frequency. The systematic uncertainty is $\pm n \times 2\pi$ radians (n is an integer). The bottom panel indicates the coherence of the oscillations. This figure is from Mitsuda *et al.* (1988).

3.3.3. *Sco X-1 (4U 1617 – 15)*

Sco X-1, the first cosmic (non-solar) X-ray source, discovered by Giacconi *et al.* (1962), was optically identified with a ~13th mag blue emission-line star (Sandage *et al.*, 1966). The orbital period of Sco X-1, as inferred from optical archival-plate photometry (Gottlieb *et al.*, 1975), and spectroscopy (Cowley and Crampton, 1975; Crampton *et al.*, 1976; LaSala and Thorstensen, 1985) is 0.787 days. The secondary star has most

probably evolved off the Main Sequence (Cowley and Crampton, 1975). Sco X-1 is a radio source with a triple morphology; one variable (core) component coincides with the X-ray binary, and two radio lobes are at opposite positions $\sim 1'$ from the core (Hjellming and Wade, 1971a; Geldzahler and Fomalont, 1986).

The X-ray behaviour of Sco X-1 is irregular. It was the first source in which X-ray flaring (time-scale of ~ 30 min) was discovered (Lewin *et al.*, 1968). Later observations showed that the X-ray flux of Sco X-1 exhibits a very complex behaviour (for a review of X-ray observations up to 1977, see Miyamoto and Matsuoka, 1977). Except for a possible 341 Hz pulsation recently reported by Leahy (1987), but not confirmed by Hasinger and Van der Klis (1987) in a much larger data set, no periodicity has been found in the X-ray flux variations, neither at the orbital period (cf. Holt *et al.*, 1976; Holt, 1987) nor at high frequencies (Friedman *et al.*, 1969; Boldt *et al.*, 1971). Sco X-1 shows active and quiescent states with a duration between ~ 1 and ~ 5 days (Bradt *et al.*, 1975; Canizares *et al.*, 1975). During the quiescent state the X-ray flux varies on a time-scale of about half a day. During active states brightness variations of up to a factor 3 occur on time-scales of seconds to minutes (see, e.g., Petro *et al.*, 1981). A positive correlation between the source intensity and the hardness of the spectrum has been observed (White *et al.*, 1976a). Such a correlation has at times been referred to as 'Sco X-1 behaviour' (e.g., White *et al.*, 1980), and the observation of this behaviour in other X-ray sources (in particular bursters; White *et al.*, 1980) was one of the arguments that led to the identification of the class of low-mass X-ray binaries.

The optical brightness of Sco X-1 also varies on time-scales ranging between a few seconds to days (Bradt *et al.*, 1975; Canizares *et al.*, 1975; Petro *et al.*, 1981). The relation between the optical and X-ray emission of Sco X-1 appears to have a bimodal character. X-ray active states, with optical flaring and flickering only occurring when the source is optically bright ($B < 12.7$). The X-ray and optical brightness variations are then often correlated in a way similar to that observed in other optically identified LMXB, which suggests that at least part of the optical emission is due to reprocessing of X-rays in the accretion disk (see Van Paradijs, 1983, and references therein). However, X-ray flares have been observed without optical flares, and *vice versa* (Canizares *et al.*, 1975; Ilovaisky *et al.*, 1980). During the X-ray quiescent state the optical brightness can change by ~ 0.5 mag without detectable variations in the X-ray flux.

QPO with properties that appeared rather different from those observed from GX 5–1 (see Section 3.2.1) and Cyg X-2 (see Section 3.2.2), were discovered in Sco X-1 by Middleditch and Priedhorsky (1985, 1986) during an ~ 9 hr EXOSAT observation in February 1985. During the second half of this observation, when the source was in a quiescent state (no flares) the power spectrum showed a strong QPO peak at ~ 6 Hz with FWHM ~ 1 Hz; this was not seen in the first half of the observation when the source was flaring.

An analysis of earlier EXOSAT observations (Van der Klis *et al.*, 1985c; see also Van der Klis and Jansen, 1986) confirmed the presence of QPO in Sco X-1, but the QPO properties were quite different from those seen by Middleditch and Priedhorsky (1985).

When Sco X-1 was in the active state, 10–17 Hz QPO were seen during ~20 min intensity dips between flaring episodes; the frequency of these QPO was strongly correlated with source intensity, a 13% increase in intensity corresponding to a 70% increase in frequency. During the transition from the active to the quiescent state, the QPO frequency varied from 7 to 11 Hz, without an obvious correlation with intensity (see Figure 3.15). The power spectrum showed red noise, which was strongest during periods of flaring, when the QPO were absent, and contained much less power than the QPO when these were present.

A further analysis of the February 1985 data (Middleditch and Priedhorsky, 1986) showed that during the first half of this observation, when the source was in a active state, with >25% flares on time-scales of 1–10 min, the power spectrum exhibited a broad distribution of excess power up to ~25 Hz. The transition between this type of power spectrum and that with the strong 6 Hz peak occurred within 10 min. A mode of QPO with power in a broad band between ~14 and 24 Hz was observed during short time intervals in the active state when the X-ray flux reached the quiescent level.

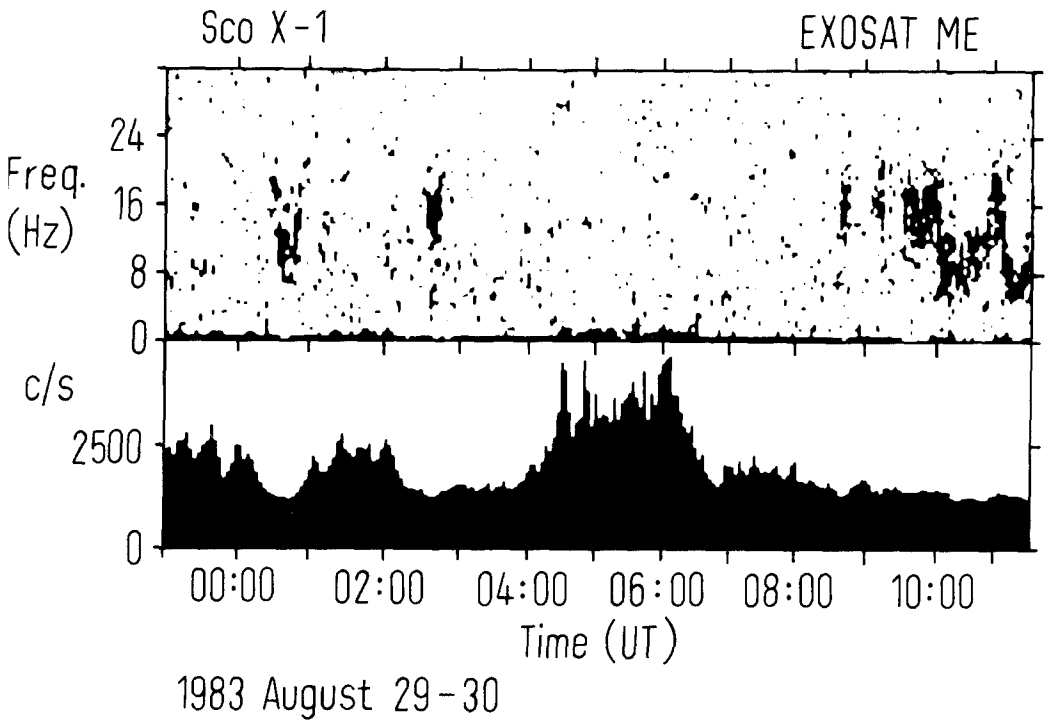

Fig. 3.15. Display of temporal variability of power spectra from Sco X-1 (*upper panel*). The shade of grey of each point indicates the excess power. The darker the shade is, the higher is the power (see also the caption of Figure 1.1). The bottom panel shows the light curve in a broad band (5–35 keV). QPO are observed during the inter-flare dips, and near the end of the EXOSAT observation during the early stages of the transition to quiescence. Note the rapid variations in QPO frequency during the latter interval. This figure is from Van der Klis *et al.* (1987b).

The frequency of the ~ 6 Hz QPO varied by $\sim 10\%$, and was anti-correlated with the source intensity; a power-law fit to the frequency-intensity relation (see Section 4.1) has an exponent $\alpha = -0.52 \pm 0.06$. The r.m.s. variation of the ~ 6 Hz QPO (average value $\sim 5\%$) increased strongly with intensity, up to a certain intensity level, above which the QPO disappeared.

The red noise, which also in this observation was strongest in the flares, had an average r.m.s. variation (in the frequency range 0.0025–0.122 Hz) of 5.5% during the active state, and 2.7% during the quiescent state.

The data were searched for the presence of coherent pulsations, correcting the data for plausible orbital Doppler shifts, using the known orbital ephemeris (Crampton *et al.*, 1976; LaSala and Thorstensen, 1985). A 220 Hz peak was seen during a single ~ 1 hr interval, which, however, did not show the expected Doppler-induced frequency shift, and was therefore tentatively rejected by Middleditch and Priedhorsky (1986), in spite of its apparent significance. The upper limits (90% confidence level) to the amplitude of coherent pulsations are 0.8% (frequencies up to 250 Hz) and 0.5% (up to 128 Hz). A more sensitive search, using data from a 4304-s time interval around quadrature gave upper limits of 0.55% (for frequencies below 256 Hz) and 0.35% below 128 Hz.

Follow-up EXOSAT observations (Priedhorsky *et al.*, 1986) confirmed the above results, and also showed that the relation between the QPO properties and spectral state (active or quiescent) is strict (although in a different way than in e.g., Cyg X-2 and GX 5–1). Sco X-1 was found in a flaring state during the first 6 hr, with a transition to a quiescent state that took place in ~ 1000 s. In the active state QPO between 10 and 20 Hz were seen during dips in the intensity that lasted typically 20 min. The frequency of these active-state QPO was strongly correlated with source intensity (exponent $\alpha = 3.15 \pm 0.2$ in a power law fit to the frequency-intensity relation; see Section 4.1 and Figure 3.16). Their r.m.s. variation (typical value $\sim 8\%$) was anti-correlated with the source intensity ($\propto I^{-1.8}$). During the X-ray flares the QPO peak in the power spectrum dissolved into a broad continuum excess power, for which a centroid frequency could not be determined.

During the quiescent state ~ 6 Hz QPO was observed. Although its centroid frequency was again anti-correlated with the intensity the frequency-intensity relation (see Figure 3.16) differed slightly from that observed earlier ($\nu \sim I^{-0.87 \pm 0.15}$). The r.m.s. variation in the 6 Hz QPO was typically 6%, and decreased with source intensity according to $I^{-1.3}$. The photon-energy dependence of the QPO could be inferred for ~ 1 hr of data; it appears that the 6 Hz QPO is significantly harder than the average X-ray spectrum (Priedhorsky *et al.*, 1986), with the r.m.s. variation increasing from $2.5 \pm 0.4\%$ (0.7–4.7 keV) to $6.0 \pm 0.2\%$ (8–20 keV) (see also Van der Klis *et al.*, 1987b).

Analysis of the GSPC data showed that the active and quiescent states of Sco X-1 correspond with two distinct branches in a hardness-intensity diagram, on both of which the spectral hardness is positively correlated with the intensity (see Figure 3.17). The two branches are smoothly connected at low-intensity; thus the topology of these branches is very different from that of the normal- and horizontal branches observed

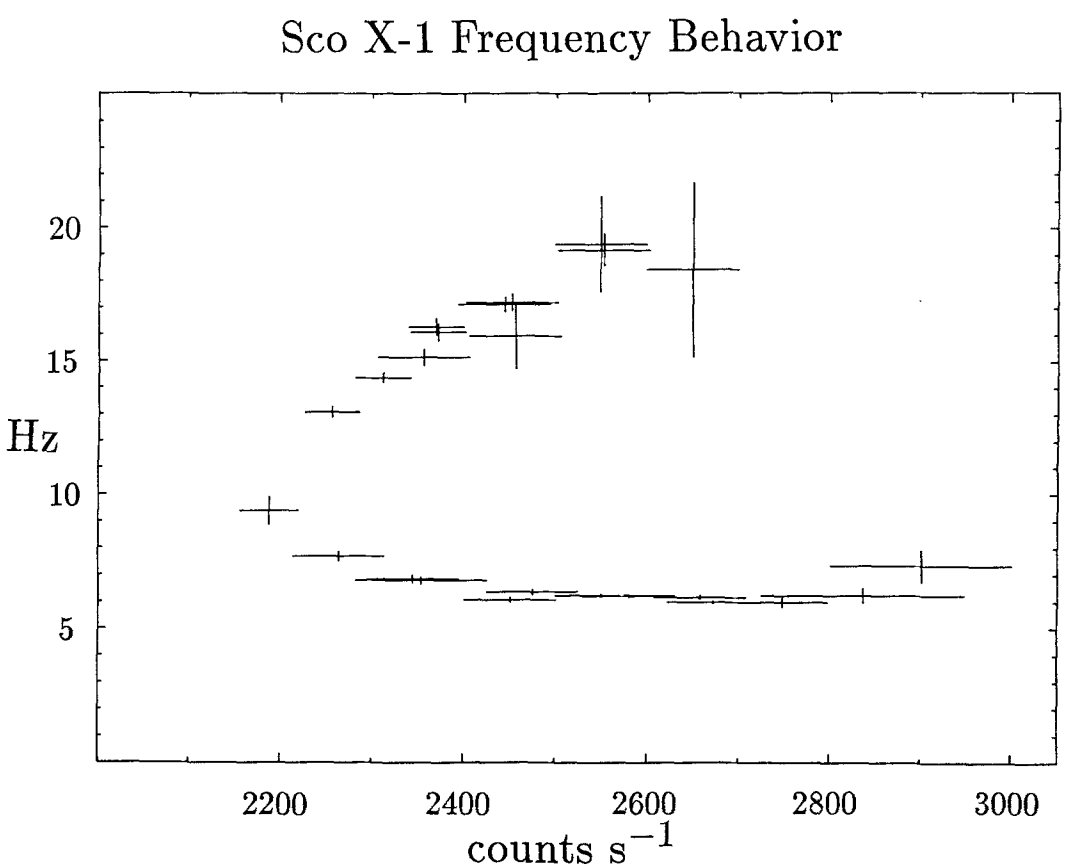

Fig. 3.16. QPO centroid frequency vs ~8–20 keV counting rate (background subtracted) of the EXOSAT ME xenon detectors (full array of 8 detectors; see Section 3.1), for those intervals when QPO was clearly present during an ~ 3-day observation of Sco X-1 in August, 1985. In the upper branch in this figure (which corresponds to the low-intensity region of the 'flaring branch' in the hardness-intensity diagram, HID, and in the colour-colour diagram), the QPO frequency is correlated with the source intensity. In the lower branch (which corresponds to the 'normal branch'), the two are anti-correlated. See also Figures 1.4 and 3.17. This figure is from Priedhorsky *et al.* (1986).

in, e.g., GX 5–1, and Cyg X-2 (see Figures 3.4 and 3.8). The two spectral branches observed for Sco X-1 have a one-to-one relation to the QPO behaviour. When the QPO is near 6 Hz, Sco X-1 is on the quiescent branch; on the active branch the 10–20 Hz QPO is observed. Transitions between the QPO modes occur simultaneously with transitions between the two spectral branches. Both transitions involve a simultaneous and continuous turning around the apexes of the *V*-shaped relations between hardness and intensity, and between frequency and intensity. Priedhorsky *et al.* (1986) suggest that this bi-modal QPO and spectral behaviour is possibly related to the likewise bi-modal behaviour seen in optical and radio observations of Sco X-1 (see Figure 3.17).

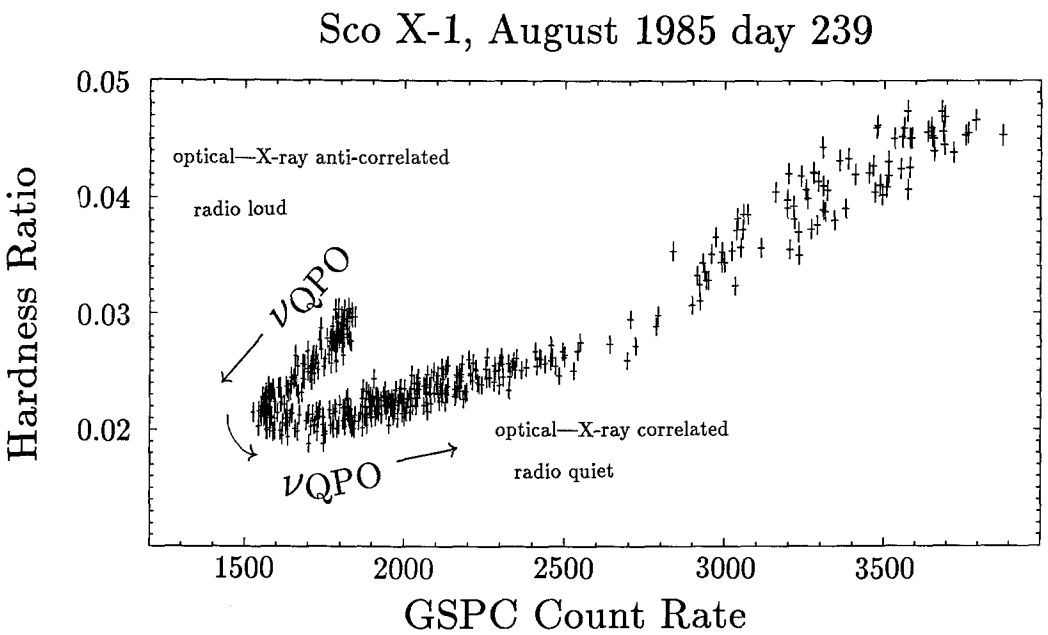

Fig. 3.17. Hardness ratio (14–21 keV/2–7 keV) as a function of EXOSAT's GSPC (see Section 3.1) countrate, background and deadtime corrected, obtained from Sco X-1 on August 27, 1985. The QPO frequency increases from ~6 to ~20 Hz as we descend the normal branch and ascend the flaring branch (see arrows). In the normal branch, a decrease (increase) in source intensity causes an increase (decrease) in QPO frequency; the two are anti-correlated. In the flaring branch, the two are correlated (see also Figure 3.16). This figure is from Priedhorsky *et al.* (1986).

Priedhorsky *et al.* (1986) suggested that the monotonic increase of the QPO frequency along the two branches reflects an increase in mass-accretion rate. The consequence of this is that on the quiescent (6 Hz QPO) branch the source intensity is anti-correlated with the accretion rate. Priedhorsky (1986a) proposed that this anti-correlation is the result of accretion-torque related energy flows from the rotational energy of the neutron star into the disk, during periods of spin-down when the mass accretion rate is low, but accretion can still take place (cf. Ghosh and Lamb, 1979).

Further analysis of the earlier EXOSAT observations (Van der Klis *et al.*, 1987b) confirmed the above bi-modal X-ray spectral behaviour. Apart from the intensity dependent 10–20 Hz QPO in the active state, it was found that when the source entered a long quiescent state the QPO frequency settled near 6 Hz, and was slightly anti-correlated with intensity.

During most of these observations Van der Klis *et al.* (1987b) found that the red noise is substantially weaker than the QPO, when these were present (typical r.m.s. variations of 5% in quiescence, and ~8% in the active state). In the range between 0.016–1.0 Hz the red noise could then be described by a power law (Equation (2.31e)), with exponent γ between ~1.4 and ~2, and r.m.s. variations of ~2%. When the QPO disappeared during flares, the r.m.s. variation in the red noise (0.016–1.0 Hz) increased to ~8%.

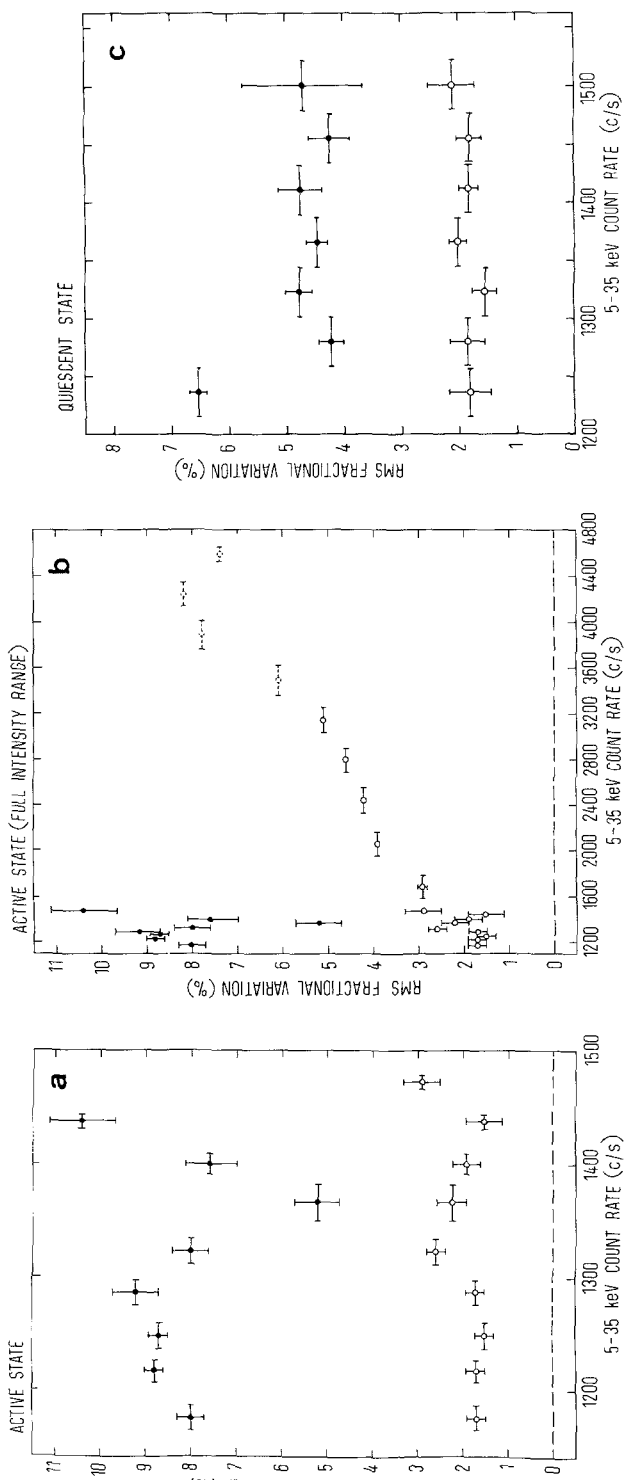

Fig. 3.18. The dependence of the strength (percentage r.m.s. variation) of QPO (solid dots), and red noise (open circles) on the observed counting rate of Sco X-1 in the 5–35 keV energy band (EXOSAT ME xenon detectors; see Section 3.1). (a) During the low-intensity episodes in the active state (flaring branch). (b) During the flaring episodes in the flaring branch. (c) During quiescence (normal branch). The red noise (VLFN component) is always considerably weaker than the QPO (see also Figure 3.6); only in strong flares is the VLFN strength similar to that of the QPO (when these are present). In (a), (b), and (c), the QPO strength (and in (b) also the red noise strength), were calculated from fits to the power spectra. In (a) and (c) the red noise was too weak to be reliably measured by fitting a function to the power spectrum. Instead, the excess power between 0.016 and 1 Hz was directly summed. Dashed bars in (b) correspond to cases where the power law slope of the red noise (VLFN component) was close to, or exceeded 2; see Section 2.3.3). Deadtime corrections were made (only needed in (c)). This figure is from Van der Klis *et al.* (1987b).

This red noise vs QPO behaviour (see Figure 3.18) is very different from that observed for the intensity-correlated high frequency QPO in GX 5–1 and Cyg X-2 (see Sections 3.3.1 and 3.3.2). It was proposed by Van der Klis *et al.* (1987a) that the red noise in Sco X-1 can be identified with the VLFN component of the red noise observed in GX 5–1 and Cyg X-2.

Van der Klis *et al.* (1987b) described the correlation between the properties of the QPO and the X-ray spectrum, using two-component spectral fits (black-body plus unsaturated Compton model; see White *et al.*, 1985, 1986). They find that the frequency of the QPO is approximately linearly related with the luminosity of the blackbody component, according to a relation that is independent of the spectral state of the source. Although there are doubts (Lewin and Van Paradijs, 1985b; Vrtilek *et al.*, 1988) as to the interpretation (and applicability) of two-component spectral models, this result seems to indicate that there exists a considerably simpler relation between QPO and X-ray spectrum than suggested by the above result found by Priedhorsky *et al.* (1986). Since the blackbody luminosity varies monotonically along the quiescent and active branches, the two results are consistent.

3.3.4. *Cir X-1 (4U 1516 – 56)*

The X-ray variations of Cir X-1 are very complicated (for a review see, e.g., Dower *et al.*, 1982). Irregular variability on a time-scale of tenths of seconds is well established (Jones *et al.*, 1974), and X-ray flares lasting less than 10 msec have been reported (Toor, 1977). Apart from the sometimes very large irregular flux variations on time scales of minutes to days the long-term behaviour of Cir X-1 is characterized by rather unusual variations with a period of 16.6 days, generally accepted to be the orbital period of the system (Kaluzienski *et al.*, 1976). The orbital variation is characterized by a sudden drop of the X-ray intensity, which generally occurs in about an hour (downward intensity transitions as fast as a minute have been observed, see Dower *et al.*, 1982). After this transition the X-ray intensity is low for days, and then gradually increases, until the next fast transition. Cir X-1 also emits type-1 X-ray bursts (Tennant *et al.*, 1987a, b), indicating once more that rapid irregular variability does not make an X-ray source a good black-hole candidate (see also Stella *et al.*, 1985b). The characteristics of the orbital X-ray variations have recently changed drastically: at the expected time of the above fast intensity decrease, a transition from a low state to a high state was observed (Tennant, 1987b).

Cir X-1 is a radio (Clark *et al.*, 1975) and infra-red source (Glass, 1978), and has a heavily reddened optical counterpart with very strong Hα emission (Whelan *et al.*, 1977; see also Argue *et al.*, 1984). Variability, correlated with the orbital cycle, is observed throughout the observed electromagnetic spectrum. From 21 cm neutral hydrogen line absorption the distance of Cir X-1 was found to be at least 8 kpc (Goss and Mebold, 1977). Hence, at times, the luminosity of Cir X-1 (for assumed isotropy of the X-ray emission) is well in excess of 10^{38} erg s^{-1}, which makes it one of the most luminous X-ray sources in the Galaxy.

Haynes *et al.* (1986) found that Cir X-1 is embedded in a radio nebula (diameter of

several parsecs), which does not look like a supernova remnant. This nebula is probably the result of ejection of matter from a compact star accreting at a super-Eddington rate, as proposed by Helfand and Becker (1985) for the axially-symmetric non-thermal radio sources recently found in the galactic bulge (Shaver *et al.*, 1985; Becker and Helfand, 1985; Fuerst *et al.*, 1985). De Kool and Van den Heuvel (1985) have argued that if the accreting compact object is a neutron star (as we know Cir X-1 is, as it emits type-1 X-ray bursts; see above), it must be part of a low-mass X-ray binary in a wide orbit.

Tennant (1987b, 1988a, b) has presented the results of a timing analysis of two EXOSAT observations, made in 1985 July (duration 23 hr; time resolution 7.8 ms in two energy channels), and 1986 March (duration 21 hr; time resolution 7.8 ms in 4 energy channels; during part of the observation the time resolution was 0.25 ms in one energy channel, which was selected at either 1–4 keV or 4–10 keV). During both observations, which were centered on the expected times of the transitions in the X-ray light curve (see above), the X-ray light curve is dominated by a large and rapid *upward* brightness transition.

During the 1985 observations Cir X-1 returned to its pre-transition brightness level within ~ 4 hr. Apart from the large flare corresponding to this transition, the X-ray light curve shows several other, much smaller, short flares. The power spectrum for the whole observation shows LFN, whose overall shape between $\sim 10^{-5}$ and 0.1 Hz can be described by a power law (Equation (2.31e)) with exponent $\gamma \sim 1$, but with significant deviations (likely due to the fact that the light curve appears to consist of discrete events). Analysis of the data during the rise part of the main event shows that a QPO peak is present in the power spectrum at 1.4 Hz, and that above ~ 0.02 Hz the red noise steepens ($\gamma \sim 2.3$). The QPO was visible in both the 1–4 keV and the 4–8 keV bands. Gaussian fits to the QPO peak showed that its centroid frequency (average value 1.40 Hz) changed by less than 5% as the source flux went up by a factor ~ 4. (It is unclear whether these flux changes reflect changes in luminosity, or are the result of variable obscuration.) The QPO peak is remarkably narrow, with a FWHM between 0.03 and 0.06 Hz. The r.m.s. variation of the QPO was 1.7–1.9 ($\pm$ 0.4)% in the 1–4 keV band, and 3.0–4.1 ($\pm$ 0.5–1.0%) in the 4–8 keV band. During the main flaring event the source luminosity (for assumed isotropy of the emission, and a distance of 8 kpc) went up to $\sim 10^{39}$ erg s^{-1}; its spectrum was very soft (fitted black-body temperature between 0.8 and 1.4 keV), and showed an anti-correlation between spectral hardness and source intensity.

During the 1986 observation the flare in which Cir X-1 reached a maximum luminosity of $\sim 3 \times 10^{38}$ erg s^{-1}, decayed by a factor ~ 3 on a time-scale of ~ 6 hr, after which the X-ray flux did not change appreciably. During the brighter part of the X-ray light curve the spectral hardness was approximately constant; when the source intensity had decreased to about half its maximum value the spectral hardness and the intensity were anti-correlated. From an analysis of the 7.8 ms resolution timing data it appears that when the luminosity had decreased to $\sim 10^{38}$ erg s^{-1} QPO was present at a frequency of ~ 18 Hz. The QPO frequency decreased with the source intensity, and appeared to saturate at a value of 5.7 $\pm$ 0.3 Hz in the lowest observed intensity range

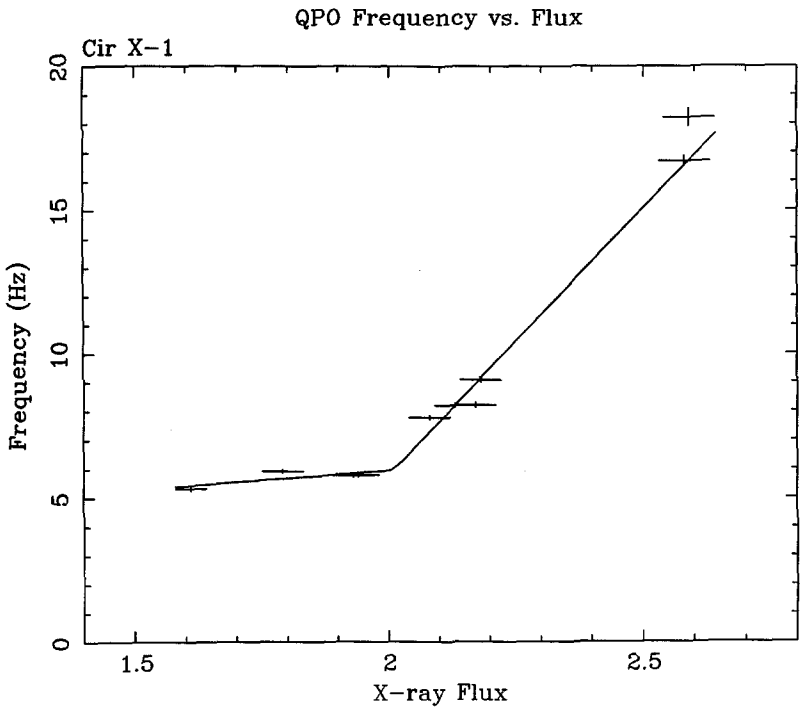
QPO Frequency vs. Flux
Cir X-1
Frequency (Hz)
0
5
10
15
20
1.5
2
2.5
X-ray Flux

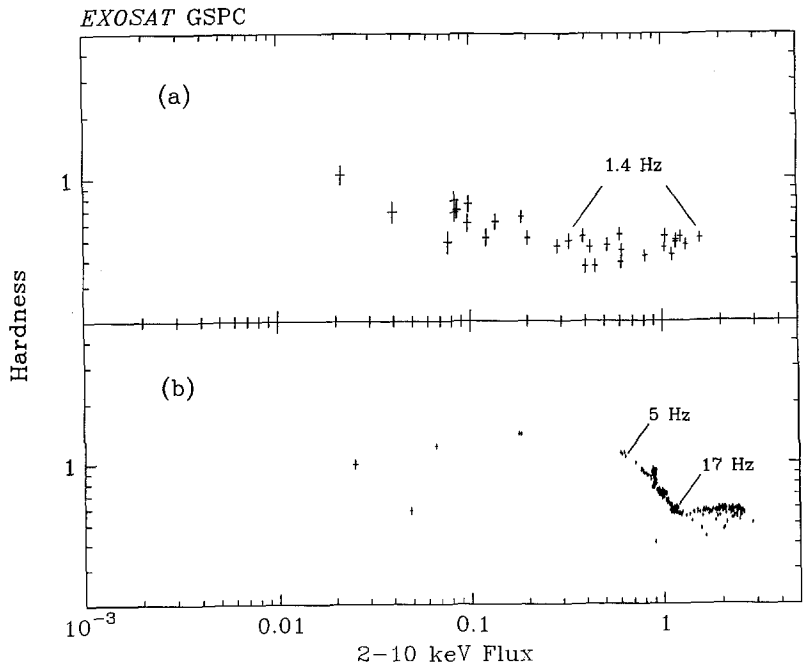
EXOSAT GSPC
(a)
1.4 Hz
(b)
5 Hz
17 Hz
Hardness
1
1
10^-3
0.01
0.1
1
2-10 keV Flux

(see Figure 3.19). The numerical value of this frequency coincides remarkably with that of the 'stationary' QPO observed in the normal-branch state of, e.g., Cyg X-2 (see Section 3.2.2) and GX 5–1 (see Section 3.2.1). Perhaps the connection between the 5.7 Hz QPO and the high-frequency QPO (up to ~ 18 Hz) is like that in Sco X-1; the hardness-intensity diagram could be different because of different energy bands used in defining the source brightness and the spectral hardness ratio. The strength of these 5.7–18 Hz QPO (average r.m.s. variation $\sim 4\%$) increases with photon energy. A comparison of the hardness-intensity diagrams (based on the GSPC data; see Figure 3.19), shows that the 1.4 Hz and the ~ 5–18 Hz QPO occurred at different spectral states. When 1.4 Hz QPO were observed, the spectral hardness was approximately constant, independent of source intensity, whereas the hardness was anti-correlated with intensity when the high-frequency (~ 5–18 Hz) QPO was observed.

From the analysis of two ~ 1.5 hr stretches of data at 0.25 ms time-resolution Tennant (1987b) found that, independent of the presence of the above ~ 5–18 Hz QPO, there is a broad peak near ~ 200 Hz in the power spectrum for the 1–4 keV channel (see Figure 3.20). This broad peak was not present in the power spectrum for the 4–10 keV data. The centroid frequencies (68% confidence limits), obtained from Lorentzian fits to the peaks, were 138 ($+21$, -26) Hz, and 195 $\pm$ 17 Hz, during the two data stretches, respectively. The r.m.s. variation in this very-high-frequency QPO (which could perhaps also be interpreted in terms of band-limited red noise) is $\sim 9\%$.

3.3.5. *GX 340 + 0 (4U 1642 – 45)*

The X-ray flux of the galactic bulge source GX 340 + 0 (Bradt *et al.*, 1971) varies irregularly from 4×10^{-9} to 1.5×10^{-8} erg cm^{-2} s^{-1} (Forman *et al.*, 1978; Markert *et al.*, 1979; Warwick *et al.*, 1981; Wood *et al.*, 1984), without evidence for periodicity (Rappaport *et al.*, 1971). GX 340 + 0 has a soft X-ray spectrum, with reported values of kT for thermal bremsstrahlung fits of ~ 5 keV (Jones, 1977; Parsignault and Grindlay, 1978; Ercan and Cruise, 1984). Ponman (1982b) found that the X-ray spectral hardness is sometimes correlated with the source intensity. The low-energy cut off in the X-ray spectrum (Ercan and Cruise, 1984; Hertz and Grindlay, 1984) corresponds to an equivalent hydrogen column density of $\sim 10^{23}$ cm^{-2}; this indicates that the interstellar reddening is large (Gorenstein, 1975; Ryter *et al.*, 1975), and accounts for the absence of an optical counterpart. Radio emission from GX 340 + 0 has not been detected (Grindlay and Seaquist, 1986).

Fig. 3.19. Results from EXOSAT observations of Cir X-1. *Top.* The QPO frequency vs the 2–10 keV flux in units of 10^{-8} erg cm^{-2} s^{-1}. The line plotted through the data does not represent a physical model. See also Figure 3.16 for a comparison with Sco X-1. This figure is from Tennant (1987b). *Bottom.* Spectral hardness ratio (5–10 keV/2–10 keV; GSPC data, see Section 3.1) vs the 2–10 keV flux in counts cm^{-2} s^{-1} (1 count cm^{-2} s^{-1} $\sim 2 \times 10^{-8}$ erg cm^{-2} s^{-1}). Data taken in July, 1985 are plotted in the top panel (a), and February 1986 data are shown in the bottom panel (b). The flux range, when the 1.4 Hz QPO were observed in July 1985, is indicated. Also the occurrence of the ~ 5–17 Hz QPO (panel b) is indicated. Note that the flux in this hardness-intensity diagram (HID) varies by about two orders of magnitude; this is very different from the flux changes observed in most other LMXB that exhibit QPO. This figure is from Tennant (1988a).

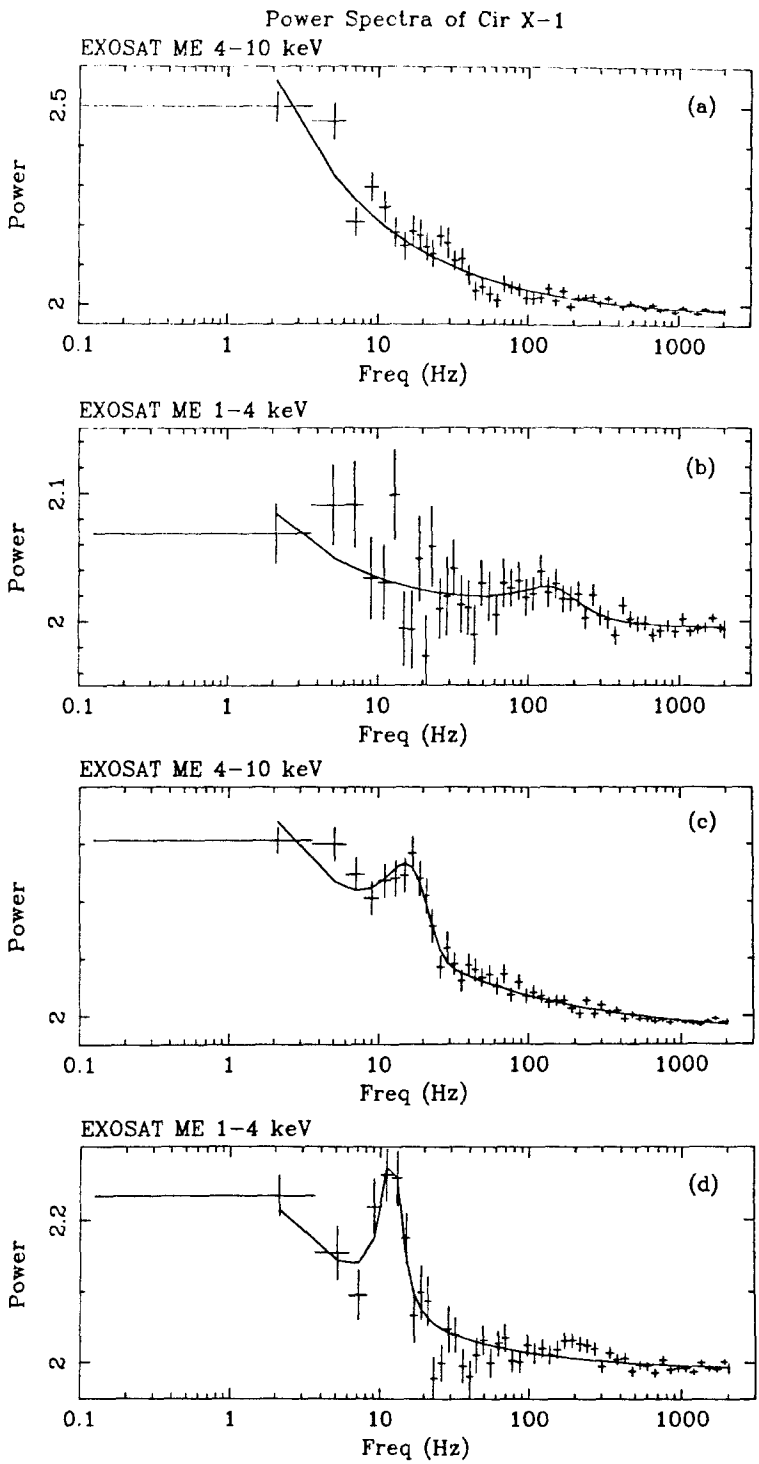

Fig. 3.20. Power spectra from EXOSAT ME data (see Section 3.1) of Cir X-1, in different energy bands at different times (the times mentioned in the caption below indicate the number of seconds after 0 hours UT on day 59 of 1986). (a) 4–10 keV band, 52000–53900 s. (b) 1–4 keV band, 54000–56100 s. (c) 4–10 keV band, 75300–78300 s. (d) 1–4 keV band, 78500–80300 s. This figure is from Tennant (1987b).

Van Paradijs *et al.* (1988) reported on two EXOSAT fast-timing observations of GX 340 + 0, made in May 1985 (duration 13 hr, time resolution 31 ms, no energy resolution), and in April 1986 (duration 12 hr, time resolution 1 ms, no energy resolution, but energy-resolved data available at 0.6 s time resolution).

The source flux ranged between 9×10^{-9} and 1.3×10^{-8} erg cm^{-2} s^{-1}, within the range previously observed. During the 1985 observation the spectral state of the source varied between the horizontal branch and the upper part of the normal branch in the hardness-intensity diagram. During the 1986 observation the source was always on the normal branch.

A power spectrum analysis of the whole 1986 data set showed no evidence for the presence of coherent pulsations, with a 99% confidence level upper limit to the r.m.s. variation of 0.5–0.7% between 0.03 and 512 Hz. QPO were detected during a 3.5 hr interval in the 1986 data; the source then occupied the middle part of the normal branch. Red noise below ~ 0.1 Hz (which corresponds to the VLFN component), was clearly detected in the 1985 and 1986 observations.

In the analysis of the power spectra for six data sets (one of which showed QPO) the QPO was described by a Lorentzian, the red noise by a power law. The centroid frequency and FWHM of the QPO peak are 5.6 ± 0.3 and 2.7 ± 0.9 Hz, respectively; the corresponding r.m.s. variation is $1.8 \pm 0.2\%$. The 2-σ upper limits to the r.m.s. variation for similar QPO in the other five data sets range between 1 and 2.5%. The power-law fits (Equation (2.31e)) to the red noise in the average power spectra for 1985 and 1986, which are good over a frequency range down to 4×10^{-3} Hz, gives exponents $\gamma = 1.23 \pm 0.11$ and 1.58 ± 0.04, respectively. (The power spectra for the six data sets separately do not extend down to sufficiently low frequencies to make a meaningful study of the variation of γ with the spectral state of the source.) The power in the red noise (between 4×10^{-3} Hz and 0.1 Hz) varies between 0.7 and 0.9% for the 1985 data, and between 1.2 and 1.7% for the 1986 data.

Analysis of the photon-energy dependence of the red noise, using the 0.6 s time-resolution (1986) data, shows that between ~ 2 and ~ 10 keV the exponent γ (Equation (2.31e)) does not vary significantly; the r.m.s. variation of the red noise, however, increases steadily from 2.1 ± 0.1 to $3.7 \pm 0.1\%$ over this X-ray energy range.

The power spectra of some of the six data sets show broad-band power, roughly between 0.5 and 10 Hz, in excess of the Poisson noise level (the above power law contribution is insignificant in this frequency range). It appears that the r.m.s. variation in the 0.5–10 Hz range decreases systematically from $\sim 3\%$ to $< 1.5\%$, when going from the horizontal branch to the normal branch in the hardness intensity diagram. Van Paradijs *et al.* (1988) interpret this excess power as LFN, and suspect that it signifies the presence of high-frequency intensity-correlated QPO, such as observed in GX 5–1 (see Section 3.3.1) and Cyg X-2 (see Section 3.3.2). The horizontal-branch QPO in these sources is accompanied by LFN extending up to frequencies much higher than in the above power-law VLFN. The time resolution of the 1985 (horizontal-branch) data was insufficient to detect these high-frequency QPO.

3.3.6. *GX 349 + 2 (4U 1702 – 36/Sco X-2)*

GX 349 + 2 is a bright galactic bulge source (Bradt *et al.*, 1971), with an X-ray flux that varies irregularly (on time-scales of hours and days) between ~ 400 μJy and $\sim 10^3$ μJy (Forman *et al.*, 1978; Markert *et al.*, 1979; Warwick *et al.*, 1981; Wood *et al.*, 1984; Ponman, 1982b). At least some of the time the X-ray intensity variations are positively correlated with the hardness of the X-ray spectrum (Mason *et al.*, 1976; Ponman, 1982b). Ponman (1982a) reported a 8.7 day periodic variation of the source intensity (cf. Matsuoka, 1985); we feel this result needs further study. Matsuoka (1985) reported very low-frequency QPO (with periods between 100 and 200 s). It is unclear whether this QPO is related to the ≥ 1 Hz QPO discussed here. X-ray bursts have not been observed from GX 349 + 2. The source has not been optically identified, neither has it been detected in infra-red or radio emission (Hertz and Grindlay, 1984; Grindlay and Seaquist, 1986).

Lewin *et al.* (1986) reported on two EXOSAT observations of GX 349 + 2, covering 6 hr in August 1983 (time resolution 31 ms), and 7 hr in September 1984 (time resolution 0.25 ms – alternately 2 s data, 15 s no data; independently data were taken continuously with 31 ms resolution). No energy resolution was available in these fast timing observations. On both occasions the hardness of the X-ray spectrum of GX 349 + 2 (ratio of GSPC count rates in the energy bands 5–15 and 2–5 keV) increased approximately linearly with the source intensity; the two hardness-intensity diagrams are very similar. The power spectrum shows red noise below about 1 Hz, which over the range 0.008–2 Hz can be well fit with a power law (Equation (2.31e)) with exponent $\gamma = 1.67 \pm 0.05$ (1983 data), and $\gamma = 1.54 \pm 0.04$ (1984 data). An exponential function does not fit the red noise. This VLFN is stronger when the source shows 'flares' (i.e., flux variations in excess of a few tens of percents on a time-scale longer than about 5 min), with r.m.s. variations (integrated over the range 0.008–0.5 Hz) between 2% (1984 data) and 3% (1983 data) in the 'flaring' state, and about 1% in the 'quiescent' state. During the 1983 observations no QPO were detected, with a 2-σ upper limit to the r.m.s. strength of the QPO (with centroid frequencies between 5 and 10 Hz, and FWHM between 2 and 6 Hz) of about 1.3%. QPO was detected in 1984 at a ~ 2.5-σ level of confidence only, with a centroid frequency of 11 ± 1.5 Hz, a FWHM of 7.5 ($+9$, -5) Hz, and an r.m.s. strength of 2 ± 1%. The presence of QPO seems to be confirmed from the continuous 31 ms data which were taken simultaneously with, but which were largely independent of the 0.25 ms data (taken only 2 s out of every 17 s; see above). However, the significance of the signal detected in the 31 ms data depends sensitively on our knowledge of the deadtime of these data. As yet, this knowledge is inadequate to allow for an accurate statement about the joint significance of the signal in the 0.25 and 31 ms data.

Ponman *et al.* (1988) observed GX 349 + 2 for 25 hr in September 1985 (time resolution ~ 4 ms). During 12 hr the fast timing observations were carried out in four relatively broad energy channels simultaneously. Also during this observation the spectral hardness (ratio of ME count rates in the ranges 5–10 and 1.5–5 keV) was

linearly related to source intensity (the latter varied between about 1600 and about 3500 c/s). QPO was detected when the source was in the lower half of its observed intensity range. It shows up as a very broad shoulder on top of, but well separated from, the red noise. The centroid frequency and the FWHM of the QPO peak (average values 5.5 and 10 Hz, respectively, for assumed Lorentzian shape of the QPO peak) do not vary significantly with source intensity. The r.m.s. fractional variation of the QPO signal varied from $\sim 3\%$ (below 2100 c/s) to 2% (between 2100 and 2600 c/s); for source intensities in excess of 2600 c/s the upper limit (90% confidence level) to the r.m.s. fractional QPO strength is 0.7%. (A more detailed correlation of the QPO strength, as measured by the integrated power in the range 2–12 Hz, shows some evidence for a maximum in the strength of the QPO at an intermediate source-intensity level, near 2000 c/s).

Throughout the observation the power spectrum showed red noise below about 1 Hz, which Ponman *et al.* (1988) fitted with a Lorentzian profile (Equation (2.31a)) centered at zero frequency. The r.m.s. fractional strength and the FWHM of this Lorentzian increase monotonically with source intensity, from 0.8 to 2.2% and 0.5 to 1.2 Hz, respectively. Below 0.1 Hz an additional power-law component with an exponent $\gamma \sim 1$ (Equation (2.31e)) is required to describe the red noise, which can probably be identified with the VLFN component found in other QPO sources (see Sections 3.3.1 and 3.3.2).

The energy-resolved (four channels) fast timing data show that the strength of the QPO tends to increase slightly toward higher X-ray energy; however, the data is consistent with an energy-independent QPO strength (i.e., with a QPO spectrum similar to that of the total emission). A cross-spectral analysis of these data shows no evidence for a time lag between low-energy (1–5 keV) and high-energy (5–10 keV) photons, with 90% confidence upper limits of 4 ms for a lag, and 6 ms for a lead of the high-energy oscillations compared to those at low energy (integrated between 2–9 Hz).

3.3.7. *Rapid Burster (MXB 1730 – 335)*

The Rapid Burster, discovered by Lewin *et al.* (1976), is unique among the galactic X-ray sources in producing two very different kinds of X-ray bursts (type 1 and 2; Hoffman *et al.*, 1978). The type-1 bursts, which are most likely due to thermonuclear flashes on the surface of an accreting neutron star (Woosley and Taam, 1976; Maraschi and Cavaliere, 1977; Hoffman *et al.*, 1978; Joss, 1978), are characterized by a distinct spectral softening as they decay; they have been observed from another ~ 35 sources (for reviews see Lewin and Joss, 1981, 1983). The type-2 bursts do not show such a spectral evolution; they show a considerable range in duration (from a few seconds to ~ 12 min), and in recurrence interval (from ~ 10 s to ~ 1 hr). They behave like a relaxation oscillator: the time interval to the next burst is roughly proportional to the integrated flux in the previous burst (Lewin *et al.*, 1976). Attempts have been made to describe this recurrence behaviour of the Rapid Burster in terms of deterministic chaos (Celnikier, 1977).

The Rapid Burster is a recurrent transient with intervals of about half a year (Lewin,

1977; Grindlay and Gursky, 1977). During its active periods it has shown a variety of combinations of burst behaviour and persistent flux levels. At times only type-2 bursts are observed, with high or low level persistent emission between them, at other times both type-1 and type-2 bursts are observed, and there have also been periods when strong persistent emission and only type 1 bursts are observed (Lewin and Joss, 1981, 1983; Lewin, 1985; Stella *et al.*, 1988a). The Rapid Burster is located in the heavily reddened globular cluster Liller 1 (Liller, 1977), at a distance of ~ 10 kpc (Kleinmann *et al.*, 1976).

It is likely that the type-2 bursts are the result of instabilities in the accretion flow onto the neutron star. Well established models for the accretion instability can be divided into two classes, involving either a gating mechanism associated with the neutron star magnetosphere (Lamb *et al.*, 1977; Baan, 1977, 1979; Michel, 1977), or with viscous and thermal instabilities of the inner radiation-dominated region of the accretion disk (Taam and Lin, 1984). Recently, Milgrom (1987) suggested that the instability occurs between the neutron star surface and the radius of the marginally stable orbits in a Schwarzschild metric (the possible relevance of this model for QPO has been discussed by Paczynski, 1987).

During Hakucho observations of the Rapid Burster in 1979 pulsations with a frequency of ~ 2 Hz were detected in 2 out of 63 type-2 bursts (Tawara *et al.*, 1982; see Figure 1.3). Since the frequency measured during the two bursts differed by $\sim 1\%$, Tawara *et al.* (1982) ruled out that the pulsations were the signature of the rotation of the neutron star.

During a 1983 EXOSAT observation (Barr *et al.*, 1987) the Rapid Burster showed only persistent emission and type-1 bursts; no QPO were then detected, with upper limits to its r.m.s. variation of $\sim 10\%$.

Two EXOSAT observations were made of the Rapid Burster in August 1985, lasting ~ 17 hr and ~ 13 hr, respectively. The time resolution of the fast-timing data varied between ~ 1 and 8 ms; energy resolved data were obtained at time resolutions of 156 and 312 ms (32 energy channels), 94 ms (8 energy channels), and 4 and 8 ms (4 energy

Fig. 3.21. Power spectra (*upper panels*), and 1–15 keV count rates (*lower panels*) vs time during the 1985, August 29–29 EXOSAT observation of the Rapid Burster (MXB 1730 – 335). Count rates are background subtracted and refer to 7 co-aligned ME detectors (see Section 3.1). After 17 : 46 UT the Rapid Burster was observed with a 48% collimator efficiency to avoid contributions from the nearby source 1728 – 34. The shade of grey of each point in the upper panels indicates the power; the darker the shade, the higher is the power (see also Figure 1.1). QPO are observed during almost all type-2 bursts which last longer than ~ 2 min, and during some which last shorter. QPO were also detected during many intervals between those bursts that were only ~ 1–2 min long; in several instances there was a frequency evolution from ~ 4 to ~ 2 Hz. From 15 : 30 to 17 : 46 UT 1728 – 34 was in the field of view; between 16 : 33 and 16 : 50 three ME detectors were offset so as to exclude the Rapid Burster from their fields of view. All type-2 bursts are numbered in sequence of their occurrence; the relatively short burst that occurred a few minutes after burst # 8 was from 1728 – 34. Excess power is observed over a wide range of frequencies on several brief occasions; this was caused by variability in the background. Three such events can be clearly seen within ~ 20 min of burst # 33. This figure is from Stella *et al.* (1988a).

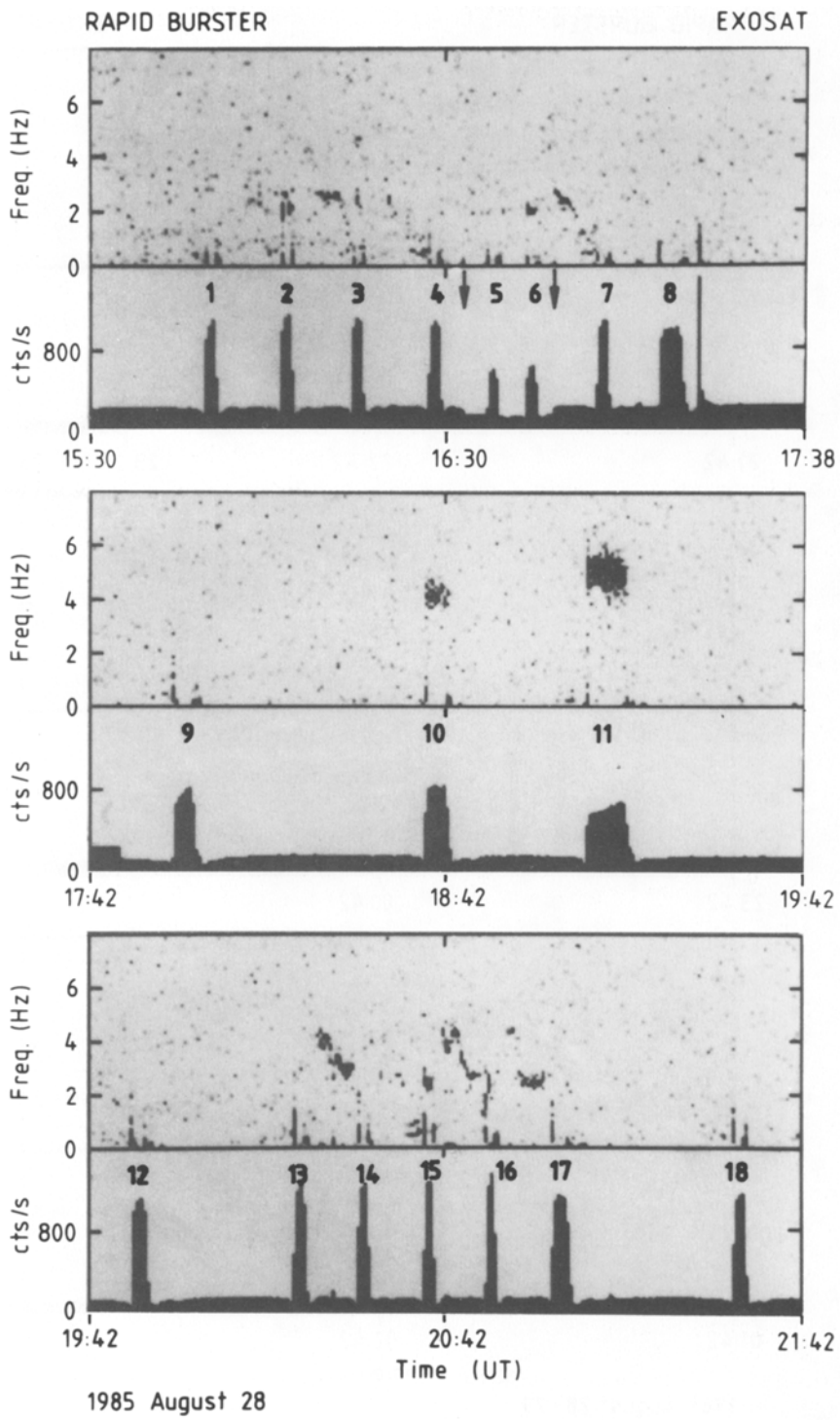
RAPID BURSTER
EXOSAT
Freq. (Hz)
cts/s
1
2
3
4
5
6
7
8
9
10
11
12
13
14
15
16
17
18
15:30
16:30
17:38
17:42
18:42
19:42
19:42
20:42
21:42
Time (UT)
1985 August 28

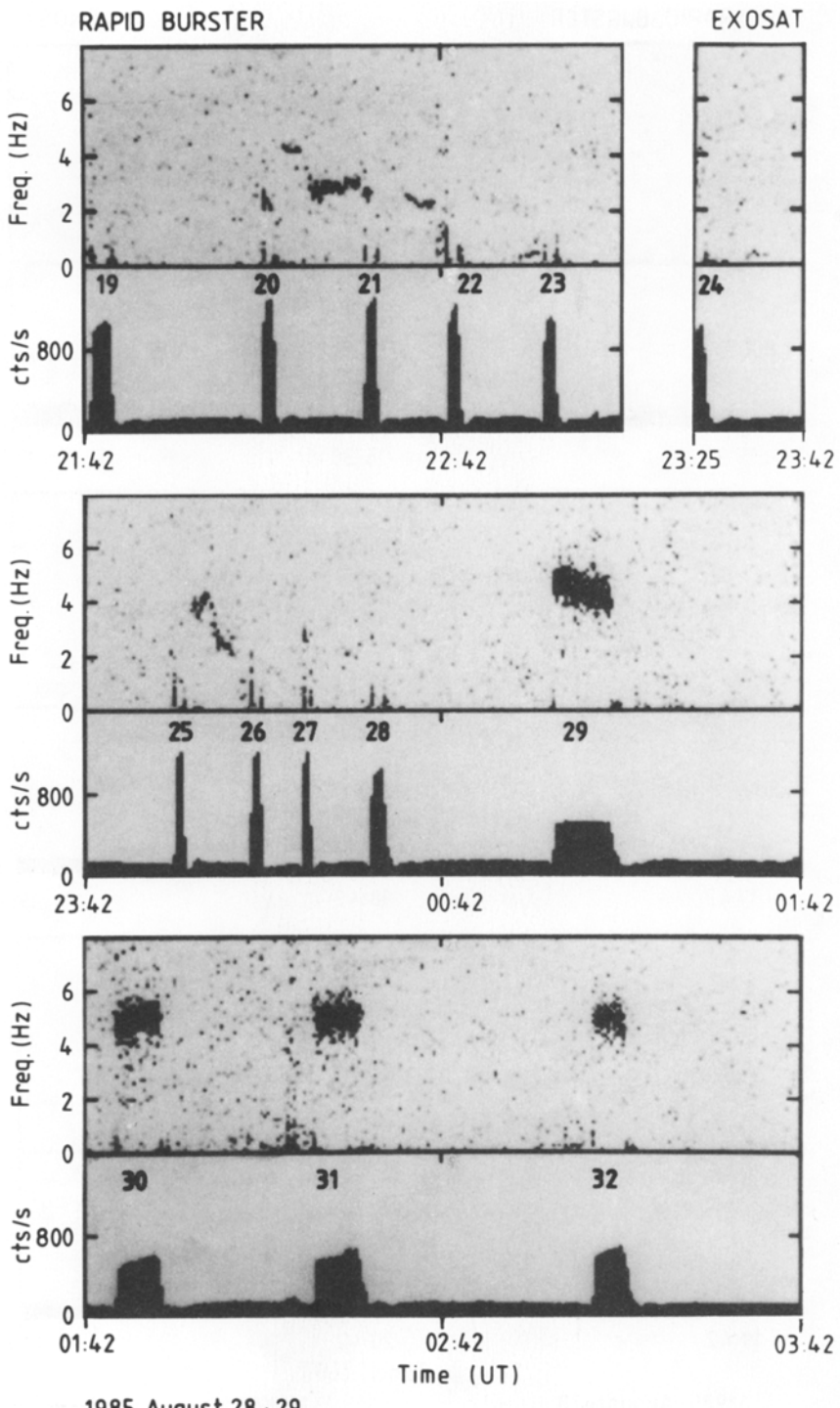
RAPID BURSTER
EXOSAT
Freq. (Hz)
cts/s
19
20
21
22
23
24
25
26
27
28
29
30
31
32
21:42
22:42
23:25
23:42
23:42
00:42
01:42
01:42
02:42
03:42
Time (UT)
1985 August 28-29

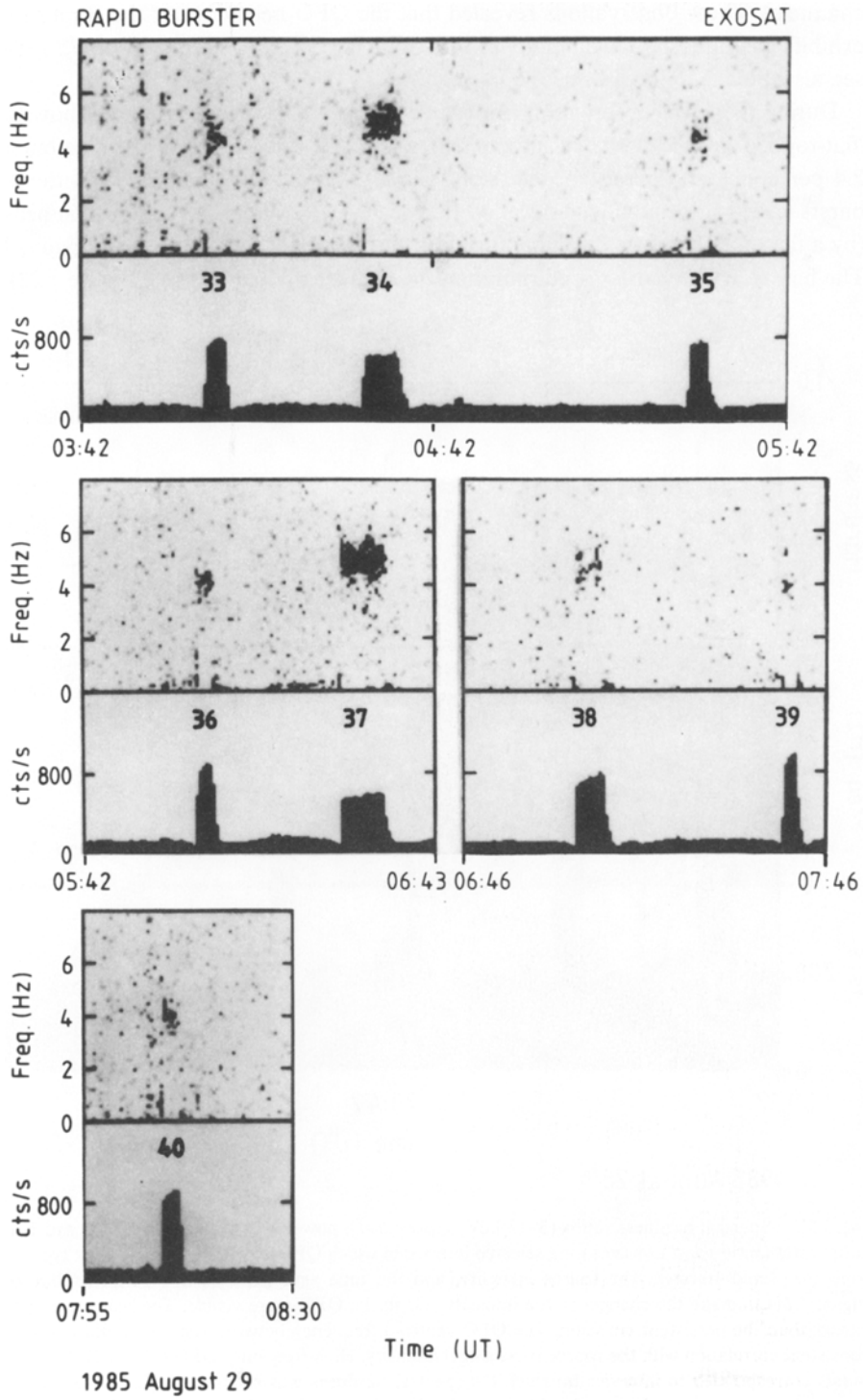
RAPID BURSTER
EXOSAT
Freq (Hz)
6
4
2
0
33
34
35
cts/s
800
0
03:42
04:42
05:42
Freq. (Hz)
36
37
38
39
05:42
06:43
06:46
07:46
40
07:55
08:30
Time (UT)
1985 August 29

channels). These observations revealed that the QPO behaviour of the Rapid Burster exhibits a complexity which matches that of its burst behaviour (Stella *et al.*, 1988a, b; see also Stella, 1986; Lewin, 1987a).

During the 17-hr observation (Stella *et al.*, 1988a), the Rapid Burster showed long 'flat-topped' type-2 bursts, at intervals between ~ 7 and ~ 60 min (average burst rate 2.4 per hour), and persistent emission (variable by a factor ~ 2) between them. The bursts varied substantially in duration (between ~ 90 s and ~ 11 min) and in peak flux (by a factor ~ 3); burst duration and peak flux were anti-correlated (see Figure 3.21). The bursts have a harder spectrum than the persistent emission (see Figure 3.22). The

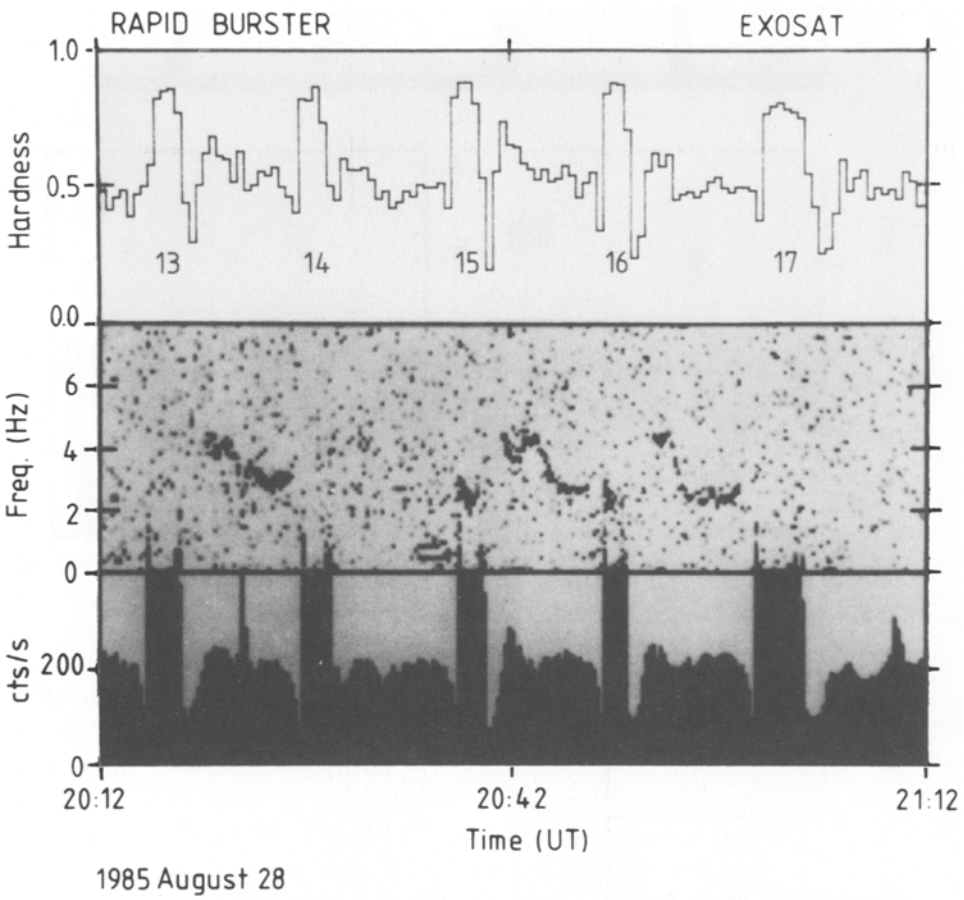

Fig. 3.22. Spectral hardness ratios (5–15 keV; *upper panel*), power spectra (*middle panel*), and 1–15 keV count rates (*lower panel*), vs time for a selected interval in which QPO were observed between type-2 bursts from the Rapid Burster. The source intensity, and the time axes have been expanded (compared to Figure 3.21) to make the changes in the intensity and in the QPO more visible. The bursts are spectrally harder than the persistent emission. The QPO centroid frequency between the bursts did not show any consistent correlation with the source (persistent) intensity. High-frequency QPO (of ~ 4 Hz) between the bursts corresponded to intervals in which the spectral hardness was relatively high. The burst numbers correspond to those of Figure 3.21. This figure is from Stella *et al.* (1988a).

persistent emission showed dips shortly before and after the bursts (Van Paradijs *et al.*, 1979), during which the spectrum softened (indicating that the dips are not the result of increased photoelectric absorption). For assumed isotropic radiation, and a source distance of 10 kpc (Kleinmann *et al.*, 1976) the average peak burst luminosities varied from 1.3×10^{38} erg s^{-1} to 4.0×10^{38} erg s^{-1}; the time averaged burst luminosity was 2.6×10^{37} erg s^{-1}, i.e., $\sim 80\%$ of the average persistent luminosity. While no coherent pulsations were detected, strong QPO were observed with frequencies between 0.4 and ~ 5 Hz.

QPO were seen at frequencies near 5 Hz in almost all bursts longer than 3 min; QPO (near 2 Hz) were also seen in 8 out of 23 shorter bursts (see Figure 3.21). The average QPO centroid frequency (as obtained from a Lorentzian fit to the QPO peak) during a burst is strongly anti-correlated with the *average* burst flux (a power-law fit to the frequency-intensity relation has an exponent $\alpha = -0.75 \pm 0.09$; see Section 4.1 and Figure 3.23). *Within individual bursts* the QPO frequency varied by up to $\sim 10\%$; these frequency variations were sometimes correlated, sometimes anti-correlated, and sometimes not correlated with the variations of the burst flux. The average r.m.s. variation of the QPO during bursts is anti-correlated with the average burst flux; it was as high as $\sim 20\%$ during the longest, low-intensity bursts. The average FWHM of the QPO peaks during bursts varied between 0.04 and 1.3 Hz (see Figure 3.24), with a tendency for broad peaks to be associated with higher frequency QPO (i.e., in long and relatively low-intensity bursts). The ratio of QPO frequency to FWHM varied between ~ 20 and ~ 8, for bursts lasting less than 2 min and more than 2 min, respectively.

QPO were sometimes seen in the persistent emission between some of the relatively short (and luminous) bursts; they were never seen between the less luminous long bursts (although the persistent flux levels were similar; see Figures 3.21 and 3.22). In most cases the QPO frequency changed from ~ 4 Hz after a burst to ~ 2 Hz prior to the next burst; however, the details of this frequency evolution showed much individual variation (see Figure 3.22; see Stella *et al.* (1988a) for a detailed description). The QPO frequency and the persistent flux were sometimes correlated, sometimes anti-correlated, and sometimes there was no correlation between them; on average, there was no general correlation between the QPO frequency and the persistent flux. However, the QPO frequency appears to be positively correlated with the spectral hardness (see Figures 3.22 and 3.27). The r.m.s. variation of the QPO in the persistent emission ranged from $\sim 8\%$ (corresponding to the limiting sensitivity that could be obtained in ~ 1 min of observing) to values as high as $\sim 35\%$ (see Figure 3.29). The FWHM of the QPO peaks in the persistent emission were between 0.03 and 0.3 Hz.

The strength of the QPO is not uniquely determined by the peak flux, total energy or spectral hardness of the burst. Two bursts, which were very similar with respect to their peak fluxes, total energies, and spectral hardness, as well as the intervals before and after the bursts, differed, in that one of them showed clear QPO, and the other did not (Figure 3.21). A similar conclusion holds for the QPO in the persistent emission.

Before some relatively short bursts significant QPO power was found in the 0.4–1.0 Hz range (see Figure 3.22). These events are not apparently connected with the

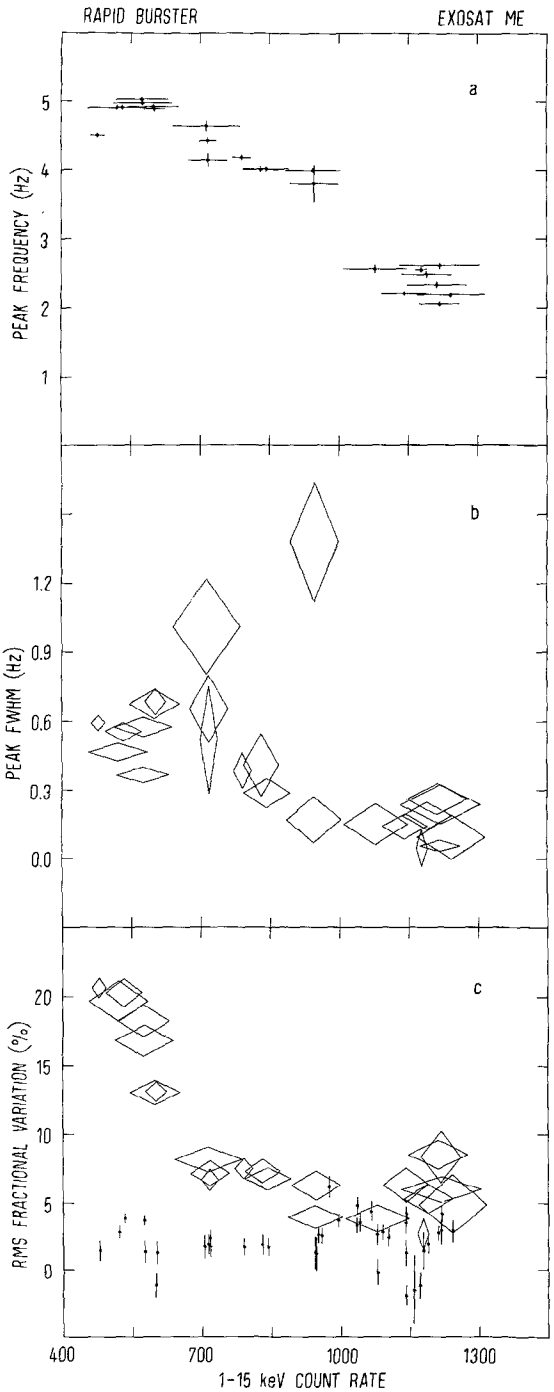

Fig. 3.23. Centroid frequency (panel a), FWHM (panel b), and the strength (r.m.s. fractional variation in %; diamonds in panel c), of the QPO observed during type-2 bursts from the Rapid Burster, plotted vs the observed average countrate during these bursts (1–15 keV EXOSAT ME data; see Section 3.1). The QPO frequency, as well as the strength of the QPO, are anti-correlated with the average type-2 burst intensity. The vertical bars in panel c represent the strength of the red noise (0.063–1 Hz) during each of the type-2 bursts in which QPO were detected; this strength (typically a few %) does not depend on the average burst flux. This figure is from Stella *et al.* (1988a).

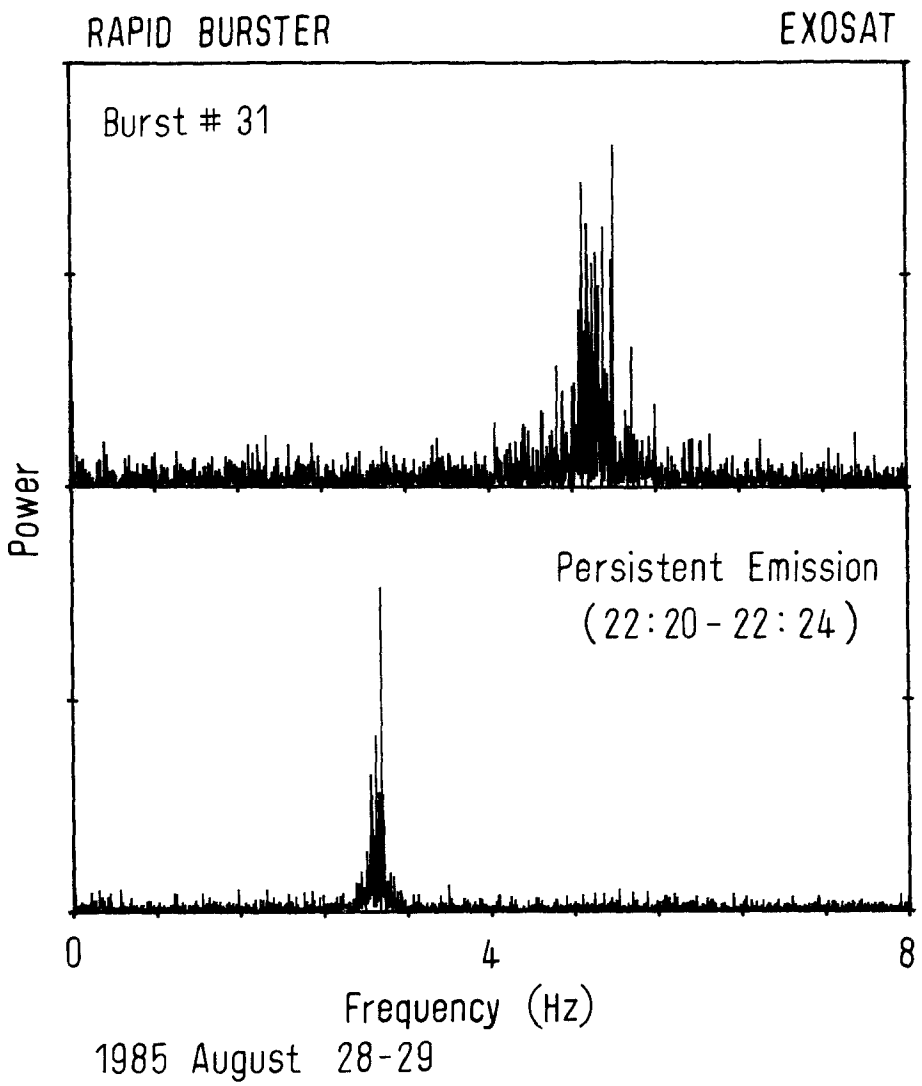

Fig. 3.24. High-resolution power spectra (2048 frequency bins) from the Rapid Burster. Upper panel: burst # 31 (4 min of data). Lower panel: a 4-min persistent emission interval between burst # 20 and # 21 (for burst numbers see Figure 3.21). The FWHM of the QPO peak during the persistent emission is much smaller than that during the burst. Notice the (near) absence of red noise in both power spectra. This figure is from Stella *et al.* (1988a).

presence of 2–4 Hz QPO in the preceding persistent interval. On one occasion QPO were observed simultaneously at frequencies of 0.44 ± 0.01 Hz, and at the second harmonic (of 0.88 ± 0.06 Hz), with FWHM of 0.007 and 0.04 Hz, respectively (see Figure 3.25).

The power spectra showed very little red noise during the persistent emission intervals and the peaks of the bursts; substantial red noise was only observed during the rise and decay parts of the bursts. During bursts, the r.m.s. variation of the red noise in the

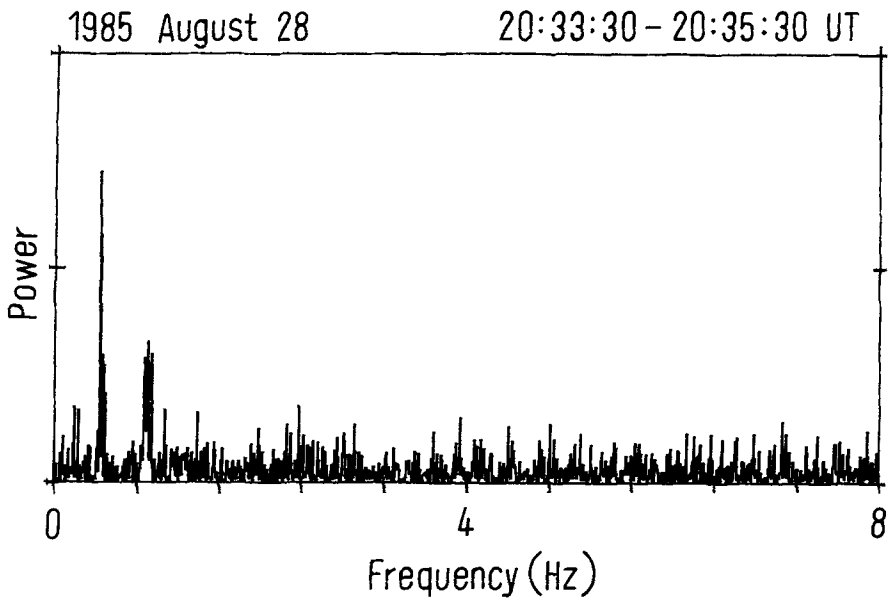

Fig. 3.25. Power spectrum (1024 frequency bins) from a 2-min interval just before burst # 15 (see Figures 3.21 and 3.22). QPO are observed at ~0.44 and at ~0.88 Hz (second harmonic). Notice the absence of red noise. This figure is from Stella *et al.* (1988a).

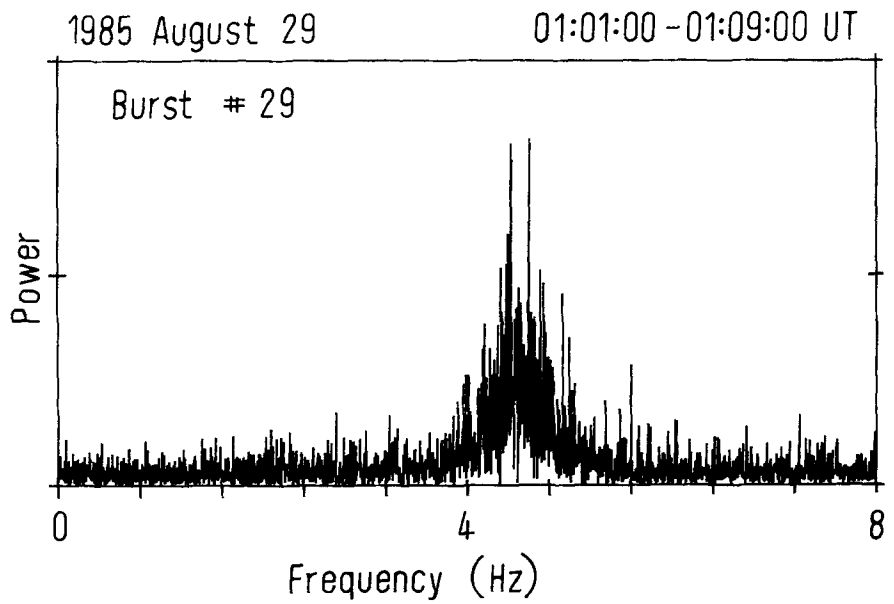

Fig. 3.26. High-resolution power spectrum (2048 frequency bins) from an 8-min interval during burst # 29 (see Figure 3.21) during which the r.m.s. variation of the QPO was ~21%. Notice the absence of red noise. This figure is from Stella *et al.* (1988a).

0.03–1 Hz range is typically 2 to 5 times smaller than that in the QPO, but sometimes it was at least 10 times smaller (see Figure 3.26). Similar results were obtained for the persistent emission (when QPO were detected).

During the second (13-hr) observation the burst was higher (~ 4.3 hr^{-1}), the bursts lasted from ~ 0.5 to ~ 3 min, and had peak luminosities between 1.3×10^{38} erg s^{-1} and 4×10^{38} erg s^{-1}. The QPO behaviour was similar to that during the previously described observation, except that no QPO were detected with frequencies below 2 Hz (Stella *et al.*, in preparation).

The energy-resolved data showed that the r.m.s. fractional variation in the QPO observed in the bursts did not change significantly with X-ray energy (with an overall average value of $\sim 10\%$). The r.m.s. variation in the persistent emission QPO as a function of X-ray energy was inconsistent with a constant value, and increased by $2.4 \pm 0.5\%$ per keV (Figure 3.29; Stella *et al.*, 1988b).

Stella *et al.* (1988b) made a cross-spectral analysis for data which showed the 2–5 Hz

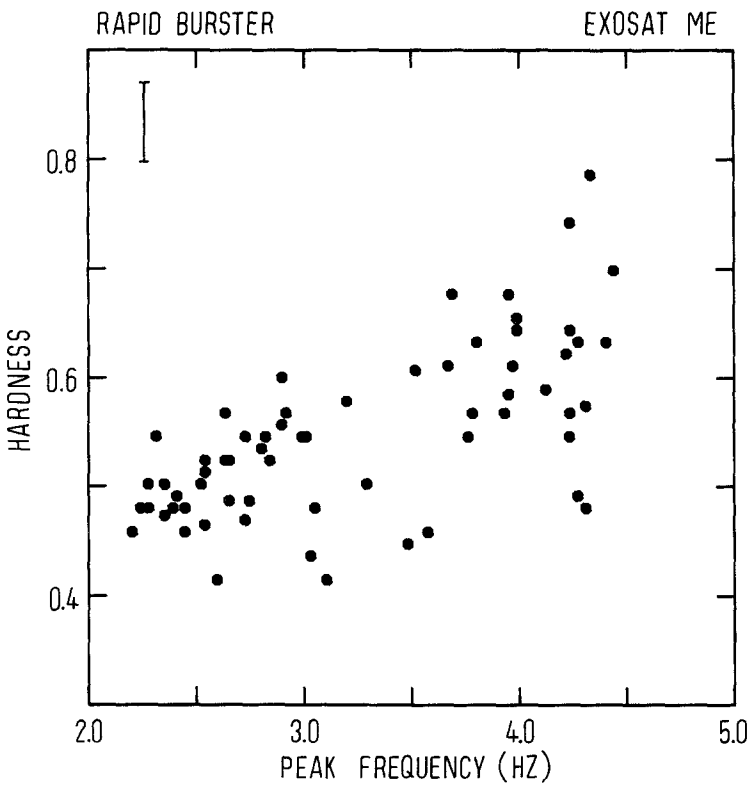

Fig. 3.27. Relation between the spectral hardness ratio (5–15 keV/1–5 keV, EXOSAT ME data; see Section 3.1), and the centroid QPO frequency in the persistent emission intervals during which QPO were detected. A characteristic error bar is shown separately (upper left). The 1-σ uncertainties in the QPO (centroid) frequency are comparable to the size of the dots. A significant correlation is found between the QPO frequency and the spectral hardness of the persistent emission between the type-2 bursts. This figure is from Stella *et al.* (1988a).

QPO; the results were averaged separately for data sets, according to whether the QPO frequency was smaller or larger than 3.6 Hz, and according to whether the source was bursting or emitting a persistent flux only. They found that in the persistent emission for the QPO with frequencies in excess of 3.6 Hz the (1–5 keV) photons lagged the (5–21 keV) photons by ~ 8 ms (at a 3.7-σ level of confidence) (see Figure 3.28). No

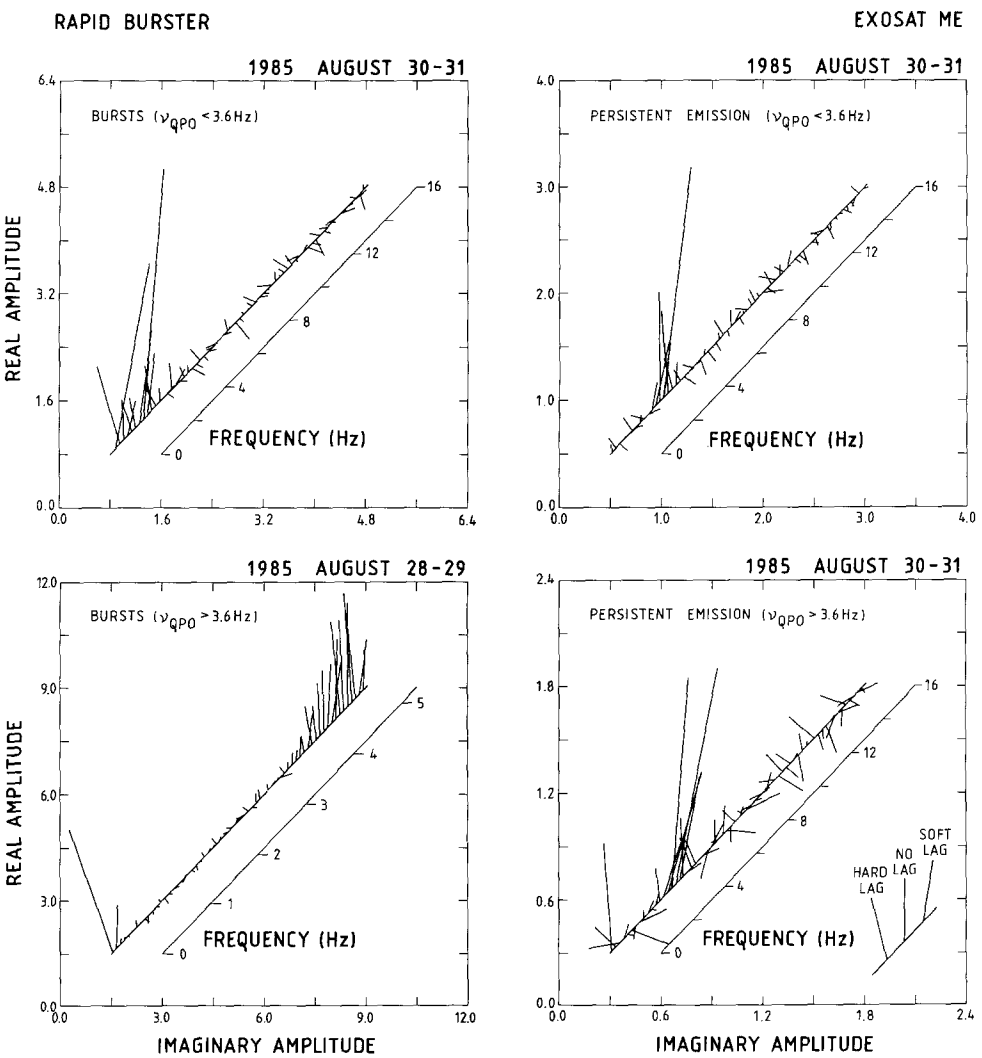

Fig. 3.28. Average complex cross-spectra (between $\sim$ 1–5 and $\sim$ 5–21 keV) in four data sets of the Rapid Burster obtained with EXOSAT during August 28–31, 1985. Two sets deal with type-2 bursts (*left panels*), and two sets with the persistent emission between the bursts (*right panels*). A division was also made according to whether the centroid QPO frequency was either smaller (*upper panels*) or larger (*lower panels*) than 3.6 Hz. The meaning of the axes, and short lines is identical to that in Figure 3.11 (for more details on the cross-spectra see Section 2.4). Vectors leaning right (left) with respect to the vertical axis indicate a soft (hard) time lag. The > 3.6 Hz QPO in the persistent emission show a significant soft lag of ~ 8 ms (lower right panel). This figure is from Stella *et al.* (1988b).

significant time lag could be measured in the QPO during the bursts and in the < 3.6 Hz QPO during the persistent emission. However, only in the case of the > 3.6 Hz QPO during bursts were the upper limits sufficiently tight (90% confidence limits on any hard lag between -0.9 and $+1.7$ ms) to exclude an ~ 8 ms delay of the low-energy signal.

3.3.8. *GX 3 + 1 (4U 1744 − 26)*

The bright galactic bulge X-ray source GX 3 + 1 (Bradt *et al.*, 1971) has an average X-ray flux density of 450 μJy, around which it varies by a factor less than ~ 3 (Forman *et al.*, 1978; Markert *et al.*, 1979; Warwick *et al.*, 1981; Wood *et al.*, 1984). Bremsstrahlung fits to the X-ray spectrum give temperatures $kT \sim 5$ keV (Jones, 1977; Parsignault and Grindlay, 1978). A positive correlation between spectral hardness and source intensity was reported by Parsignault and Grindlay (1978) and Ponman (1982b). GX 3 + 1 has been of considerable interest, as for several months in 1979 the X-ray flux of this bright galactic bulge source was relatively low; it then emitted type-1 X-ray bursts (Oda, 1980; Inoue *et al.*, 1981; Makishima *et al.*, 1983). This confirmed the suspicion that burst sources and bright galactic bulge sources are similar systems, differing mainly in their X-ray luminosities (cf. Van Paradijs *et al.*, 1979). No optical counterpart has been found for GX 3 + 1, neither has it been detected as an IR or radio source (Hertz and Grindlay, 1984; Grindlay and Seaquist, 1986).

Lewin *et al.* (1987) reported on EXOSAT observations of GX 3 + 1, made in March 1985 (8.5 hr, time resolution 2 and 0.25 ms, no energy resolution), and in September 1985 (16 hr, four energy channels, time resolution 4 ms). During both observations the source strength and the spectral behaviour were quite similar; however, QPO were detected only during the latter observation.

During the March 1985 observations the 2-σ upper limit to the r.m.s. flux variations for QPO with similar properties as those detected during the September 1985 observation (see below) is 2.7%. Red noise was clearly present below about 1 Hz. This red noise could be well described by a power law (VLFN component), with exponent $\gamma = 1.23 \pm 0.04$ (see Equation (2.31e)); an exponential function did not give a good fit to the red noise. The strength of the red noise corresponded to an r.m.s. variation of $2.32 \pm 0.04\%$ (0.01–32 Hz; 1–16 keV).

During the September 1985 observation the hardness-intensity diagram of GX 3 + 1 showed both the normal branch and the horizontal branch. QPO were detected only during a 3.3 hr interval, when the source was on the normal branch; however, the source did not always show QPO when it was on the normal branch. The centroid frequency of the QPO peak (for an assumed Lorentzian profile) is 8 ± 1 Hz; its FWHM equals 8 ± 4 Hz. The r.m.s. variation in the QPO is $3.5 \pm 0.9\%$. The red noise, which was clearly visible below ~ 1 Hz, was again best described by a power law with exponent $\gamma = 1.29 \pm 0.03$, and r.m.s. strength $3.1 \pm 0.02\%$ (0.01–32 Hz; 0.9–16 keV), i.e., very similar to the values observed in the first EXOSAT observation. These values did not change significantly during the observation. The possible energy dependence of the QPO could not be determined because of limited photon statistics. However, the r.m.s.

strength of the red noise increased substantially with photon energy; averaged over the whole observation it was 2.0% at 2 keV, 3.4% at 5 keV, and 6% at 10 keV. Also the power-law exponent γ (see Equation (2.31e)) varied with energy, from 1.85 ± 0.06, 1.28 ± 0.07, and 1.38 ± 0.05, at these three average photon energies, respectively.

3.3.9 *GX 17 + 2 (4U 1813 – 14)*

The X-ray flux of the bright bulge source GX 17 + 2 (Bradt *et al.*, 1971) varies irregularly on a time-scale of hours and longer (Forman *et al.*, 1976; Ponman, 1982b). Possible coherent variability has been reported with periods of 31.8 min (White *et al.*, 1976b), 1.4 hr (Langmeier *et al.*, 1986), 19.5 hr (Hertz and Wood, 1986), and 6.4 d (Ponman, 1982a); independent confirmation of any of these reported periodicities is, in our opinion, required. GX 17 + 2 is one of the very few galactic bulge sources that

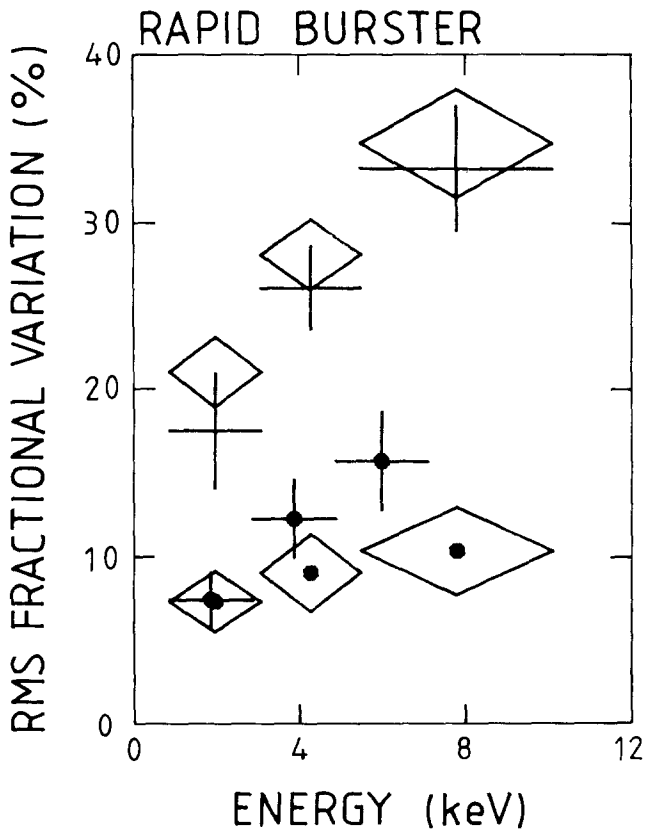

Fig. 3.29. The strength (r.m.s. fractional variation in %) of the QPO in the four data sets from the Rapid Burster (as described in the caption of Figure 3.28), as a function of the energy of the X-rays. Crosses refer to > 3.6 Hz QPO, and diamonds to < 3.6 Hz QPO; the type-2 burst data are indicated with solid dots, the remaining data hold for the persistent emission between the bursts. During the persistent emission, the strength of the QPO (with frequencies both larger and smaller than 3.6 Hz) increases with photon energy. This figure is from Stella *et al.* (1988b).

occasionally emits X-ray bursts (Kahn and Grindlay, 1984; Tawara *et al.*, 1984; Sztajno *et al.*, 1986); although the relative flux increase in these bursts, above the persistent level, is very small, and some of them last extremely long (up to ~ 5 min), these events are probably *bona fide* type-1 X-ray bursts (Sztajno *et al.*, 1986), possibly ignited in a hydrogen-rich environment (Van Paradijs *et al.*, 1988b). GX 17 + 2 is a source of variable radio emission (Hjellming and Wade, 1971b; Braes and Miley, 1973; Hjellming, 1978; Geldzahler, 1983; Grindlay and Seaquist, 1986). A 17th magnitude optical star is located inside the radio error box (Tarenghi and Reina, 1972), but this G-type star (Davidsen *et al.*, 1976) is unlikely to be the companion of the X-ray source (Lewin and Van Paradijs, 1985a).

Stella *et al.* (1988) analyzed the rapid variability behaviour of GX 17 + 2, during two observations with EXOSAT, made in August 1985 (21 hr of data at 2 ms time resolution in the 1–15 keV range), and in September 1985 (6.8 hr with 4 ms data sampling in the 1–15 keV range; 4.2 hr at 4 ms in the 5–35 keV range, and 1.5 hr with 0.25 ms sampling in the 1–15 keV range). During both observations the source intensity was within $\sim 15\%$ of 2.2×10^{-8} erg cm^{-2} s^{-1} (1–30 keV).

A search for coherent pulsations was made using the 1985 September data; none were found, with (99.9% confidence) upper limits of 0.5 and 1.9% in the frequency ranges 0.125–256 and 256–2048 Hz, respectively (Table I).

During the 1985 August observation GX 17 + 2 was on the normal branch in the hardness-intensity diagram (Langmeier, 1988); QPO were detected when the source was in the lower half of the observed intensity range. The centroid frequency of the QPO peak (fitted with a Lorentzian) showed no significant variation with source intensity (average value 7.2 ± 0.5 Hz; Stella *et al.*, 1988c). The FWHM of the QPO peak, and the r.m.s. variation in the QPO, were both anti-correlated with intensity; over the intensity range where the QPO were observed they varied between ~ 3 and ~ 7 Hz, and between $1.4 \pm 0.2\%$ and $2.8 \pm 0.4\%$, respectively. In the upper half of the observed intensity range the upper limit (90% confidence level) to the r.m.s. QPO variation was 1.2%. From a fit to the red noise in the power spectrum with a Lorentzian (see Equation (2.31a)) centered at zero frequency a FWHM of ~ 0.9 Hz was found; the r.m.s. variation in the red noise, which varied between ~ 1.2 and $\sim 2.7\%$ (similar to the values for the QPO), did not show a significant correlation with source intensity.

During the September 1985 observation GX 17 + 2 was on the horizontal branch (Hasinger, 1987b, and private communication), and showed QPO with a frequency that varied from 23.7 ± 0.7 to 28.1 ± 0.6 Hz, when the source intensity increased by $\sim 5\%$ (Figure 3.30). The r.m.s. variation in the QPO was between ~ 2 and $\sim 3\%$. The average FWHM of the QPO peak was 3.5 Hz, with some evidence for an increase when the source intensity was relatively low. Strong red noise was detectable up to ~ 60 Hz. A Lorentzian fit (around zero frequency) to the red noise yielded a FWHM of 9.4 ± 0.6 Hz, and an r.m.s. variation in the red noise of $6.1 \pm 0.2\%$, independent of source intensity. Power-law fits (see Equation (2.31e)) to the red noise in the power spectra at different source intensities gave an average value for the exponent γ of 1.2 (range between 0.7 and 1.9); however, these fits were substantially worse than the

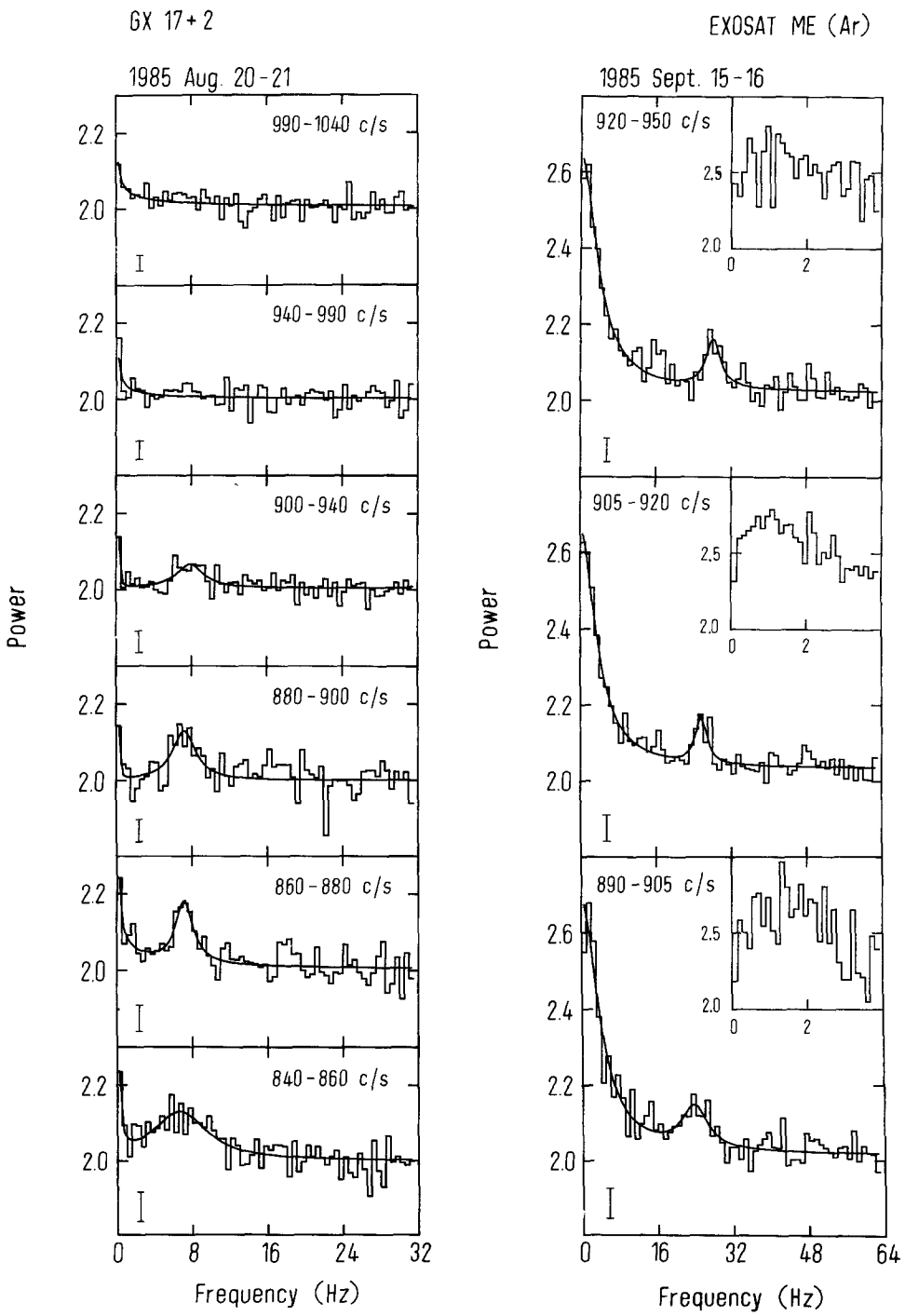

Fig. 3.30. Power spectra for data from GX 17 + 2 for various source intensities as indicated in each panel (EXOSAT ME data 1–15 keV, half array, see Section 3.1) during August 20–21, 1985 (*left panels*), and September 15–16, 1985 (*right panels*). Characteristic 1-σ error bars are shown in the lower left hand corner of each panel. The solid lines represent best fits using two Lorentzian profiles; one for the QPO peak, and one (centered on zero frequency) for the red noise (see Section 2.3.3). The top right inserts (September data) show the power spectra, with a better frequency resolution, of the red noise up to 4 Hz. Notice a turn-over of the power in the range $\sim$ 1–2 Hz. This figure is from Stella *et al.* (1988c).

Lorentzian fits, due to the fact that the power did not continue to rise toward zero frequency, but showed a slight turn-over or saturation below ~ 2 Hz. It is possible that this turn-over represents the same phenomenon as the very broad QPO peak (centroid frequency ~ 2.4 Hz, FWHM ~ 4.3 Hz) in the power spectrum found by Langmeier *et al.* (1985) during a 1.4 hr interval of an EXOSAT observation of GX 17 + 2 in August 1984 when the source was largely on the horizontal branch, but near the transition to the normal branch. The 2.4 Hz feature may be structure in the red noise (Langmeier, 1988, and private communication).

3.3.10. *4U/MXB 1820 – 30*

This X-ray source is located in the globular cluster NGC 6624 (Giacconi *et al.*, 1974; Jernigan and Clark, 1979; Grindlay *et al.*, 1984). Grindlay *et al.* (1976) discovered X-ray bursts from this source, which have only been seen when the persistent X-ray flux was relatively low (Clark *et al.*, 1977; Vacca *et al.*, 1986; Haberl *et al.*, 1987). Because of its location in the dense core of NGC 6624 no optical counterpart has yet been found. There is a weak radio source near the center of NGC 6624 (Geldzahler, 1983; Grindlay and Seaquist, 1986).

Stella *et al.* (1987a) found from EXOSAT observations that the X-ray flux of 1820–30 varies coherently with a period of 685 s. From the upper limit on the period derivative (< 4 s yr^{-1}) they concluded that this is most likely the orbital period. Analysis of archival SAS-3 data confirmed this period, and improved the upper limit on the period derivative to 0.11 ms yr^{-1} (Morgan *et al.*, 1986; Morgan and Remillard, 1988), thus supporting the conclusion that the 685-s flux variations reflect the orbital period (the smallest orbital period found so far for any binary star). The secondary star of 1820–30 is most probably a helium white dwarf with a mass of $\sim 0.05\ M_\odot$ (Stella *et al.*, 1987a; Verbunt, 1987; Rappaport *et al.*, 1987).

Long-term observations of 1820–30 with the Vela 5B satellite, covering the interval 1969–1976 led to the detection of a long period (176 days) in its X-ray flux variations (Priedhorsky and Terrell, 1984). The origin of this long-term periodicity is unknown (see Priedhorsky, 1986b, for a discussion, and a comparison with dwarf novae).

With respect to its X-ray spectrum, and the variability of its X-ray flux on time-scales ranging from seconds to days, 1820–30 is quite similar to the bright bulge sources not located in globular clusters. In particular a positive correlation has often been found between its spectral hardness and the source intensity (Ponman, 1982b; Stella *et al.*, 1984).

Observations with the *Einstein* Observatory showed that during its high state 1820–30 can display short-term flickering with a shot-noise character on a time scale of ~ 10 s; the excess variance due to these shots increases strongly toward higher photon energy (Stella *et al.*, 1984). No time lag between the signals in a low- and a high-energy band was detected, with an upper limit of 30 ms (Stella *et al.*, 1984).

1820–30 was observed with EXOSAT on four occasions. During three the source was in the high state of the 176-day cycle, and aperiodic variability was then detected on time scales of hours and less (Stella *et al.*, 1987b; see also Stella *et al.*, 1987a). The

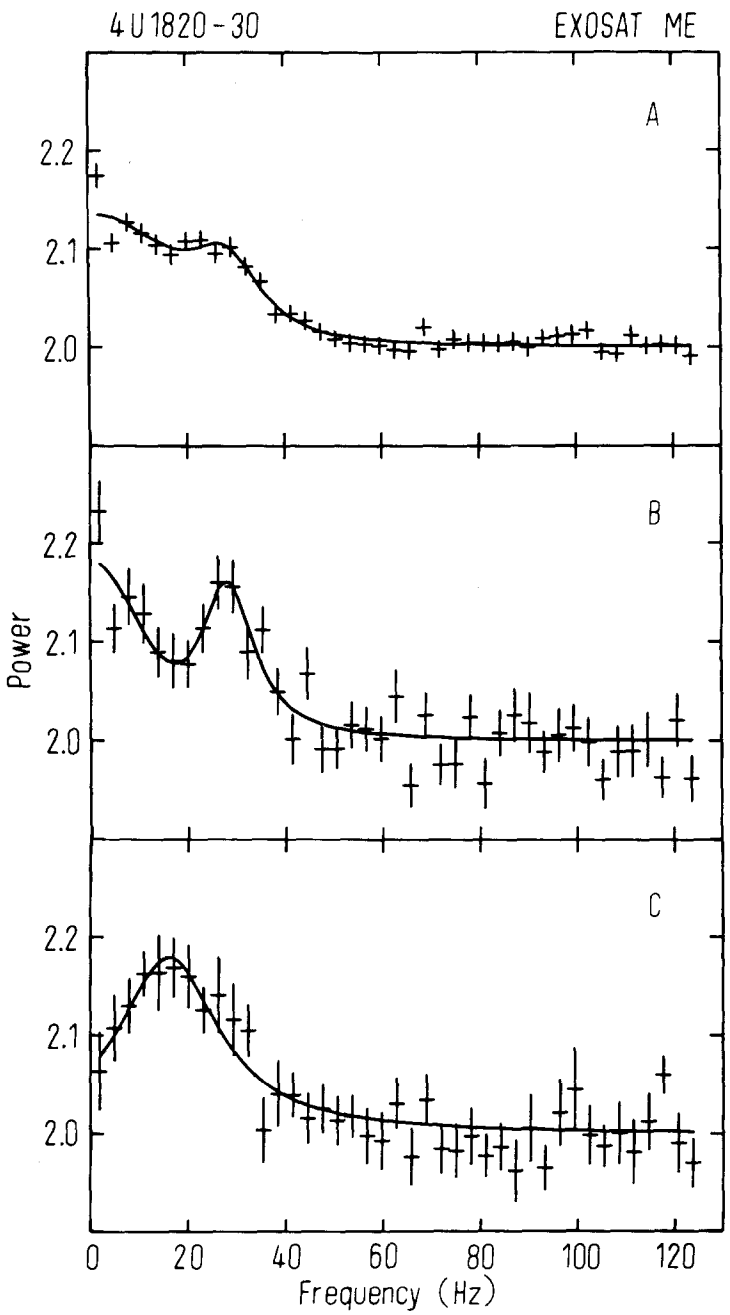

Fig. 3.31. Power spectra from EXOSAT ME 1–15 keV data (see Section 3.1) from 1820–30. (a) ~ 5 hr of data on September 22–23, 1985. (b) A 42-min interval near the middle of the observations. (c) A 30-min interval near the end of the observations. The solid lines indicate the best fits using a Lorentzian profile to describe a QPO peak, and a Gaussian (centered on zero frequency) to describe the red noise. This figure is from Stella *et al.* (1987b).

strength of this LFN increased with photon energy (this is similar to the above-mentioned findings of Stella *et al.* (1984); however, the frequency range is very different). On these longer time-scales there is a positive correlation between the hardness of the X-ray spectrum and the source intensity.

QPO were detected from 1820–30 (Stella *et al.*, 1987b) during one of the EXOSAT high-state observations, which was made with time resolutions varying between 0.25 and 2 ms (but no spectral resolution). The power spectrum of 1820–30 changed rapidly, on a time-scale as short as ~ 3 min (similar to the time resolution with which statistically significant power spectra could be made). During most of this observation red noise was found; in addition during several time intervals, lasting between 10 and 40 min, QPO were detected (Figure 3.31). Fits were made to the power spectrum, as obtained during two such intervals, with the red noise represented by a Gaussian (centered at zero frequency), and the QPO as a Lorentzian profile. The QPO centroid frequencies were 16.1 ± 1.2 and 28.2 ± 1.2 Hz; the corresponding values of the FWHM, and of the strength of the QPO (in terms of r.m.s. variation) are 13.3 ± 2.7 and 25 ± 4 Hz, and 5.9 ± 0.8 and $7.8 \pm 0.7\%$, respectively. The strength of the red noise was $4.4 \pm 0.6\%$ in the first of the two time intervals where QPO was detected; it was not detected during the second interval (the upper limit was 2.6% at a 90% confidence level). No dependence of the properties of the QPO and the red noise on the source intensity, spectral hardness, or orbital phase was found.

During part of this high-state observation the data were sampled in four energy channels with a sampling rate of ~ 256 Hz. No QPO was then detected, but the red noise was strong, with the r.m.s. variation increasing from $\sim 6\%$ r.m.s. in the photon energy range between 1–3 keV, to $\sim 13\%$ between 5–8 keV. The time resolution used in the two other high-state observations of 1820–30 (32 ms) made detection of QPO in the 15–30 Hz range difficult. During these observations red noise was present with an r.m.s. strength of 3% (integrated between 0.1–16 Hz).

During the one low-state observation the red noise was visible in the power spectrum up to ~ 50 Hz, with an r.m.s. strength of $14.3 \pm 0.3\%$ (i.e., three times that observed during the high state). QPO was then not detected, although the upper limit to the r.m.s. variation (6%) is not particularly strong.

No coherent pulsations were detected during any of the above EXOSAT observations; the 99.9% confidence limits on the pulsed fraction range between 1.5% (0.25–512 Hz) and 2.8% (512–2048 Hz) during the high state observations, and are less than 1.5% (0.125–256 Hz) during the low-state observation (Table I).

3.4. QPO IN CATACLYSMIC VARIABLES

Quasi-periodic oscillations (QPO) are commonly observed in the optical flux (in a few cases also in the X-rays) of dwarf novae in outburst (dwarf novae are accreting white dwarfs; see, e.g., Robinson and Nather, 1978; Patterson, 1981; Cordova and Mason, 1983). The time-scale of these oscillations ranges from ~ 10–10^3 s (frequency ~ 1 mHz–0.1 Hz), and the coherence ranges from a few oscillations up to $\sim 10^5$ oscillations. Optical QPO with very different coherence can be observed simultaneously

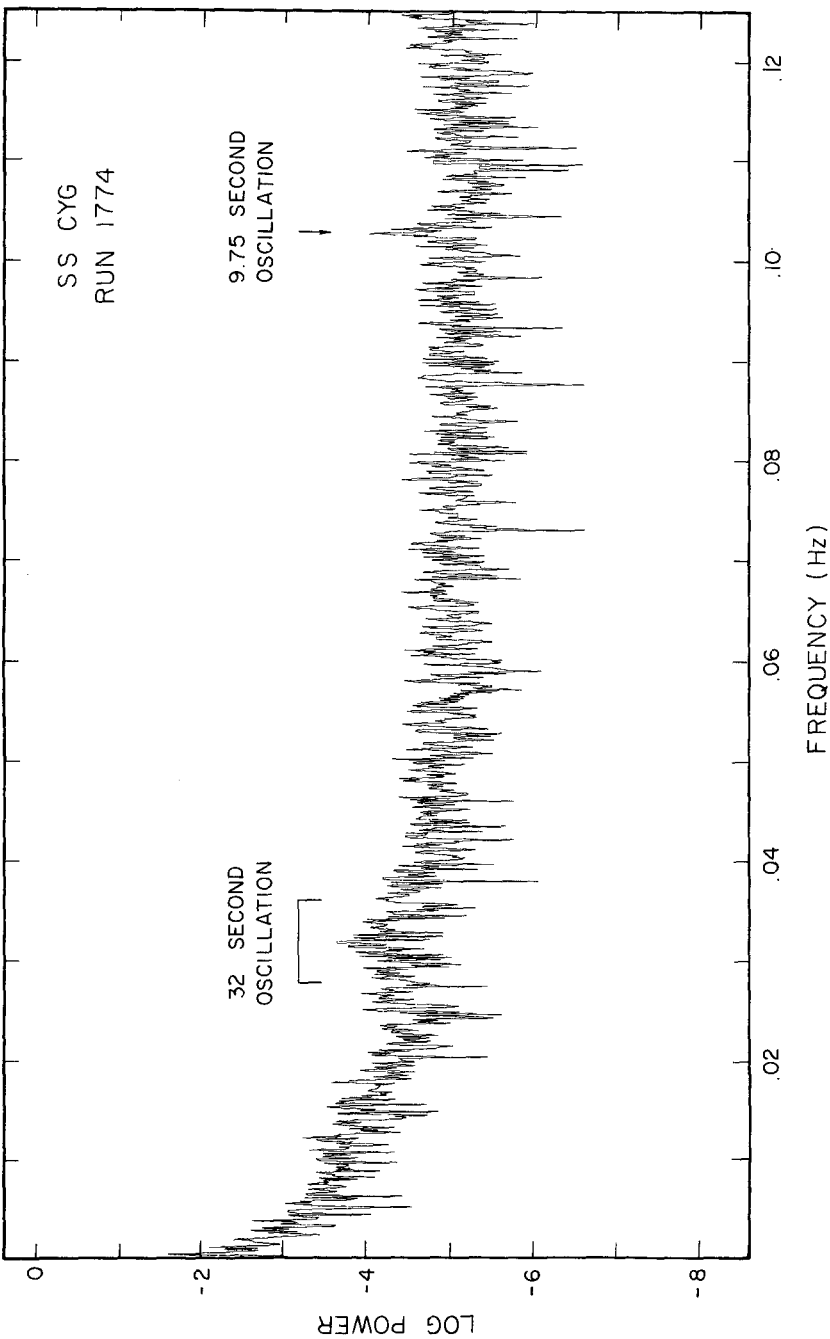

Fig. 3.32. Power spectrum of ~ 3.5 hr of optical data (4 s time resolution; Nyquist frequency of 0.125 Hz) from the cataclysmic variable SS Cyg taken at maximum of its eruption cycle. The spectrum shows quasi-periodic oscillations with a centroid frequency of ~ 0.32 Hz, and oscillations of ~ 0.103 Hz with a much higher coherence than the former. Note the red noise below ~ 0.04 Hz. This figure is from Robinson and Nather (1979).

at two frequencies (Figure 3.32). The strength of the optical oscillations is typically less than 1%. Many models have been proposed to explain these oscillations. Not one alone can explain the whole range of complex phenomena; it is almost certain that more than one mechanism is at work.

It is not surprising that several models on high-frequency QPO in the bright LMXB (see next chapter) reflect some earlier ideas for optical QPO in the cataclysmic variables. In scaling the geometry of an accreting white dwarf to that of an accreting neutron star, it is not too difficult to imagine a frequency increase by a factor of order $\sim 10^{2-3}$. Van der Klis *et al.* (1985b) explicitly examined the QPO models proposed for CV's for their applicability to LMXB.

4. QPO Models and a Confrontation with Observations

A variety of models has been proposed to explain some of the salient features of the QPO and the LFN. There are models where the QPO are the result of an oscillatory variation in the X-ray luminosity, in others (e.g., obscuration and disk oscillation models) the oscillations are the result of a modulation of a near-constant luminosity. Some models require the presence of a magnetosphere, others do not. Fast rotation of the neutron star is required by some models, but not by others. In most models (but not all) the radiation that is modulated in a quasi-periodic fashion originates at (or very near) the surface of the neutron star.

4.1. Application of Bath's model

More than a decade ago Bath (1973) suggested a model to explain optical QPO in cataclysmic variables (see Section 3.4). He suggested that the QPO frequency was that of the Kepler motion of matter orbiting a magnetized white dwarf at the magnetopause (inner edge of the accretion disk). This idea can be adapted to magnetized accreting neutron stars in an effort to explain the observed high-frequency QPO in X-rays. The radius, r_m, of the inner edge of the accretion disk for a gas-pressure dominated case (see Equation (1.1); however, for a radiation dominated case, see White and Stella, 1988) depends on the mass transfer rate, $\dot{M}$, at that radius, on the mass and radius of the neutron star, and on the magnetic dipole field strength, B, at the surface of the neutron star (Pringle and Rees, 1972; Davidson and Ostriker, 1973; Lamb *et al.*, 1973; however, see White and Stella, 1988). Combining the relation between r_m and $\dot{M}$ with Kepler's third law, and assuming that the Kepler frequency, ν_K (see Equation (1.2)), equals the QPO frequency, ν (Bath, 1973) one can easily find that

$$\nu \propto \dot{M}^{3/7} . \tag{4.1}$$

If we make the assumption that $\dot{M}$ depends linearly on the observed broad-band X-ray intensity, I, we find that the observed QPO frequency, ν, should be proportional to I to the power $\frac{3}{7}$, thus

$$\nu \propto I^{3/7} . \tag{4.2}$$

This was not observed when the intensity-dependent QPO in GX 5–1 were discovered; the exponent $d(\log \nu)/d(\log I)$, which we will call α, was ~ 2 (Van der Klis *et al.*, 1985a, b), instead of $\sim \frac{3}{7}$.

The disagreement between the expected value of α and the observed one was at first considered a strong reason to reject this model in favor of a beat-frequency scenario (see below) which allows for larger values of α. It was later realized that the observed X-ray flux may not depend linearly on the mass accretion rate, and a β parameter was introduced to take this into account (see Equation (4.7)). Equation (4.2) would then become

$$\nu \propto I^{3/(7\beta)}, \tag{4.3}$$

[thus $\alpha = 3/(7\beta)$]. A very large range of values for α is now allowed, and the model has lost its predictive power as far as α is concerned, but that alone is not a valid reason to reject it. For GX 5–1 a value for $\beta \sim 0.21$ is required, to 'explain' the observed value of $\alpha \sim 2$. (*Note*: according to J. Shaham, private communication, the most probable value for β in the horizontal branch is $+1$.)

This model may have difficulties explaining the 0.44 Hz and the ~ 2 Hz QPO in the Rapid Burster, and perhaps also the ~ 6 Hz QPO, observed in several sources (see Table I, and Section 3) as it would lead (for a $1.4\,M_\odot$ neutron star) to large magnetospheric radii of $\sim 3 \times 10^3$ km (0.44 Hz) and $\sim 5 \times 10^2$ km (6 Hz). Such large radii imply very strong magnetic fields, similar to those of X-ray pulsars, and they would probably reveal themselves in the form of coherent X-ray pulsations.

4.2. Beat-frequency models (BFM)

In the beat-frequency model (Alpar and Shaham, 1985a, b), the observed QPO frequency is the difference between the Kepler frequency at the magnetopause, ν_K, and the rotation frequency, ν_n, of the neutron star

$$\nu = \nu_K - \nu_n . \tag{4.4}$$

In this model, small changes in ν_K can lead to large changes in ν. If again the assumption is made that the mass transfer rate, $\dot{M}$, at the magnetopause depends linearly on the observed broad-band X-ray intensity, and if one adopts Equation (1.2), which holds for a gas-pressure dominated case (for radiation dominated cases, see White and Stella, 1988), one finds that

$$\alpha = 3\nu_K/7\nu . \tag{4.5}$$

Combining Equations (4.4) and (4.5) leads to

$$\nu_n = \nu(7\alpha/3 - 1) . \tag{4.6}$$

If, as an example, we take an approximate average value for the observed QPO frequency, ν, in GX 5–1 of 30 Hz, then, with $\alpha \approx 2$ (as observed), $\nu_K \approx 140$ Hz (Equation (4.5)), and $\nu_n \approx 110$ Hz (Equation (4.6)). Assuming a mass for the neutron star of $1.4\,M_\odot$, with Kepler's law we can then also find the radius of the inner edge of

the accretion disk (here ≈ 55 km). If, in addition, one assumes a radius for the neutron star (e.g., 10 km), and one estimates the mass transfer rate at the magnetopause (this can be done from an estimate of the distance to the source, and from the observed broad-band X-ray intensity), one also finds the magnetic dipole field strength, B, at the surface of the neutron star, using the equations given by Lamb *et al.* (1973). For GX 5–1, $B \approx 6 \times 10^9$ G. Somewhat similar values for B and ν_n can be inferred for Cyg X-2, Sco X-1, and GX 17 + 2 from the QPO data in the range above ~ 15 Hz where the observed values for α were positive (however, not for the QPO in the range near ~ 6 Hz; see below).

It was at first puzzling (and perhaps it still is) why, if the BFM were correct, in GX 5–1 no coherent X-ray pulsations (of ~ 110 Hz) were observed. However, a number of studies have shown that for certain geometries the observable fraction of coherent pulsations can be strongly suppressed (Bussard *et al.*, 1988; Brainerd and Lamb, 1987; Kylafis and Klimis, 1988; Wang and Schlickheiser, 1987; Mészáros *et al.*, 1988). The best upper limits on coherent pulsations in the range of a few Hz to 512 Hz are 0.4–1% for GX 5–1 (Section 3.3.1; Van der Klis *et al.*, 1985b), 0.3–0.5% for Sco X-1 (Middleditch and Priedhorsky, 1986; Hasinger and Van der Klis, 1987)*, $\sim 0.4\%$ for Cyg X-2 (Norris and Wood, 1987).

There is strong evidence that the observed X-ray flux (even observed in a broad band) is not always linearly proportional to the mass accretion rate $\dot{M}$. It has been suggested that at times (when the source is in the 'normal branch') $\dot{M}$ might increase (decrease) while the observed flux decreases (increases) (see, e.g., Figure 3.17; Priedhorsky *et al.*, 1986). In the context of the BFM this could then explain why, for instance in Sco X-1, the QPO frequency goes down, while the source flux increases (Priedhorsky *et al.*, 1986; Van der Klis *et al.*, 1987b).

Therefore, Lamb *et al.* (1985) do not assume that the observed X-ray intensity is linearly proportional to $\dot{M}$, but rather

$$I \propto \dot{M}^{\beta} . \tag{4.7}$$

For n-fold symmetry in the magnetic field pattern (Lamb *et al.*, 1985), Equation (4.4) becomes

$$\nu = n(\nu_K - \nu_n) \quad (n = 1, 2, 3, \ldots) . \tag{4.8}$$

We then find for a gas-pressure dominated case (i.e., under the assumption that Equation (1.2) holds)

$$\alpha = 3n\nu_K / 7\beta\nu . \tag{4.9}$$

Notice that α and β can be both negative or both positive, but they cannot have opposite signs. Combining Equations (4.8) and (4.9), leads to

$$n\nu_n = \nu(7\alpha\beta/3 - 1) . \tag{4.10}$$

* There is a recent report by Leahy (1987) of 2.93 ms coherent pulsations in Sco X-1 in the energy range 20–120 keV (the r.m.s. amplitude of the pulsations are $\sim 20\%$, private communication). However, see also Hasinger and Van der Klis (1987).

Priedhorsky *et al.* (1986) found in Sco X-1 a '6-Hz QPO branch' in which the QPO frequency was *anti-correlated* with the source intensity ($\alpha \approx -0.6$). A '15–20 Hz QPO branch' in which the QPO frequency was correlated with the source intensity ($\alpha \approx +3$) was also found (Van der Klis *et al.*, 1985c, 1987b; Priedhorsky *et al.*, 1986). With the observed values for ν and α (using Equation (4.10)), we can now only find the neutron star rotation rate* if w eknow the β* values (or, if we know the neutron star's rotation we can calculate the values for β for the various source states). Priedhorsky (1986a) has proposed that the X-ray luminosity may at times be tapped at the expense of rotational energy of the neutron star. This could explain how a decrease in mass accretion could lead to an increase in the observed X-ray flux (β and α would then be negative).

There may be other ways to explain an anti-correlation between QPO frequency and source intensity in the framework of the BFM. For instance, one could assume that the magnetospheric radius is larger than the co-rotation radius (i.e., $\nu_K < \nu_n$). However, in this case accretion may be inhibited by centrifugal forces. Priedhorsky (1986a) proposed that the anti-correlation is the result of accretion-torque related energy flows from the rotational energy of the neutron star into the disk during periods of spin-down when the mass accretion is low, but when accretion can still occur (cf. Ghosh and Lamb, 1979).

Tennant (1987b) suggested that Equation (4.4) may well hold but that the inner radius of the accretion disk (and the corresponding Kepler frequency) is not determined by a magnetosphere, but by another critical radius. If this critical radius were governed, for instance, by the condition L/r^2 = constant (L is the luminosity), he finds that

$$\nu = CI^{-3/4} - \nu_n \quad \text{(here, } C \text{ is a constant).}$$

Particular versions of the beat-frequency scenario have been discussed by several groups (Lamb *et al.*, 1985; Van der Klis *et al.*, 1985b; Berman and Stollman, 1985; Lamb, 1986). Lamb *et al.* (1985) suggest that the beat phenomenon is the result of inhomogeneous matter distribution ('blob formation') at the inner edge of the accretion disk. The matter in the blobs is gradually stripped off by interaction with the magnetic field which is anchored in a spinning neutron star. If the rotation axis and the dipole axis are not co-aligned, the rate at which matter can penetrate the magnetosphere will be different for different azimuthal directions in the frame of the rotating neutron star. The matter will then reach the surface of the neutron star in a quasi-periodic fashion with a frequency equal to the difference between the (variable) Kepler frequency of the blobs and the (fixed) rotation frequency of the neutron star (see Equation (4.4)) [or n times that for n-fold symmetry (see Equation (4.8))]. While a blob is 'milked' in a piecemeal fashion the X-ray flux, originating from the neutron star surface, oscillates (producing QPO), while the mean X-ray flux is temporarily increased. The latter variation gives rise to low-frequency noise (LFN). The model can be represented by

* For instance, if β were $\sim +9$ in the 15–20 Hz branch, and ~ -120 in the 6-Hz branch, the rotation frequency $n\nu_n$ would be $\sim 10^3$ Hz. On the other hand, if we knew that the rotation rate ($n\nu_n$) were $\sim 10^2$ Hz the values for β would have to be $\sim +1$, and ~ -13, respectively.

oscillating 'shots'. The oscillatory part of the shots determines the QPO characteristics; the overall envelopes of the shots determine the LFN characteristics. The blobs are produced at random times, and with a random equatorial azimuthal distribution. For a sufficiently large number of blobs, the 'crests' of the oscillations, produced by one blob, will coincide with the 'valleys' of those produced by some others. In the case that the

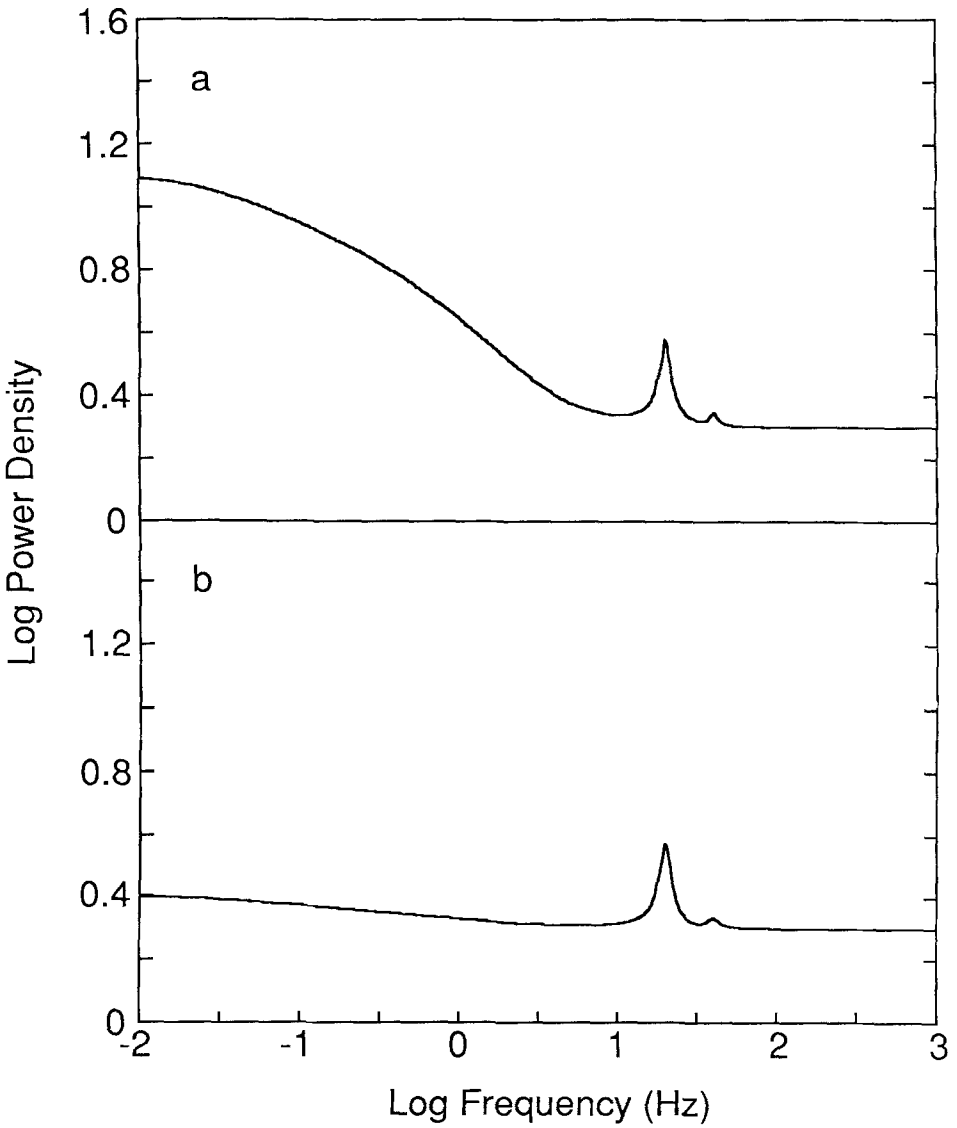

Fig. 4.1. Theoretical power spectra for a model involving oscillating shot noise without correlation between the phases of the oscillations of the different shots (panel a), and with such correlation (panel b). The strength of the red noise can be made arbitrarily small, relative to that of the QPO, by properly choosing the various parameters in the shot-noise models. This figure is from Shibazaki and Lamb (1987; for all details we refer to their paper).

flux is dominated by the contributions of the shots, the fractional r.m.s. variations of the QPO and the LFN will then decrease (see Equation (2.34)).

In this scenario, LFN is a logical consequence of the QPO, and it was proposed as an explanation for the first QPO observations of GX 5–1 where the QPO strength and the LFN strength went 'hand in hand' (Van der Klis *et al.*, 1985). However, in later observations of, e.g., Cyg X-2, Sco X-1, and the Rapid Burster this was not the case (Van der Klis *et al.*, 1985c, 1987b; Hasinger *et al.*, 1986; Van der Klis, 1986a, b; Van der Klis and Jansen, 1986; Stella, 1986; Lewin, 1986; Stella *et al.*, 1988a); QPO were observed in the near absence of LFN. In recent papers, it has been argued that for a variety of reasons the LFN can be strongly suppressed in the presence of QPO, particularly if the pulses from different blobs are partially coherent (crests from one blob support crests from other blobs); this would happen if the blobs could appear in clusters (Shibazaki and Lamb, 1987, see Figure 4.1; Shaham, 1987; Brainerd *et al.*, 1986; Elsner *et al.*, 1987).

There is another, but very different, beat-frequency scenario. Morfill and Trümper (1986) suggest that the supersonic stirring of the disk by an inclined magnetic field causes shock waves which interact with disk inhomogeneities (plasmoids) which are in Keplerian rotation. The plasmoids are hotter than their environment. This results in a quasi-periodic signal at the beat frequency given by Equation (4.4). Here the QPO signal does not come from the surface of the neutron star but from the plasmoids in the magnetopause. Thus the available energy for the QPO is dictated by the radius of the magnetopause. If the latter were, e.g., ten times that of the neutron star, the maximum available energy in the plasmoids (to produce QPO) would be $\sim 10\%$ of the total X-ray flux. The QPO mechanism could not be 100% efficient (see Lamb, 1986). This model could, therefore, perhaps explain QPO with a modest strength, but it is hard to see how it could explain the high percentages observed in, e.g., GX 5–1 (up to $\sim 6\%$ r.m.s. variation), Sco X-1 (up to $\sim 8\%$ at high-energy X-rays), and the Rapid Burster (up to $\sim 35\%$) (see Section 3).

4.3. Disk reflection model

Boyle *et al.* (1986) proposed that the QPO are produced by a hot ($> 10^7$ K) accretion disk corona. X-rays produced at the central source (the neutron star) scatter off oscillating disturbances in this corona near the inner disk. The oscillations are in a direction perpendicular to the disk plane (disk oscillations); they have a frequency approximately equal to the local Kepler frequency (see, e.g., Pringle, 1981). Thus, for a 1.4 $M_\odot$ neutron star, QPO frequencies of ~ 100 and ~ 1 Hz, would correspond to an effective scatter radius of ~ 80 km (~ 8 stellar radii) and $\sim 1.6 \times 10^3$ km (~ 160 stellar radii), respectively. No magnetic field, and no neutron star rotation are required.

The X-rays scatter off the $\tau \sim 1$ surface. Since the observed peaks (QPO) in the power spectra have widths of typically ~ 10 to $\sim 20\%$, a very restricted range of radii of this scattering surface is required. The spread in radii of the effectively contributing part of this surface (as seen from Earth) should be no larger than $\sim 30\%$. Thus this scatter surface must be very steep and well localized. The scatter surface should more or less

behave as a rising and falling 'wall' in order to obtain a strong modulation in those X-rays that are scattered. The authors predict that those systems seen at low inclinations are favored (no QPO should be seen from eclipsed systems).

It is hard to see how the disk reflection mechanism could produce the high strength of QPO (typically $\sim 5\%$ r.m.s. variation, but up to $\sim 35\%$ in the Rapid Burster). If the modulation efficiency (of scattered X-rays only) were as high as $\sim 10\%$, one would expect to observe a modulation in the total X-ray signal (scattered and non-scattered) of only $\sim 1\%$. If the central source were obscured, and only the scattered X-rays were seen, the observed modulation could be permanently much higher. This, however, is not the case for most (if not all) QPO sources as they are very bright.

4.4. The neutron star envelope

Hameury *et al.* (1985) proposed a scenario which does not require the presence of a magnetopause. The QPO are the result of hot spots rotating in the boundary layer where the accreting matter settles onto the surface of a slowly rotating (with period of order ~ 1 s) neutron star. The authors suggest that transient magnetic fields are generated locally due to turbulent dynamo action (analogous to sun spots), and that hot spots are formed locally by conduction along the magnetic field lines. QPO are then the result of repeated occultations of the hot spots when they rotate out of our line of sight to the 'back side' of the neutron star. The low-frequency noise results from the finite lifetime of the hot spots, and from contributions of those spots that are never occulted due to their high latitude. Hameury *et al.* (1985) predict that the QPO spectrum is that of a blackbody with a radius less than that of the neutron star.

The 'available' frequencies in this model range all the way from ~ 1 Hz (at the bottom of the boundary layer, rotating with the neutron star frequency) to $\sim 10^3$ Hz (at the very top of the boundary layer, rotating with the Keplerian frequency). If this scenario were operating, it is puzzling why the observed QPO frequencies vary in limited ranges (e.g., in GX 5–1, for QPO in the horizontal branch, by a factor of ~ 2), and why the peaks in the power spectra (in the horizontal branch state) are so narrow (typically ~ 10 to $\sim 30\%$). Since in this model the LFN is a logical consequence of the QPO, it may also be difficult to explain those cases where LFN is nearly absent in the presence of strong QPO. It is also unclear whether the hot spots could contain such a high fraction of the available gravitational potential energy to explain the observed high strength of QPO (typically $\sim 5\%$ r.m.s. variation, but up to $\sim 35\%$ in the Rapid Burster).

A particular hot spot would have to appear and disappear (occultation) at least three or four times to produce the observed QPO. The QPO with a fundamental frequency of ~ 0.44 Hz in the Rapid Burster would thus require a lifetime of the hot spots of at least ~ 10 s. According to Jean Paul Lasota (private communication), the lifetime of one hot spot is probably less than a few seconds. Thus, if this is so, the very low-frequency QPO could not be explained with this 'stellar spot' scenario.

Non-radial g-mode oscillations of the neutron star envelope can have periods in the frequency range observed in horizontal-branch QPO (McDermott and Taam, 1987). The frequency of these oscillations increases with temperature of the envelope. Thus,

if these oscillations are associated with the QPO, one might expect a positive correlation between QPO frequency and the luminosity from the neutron star surface. It is perhaps interesting to note here that there is some evidence that the QPO frequency in Cyg X-2 and Sco X-1 is related to the luminosity of a possible blackbody component in their X-ray spectra which is believed to originate from the neutron star surface (Hasinger, 1986a; Van der Klis *et al.*, 1987b; see, however, also Section 5.2). It is unclear how oscillations of the neutron star envelope can lead to oscillations in the observed X-ray flux with amplitudes of a few percent (and as high as $\sim 30\%$; see Section 3).

Hasinger (1987b) suggests that the ~ 6 Hz QPO often observed in the normal branch spectral state, result from a modulation of the X-ray flux by a non-radial resonant sound wave in the Eddington limited accretion flow above the neutron star surface (thus in a region which is dominated by radiation pressure; Ponman *et al.*, 1988). He argues that the frequency of the fundamental depends very weakly on the mass accretion rate ($\nu \propto \dot{M}^{1/8}$) and is mainly determined by the radius of the neutron star.

4.5. Occultation models

It was suggested by several authors (Van der Klis *et al.*, 1985b; Stella, 1986; Van der Klis *et al.*, 1987b) that QPO could be the result of quasi-periodic partial occultation of the X-ray source by orbiting clumps or by an oscillating disk. Occultation models do not suffer from a lack of available energy for the QPO (Lewin, 1986, 1987a). Van der Klis *et al.* (1987b) show that the absence of LFN in the presence of strong QPO is expected if the region which is quasi-periodically occulted is uniform in its X-ray emission properties. They suggest that this uniform emission region may be a polar funnel (cf. Lamb *et al.*, 1985) in a geometrically thick inner accretion disk filled with X-ray scattering plasma. This would provide an extended X-ray source which for a large range of inclinations can undergo partial occultation by the thick inner disk.

4.6. General relativistic instabilities

Paczynski (1987) believes that the absence of X-ray pulsations indicates that the QPO sources have no magnetospheres. He points out that in most non-rotating neutron star models the radius of the neutron star is smaller than 3 times the Schwarzschild radius ($3R_s$). In an analogy with black holes (Muchotrzeb, 1983), Paczynski (1987) suggests that a steady-state flow of matter through the marginally stable orbit at $3R_s$ may not be possible when the viscosity parameter α, which determines the angular momentum transport in the disk (see, e.g., Pringle, 1981), is larger than ~ 0.03. An unsteady flow would make the X-ray luminosity at the neutron star surface variable, possibly giving rise to QPO.

5. Time Lags

5.1. Time lags in QPO and LFN

Following the discovery of intensity-dependent high-frequency QPO, the EXOSAT Observatory team developed on-board data-processing modes which made it possible

to make high time resolution observations with spectral resolution. These observations allow measurements of the X-ray energy dependence of the strength of the QPO and LFN, and of possible time lags between the signal at different energies.

The first detection of such a time lag in the X-ray signal of an LMXB was made by Hasinger (1987a) from a cross-correlation analysis of ~ 12 hr of data (time resolution ~ 4 ms), and 20 hr of data (~ 3 ms resolution) for Cyg X-2 in the 4.5–17 and 1–4.5 keV bands. The source was then in the horizontal branch of the hardness-intensity diagram, and showed 20–50 Hz QPO. Hasinger (1987a) found that the high-energy photons were delayed with respect to the low-energy photons by a few ms (see Figure 3.10); this time lag is, therefore, called 'hard' lag. He suggested that the hard lags are the result of (inverse) Comptonization of X-rays, originating from the near vicinity of the neutron star, in a surrounding hot coronal cloud; the more scatterings an X-ray makes in the cloud, the higher will its energy be (on average), and the longer will it take to emerge from the cloud (Shapiro *et al.*, 1976; Priedhorsky *et al.*, 1979; Payne, 1980; Pozdnyakov *et al.*, 1983; Page, 1985). Hasinger (1987a) found that the time lags become smaller when the source intensity increases, and the QPO frequency becomes higher (see Figure 3.13).

A cross correlation does not allow us to identify the frequencies that contribute to the time lag; these frequencies are not necessarily those of the QPO. A Fourier cross-spectral analysis, however, does give the time lags as a function of Fourier frequency (see Section 2.4). From such an analysis Van der Klis *et al.* (1987c) found that the time lag in Cyg X-2 (horizontal-branch data) is caused by variations in the QPO frequency range (see also Van der Klis, 1986b). The average time lag in the QPO frequency range varies between ~ 4 ms and < 1 ms, and is anti-correlated with the QPO frequency, as found earlier by Hasinger (1987a).

From similar cross-correlation (Van der Klis, 1986b) and cross-spectral (Van der Klis *et al.*, 1987c) analyses of 12.5 hr of EXOSAT data for GX 5–1, it was found that for this source (in the horizontal branch state) there is also a marginally significant hard lag in the QPO frequency range; for similar QPO frequencies the lags observed for GX 5–1 are much smaller than for Cyg X-2 (average value 0.44 ± 0.17 ms). The time lags in the QPO of GX 5–1 do not show a clear trend with QPO frequency, although they are formally incompatible with a constant value.

The 5.6 Hz QPO in Cyg X-2 (observed during the normal branch) show a possible hard lag of 6.2 ± 2.7 ms (averaged over the 5.58–6.11 Hz range) between the 0.7–2.9 and 2.9–4.5 keV energy channels (Van der Klis *et al.*, 1987c).

In the frequency range below ~ 10 Hz, which during the horizontal-branch spectral state is dominated by the LFN, there is a 'soft' lag for both sources, which near 2 Hz reaches average values of ~ 15 ms (Cyg X-2), and ~ 6 ms (GX 5–1). There is some evidence that the soft lag (averaged over 1–10 Hz) changes with QPO frequency, between < 6 ms to ~ 12 ms for Cyg X-2, and between < 2 ms and ~ 4 ms for GX 5–1. Van der Klis *et al.* (1987c) showed that soft lags in the LFN do not necessarily invalidate the interpretation of the hard lags in the QPO in terms of Comptonization; they can, e.g., occur if the QPO are due to 'modulated shots' with spectral softening during their decay (see also Van der Klis, 1986b; and Shibazaki *et al.*, 1988).

A cross-spectral analysis by Stella *et al.* (1988b) shows that in the Rapid Burster 'soft' lags occur in > 3.6 Hz persistent emission QPO (Stella *et al.*, 1988a), with the 1–5 keV signal lagging the 5–21 keV signal by ~ 8 ms. No significant time lags could be measured in the QPO during bursts, and in the 0.5–3.6 Hz persistent emission QPO. However, only in the > 3.6 Hz QPO in bursts was the upper limit tight enough to exclude the 8 ms time lag found in the > 3.6 Hz persistent emission QPO. This soft lag may cast some doubt on the above Comptonization interpretation. However, it is perhaps possible that in the case of the Rapid Burster the scattering cloud is relatively cold, so that the X-rays, on average, lose energy when they scatter. Another possibility is that the sign of the lag is in some way connected with the time scale of the variation, so that the soft lags in the QPO in the Rapid Burster would have the same origin as those in the LFN in GX 5–1, and Cyg X-2. However, the following results seem to invalidate this idea.

Recently Mitsuda *et al.* (1988) presented results of QPO observations of Cyg X-2, GX 5–1, and 4U 1820 – 30, made with the Japanese X-ray satellite *Ginga*. For QPO observed during the normal branch, with frequencies in the ~ 5 Hz range, they report large 'hard' delays (over the energy range ~ 1–20 keV) for all three sources. From a cross-correlation analysis they find 80 ± 30 ms for GX 5–1, and 20 ± 10 ms for 4U 1820 – 30. A cross-spectral analysis of their Cyg X-2 data (7.9–12.3 and 1–2.9 keV) shows that the time lag is caused by variations in the QPO frequency range. There is no significant relative delay between ~ 1 and 5 keV; however, for energies above 5 keV the delay rises strongly, to 70 ± 10 ms at 15 keV.

5.2. Evidence for comptonizing coronae in LMXB?

The results summarized in Section 5.1 suggest that Comptonization of low-energy photons in a cloud or corona of high-energy electrons around the neutron star may produce the hard time lags observed in several QPO sources. (However, as discussed in Section 5.3, the observed soft lags in the QPO of the Rapid Burster, in combination with a positive correlation between the QPO strength and X-ray energy, suggest that other mechanisms possibly play a role.) Compton-scattering has also been suggested as an explanation of the very large width of the Fe emission line near 6.7 keV (White *et al.*, 1985, 1986) and as a means to suppress the amplitude of coherent pulsations in LMXB (see, e.g., Brainerd and Lamb, 1987; Kylafis and Klimis, 1988).

It should be noted that if the delays of a few milliseconds are due to Comptonization, the size of the scattering medium is $\sim 10^{7-8}$ cm (Hasinger, 1987a; Stollman *et al.*, 1987). This medium should, therefore, not be confused with the scattering accretion-disk coronae, whose much larger sizes (10^{10-11} cm) have been inferred from the partial-eclipse profiles observed in several LMXB (see Mason, 1986). [For the very large delays, up to ~ 70 ms (Mitsuda *et al.*, 1988), a possible Comptonizing cloud should have dimensions of order 10^{9-10} cm.]

Several groups have tried to derive emission mechanisms, and emission geometries from spectra of LMXB, and some report that their data show evidence for the existence of a Comptonizing hot cloud (Hirano *et al.*, 1984; Shibazaki and Mitsuda, 1984; Mitsuda *et al.*, 1984; White *et al.*, 1985, 1986, 1987). In a recent paper, Vrtilek *et al.*

(1988) point out that none of the proposed geometries, and models provide unique fits to the data and that it is often not possible to explain different observations of the same source. They also note that different instruments seem to favor different models for the same sources, and that no one can uniquely select one.

Using data from the medium resolution Solid State Spectrometer (SSS) of the *Einstein* Observatory, Vrtilek *et al.* (1988) find an enormous improvement in spectral fits of data from 5 LMXB if 'invisible' emission lines are taken into account. The lines can not be seen in the SSS spectra, but their presence is known from data taken with the *Einstein* high-resolution Objective Grating (OGS). It is evident from their work that many (if not all) interpretations of LMXB spectra taken with Hakucho, Tenma, and EXOSAT could be incorrect. Lewin and Van Paradijs (1985b) have independently expressed their reservations about the correctness of the spectral interpretations of LMXB.

It has long been recognized that an understanding of the formation of X-ray spectra of LMXB is a key element in the physics of the accretion processes in these systems. In the often-used spectral model of White *et al.* (1986), most of the X-ray emission is due to Comptonization (up-scattering) of very low-energy photons; the question then arises why most of the energy liberated during the accretion process does not originate at the surface of the neutron star, but is in the form of kinetic or thermal energy of electrons in the scattering medium (Stollman *et al.*, 1987; for a discussion of this issue, see also Shibazaki *et al.*, 1987). If Comptonization is the cause of (or at least some of) the observed time delays, a combination of spectral and timing studies could perhaps lead to a better understanding of the X-ray spectra of LMXB (Figure 5.1; see, e.g., Wijers *et al.*, 1987; Bussard *et al.*, 1987).

5.3. Consequences of the time lags for QPO models

With regard to the time lags we can divide most QPO models, but not all, between two types. In the first type of model the QPO in the X-ray signal originate at the neutron star surface (see Sections 4.2, 4.4, 4.6); in the second type of models the X-ray luminosity from the neutron star itself is constant, but the observed flux modulation originates at a large distance from the neutron star (see Sections 4.3, 4.5). As shown by Stollman *et al.* (1987) the presence of time lags cannot, by itself, decide between these types of model. However, as pointed out by Stella *et al.* (1988b), if time lags of the QPO signal are due to Comptonization of a constant signal in a cloud with an oscillating scattering optical depth (such oscillating clouds exemplify, e.g., the obscuration model of Van der Klis *et al.*, 1987b), the variation with X-ray energy of the QPO strength depends mainly on the properties of the scattering cloud. For a hot (cold), up- (down-) scattering cloud, one expects that the QPO strength increases (decreases) with X-ray energy.

The strength of the QPO in the persistent emission of the Rapid Burster, which show an ~ 8 ms soft lag, increases with X-ray energy. Within the framework of Comptonization models for time lags in QPO, the soft lag implies a cold scattering cloud. If a cold cloud, occulting the central source in an oscillatory manner, would produce the QPO,

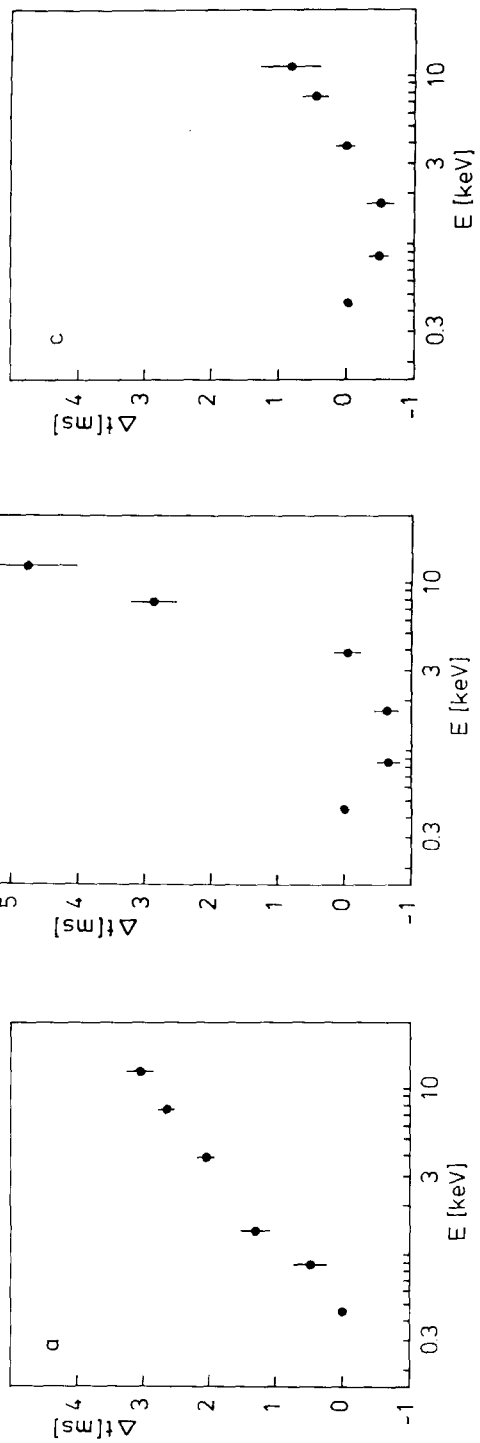

Fig. 5.1. Plots of the relative arrival times of X-ray photons in six energy bands (covering the range from 0.32–16 keV) for different input spectra, and different parameters of the Comptonizing cloud. The arrival time of the photons in the 0.32–0.63 keV band are set at zero. The parameters of the Comptonizing cloud were chosen in each case to reproduce reasonably well the observed X-ray spectrum of GX 5–1. (a) Input spectrum: a black-body with kT = 10 eV; cloud parameters: radius 10^7 cm, optical depth 9.5, electron temperature (kT) = 4.0 keV. (b) Input spectrum: a black-body with kT = 0.5 keV; cloud parameters: radius 4×10^7 cm, optical depth 5.5, electron temperature (kT) = 4.0 keV. (c) Input spectrum: a black-body with kT = 2.0 keV; cloud parameters: radius 4×10^7 cm, optical depth 6.0, electron temperature (kT) = 7.0 keV. This figure is from Wijers *et al.* (1987).

one would expect the strength of the QPO to be lower at high-energy X-rays than at low-energy X-rays, and that is the opposite of what is observed. Based on this, perhaps somewhat naive interpretation, the second type of QPO models cannot account for the QPO in the persistent emission of the Rapid Burster. The same problem exists, in principle, also for the other type of model, although in these models the initial energy dependence of the QPO strength can be appropriately chosen. It is, of course, entirely possible that in the case of the Rapid Burster the delays are due to a different mechanism.

The second type of model may also have a problem to explain the 70 ms hard delay in the 5–6 Hz QPO reported by Mitsuda *et al.* (1988). The inferred cloud size is of order 10^9 cm (Stollman *et al.*, 1987; Bussard *et al.*, 1988); it is hard to see how a cloud this big can oscillate at a 6 Hz frequency, which has a corresponding Kepler radius of only $\sim 5 \times 10^7$ cm (for a 1.4 $M_\odot$ neutron star).

If the hard lags are the result of Comptonization in a hot cloud (this remains to be seen), those models in which the QPO frequency reflects directly the Kepler frequency (e.g., Boyle *et al.*, 1986) can be excluded if it can be shown convincingly that the cloud is smaller than the corresponding Kepler radius. (Note, that for beat-frequency models this Kepler radius is not so strongly constrained, particularly not if it is not assumed that the source intensity is proportional to the accretion rate, see Section 4.2.) For the ~ 30 Hz horizontal-branch QPO in Cyg X-2 and GX 5–1 the corresponding Kepler radius would then be $\sim 2 \times 10^7$ cm (for a 1.4 $M_\odot$ neutron star). The relation between delay and cloud size depends sensitively on the assumptions made about the spectrum of the primary photons which are up-scattered in the cloud. On the basis of presently available calculations, cloud dimensions inferred from the observed delay of ~ 2 ms in Cyg X-2 range between $\sim 2 \times 10^7$ cm (Stollman *et al.*, 1987) and $\sim 10^8$ cm (Bussard *et al.*, 1988). For the < 1 ms delay observed in the 30 Hz QPO in GX 5–1 the corresponding cloud sizes are $< 10^7$ cm and $< 5 \times 10^7$ cm, which may be uncomfortably close for these models. However, we feel that until the time lags are better understood (and this may require a better understanding of the formation of the X-ray spectrum of LMXB, see Section 5.2), it is probably premature to exclude models on the basis of the observed time lags alone.

6. Discussion and Concluding Remarks

Quasi-periodic oscillations (QPO) have been detected in ten bright low-mass X-ray binaries; no known X-ray pulsars show the high-frequency ($\gtrsim 1$ Hz) QPO phenomenon as discussed in detail in this review. The characteristics of the QPO and the low-frequency noise (LFN), and their relation to the source flux are often complex.

Phenomenologically some 'order' seems to be present (Hasinger, 1987a, b; see also Stella, 1986, 1988). For most (~ 6) sources, QPO can be divided into two types: the 'horizontal-branch QPO', and the 'normal-branch QPO' (see Figure 6.1). The horizontal-branch QPO have the following characteristics: (i) they have frequencies in the range ~ 20–50 Hz, (ii) they are associated with strong low-frequency noise (LFN), and

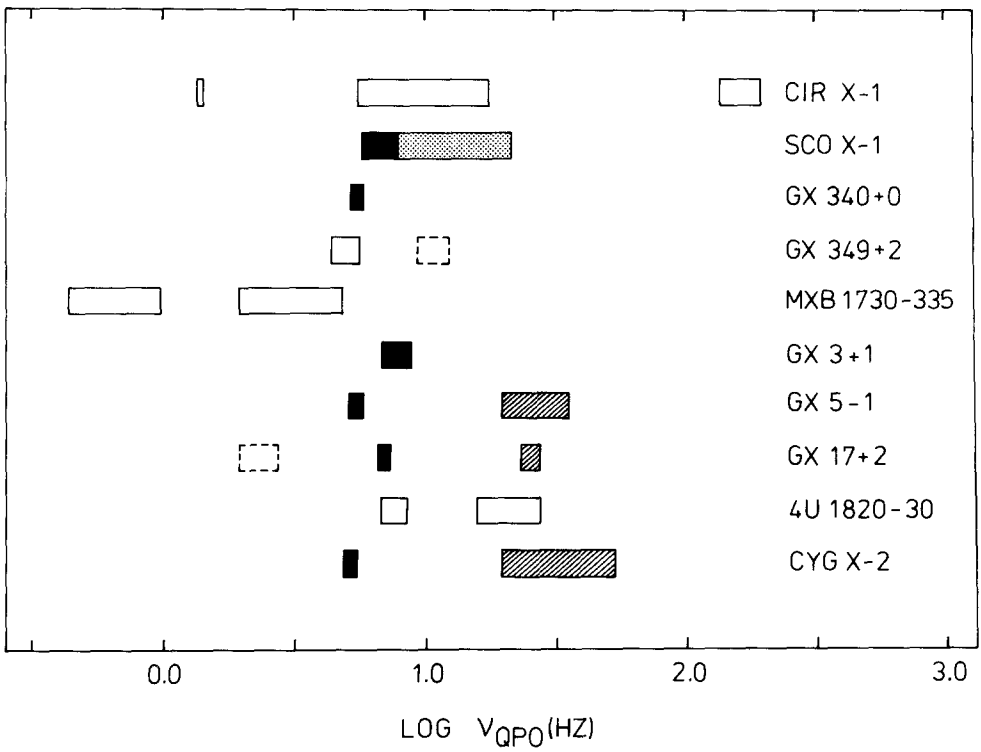

Fig. 6.1. Summary of observed QPO in the LMXB. The black areas indicate QPO observed in the normal branch (NB) state. The hatched areas refer to the horizontal branch (HB). The dotted area refers to the flaring-branch QPO in Sco X-1. The dashed boxes for GX 349 + 2 and GX 17 + 2 indicate that these QPO detections are somewhat uncertain. When the spectral state could not be determined in terms of NB, HB or flaring branch (see Section 1.5, and Table I), the boxes are open. This figure is an adapted version from Hasinger (1988).

(iii) their centroid frequency is strongly correlated with the observed source flux. The normal-branch QPO have frequencies near ~ 6 Hz, and they are not associated with strong LFN. Very low-frequency noise (VLFN) is observed in both branches. In Sco X-1 ~ 15–25 Hz QPO, whose frequency is strongly correlated with source flux, have been observed when the source was in a third spectral state, the so-called 'flaring branch' in the hardness-intensity diagram. This branch has also been observed in Cyg X-2 (Hasinger, 1987a, b). The very complex QPO behavior in the Rapid Burster does not readily fit the above phenomenological scheme, and it remains to be seen whether Cir X-1, GX 349 + 2, and 1820 – 30 fit the scheme.

The ten sources in which QPO have been detected are among the ~ 20 brightest known sources. This raises the possibility that QPO only occur in luminous sources. To date, only a few very sensitive searches for QPO in relatively weak sources were made; they were not successful (e.g., Gottwald *et al.*, 1987). Most notably, about 80 hr of EXOSAT data from the burst source 1735–44 were examined; no QPO were found with upper limits of $\sim 1\%$ (Penninx *et al.*, 1988). Moreover, low-frequency noise in the

range above a few Hz (which, on the basis of the observations of GX 5–1, Cyg X-2 and GX 17 + 2 is a good indicator for the presence of high-frequency QPO), was not observed when the source moved onto a 'horizontal branch'.

The apparent 'absence' of QPO in the weak sources, however, may be a selection effect. For QPO of given characteristics (strength, frequency, width) in two sources which differ by a factor of 5 in flux, it would take 25 times longer to detect the QPO in the weak source than in the bright one (see Section 2.2.2). Since the occurrence, and the character of QPO are highly variable, it may easily escape detection. Clearly, there is a strong bias against the detection of QPO in weak sources.

In most of the models proposed to date, a high luminosity (i.e., a high mass accretion rate) is not the key element that determines the presence of the QPO (see, however, Van der Klis *et al.*, 1987b; Paczynski, 1987). Yet, this can not be excluded. Distance estimates for Cyg X-2 (Cowley *et al.*, 1979), 4U/MXB 1820 – 30 (Vacca *et al.*, 1986), Sco X-1 (Cowley and Crampton, 1975), Cir X-1 (Goss and Mebold, 1977), and an average distance of ~ 8 kpc for the remaining sources, located in the galactic bulge (see, e.g., Kerr and Lynden-Bell, 1986; Wesselink, 1987), show that all QPO sources are intrinsically quite luminous ($> 5 \times 10^{37}$ erg s^{-1}). It seems, therefore, possible that QPO are only present in very luminous sources.

An indirect connection between the presence of QPO and the mass-transfer rate has been suggested by Van der Klis *et al.* (1985b), Lewin and Van Paradijs (1986), and Van Paradijs and Lewin (1986). Under the assumptions that (i) QPO is a magnetospheric phenomenon, and (ii) that the neutron star magnetic fields decay on a time scale of $\sim 10^7$ yr, they proposed that a necessary condition for QPO might be a mass-transfer rate high enough to produce a young neutron star in an old binary system through the accretion-induced collapse of a white dwarf (cf. Isern *et al.*, 1987; Van den Heuvel and Verbunt, 1988, and references therein). Such a mass-transfer rate could be driven by an evolved companion which is moving up the giant branch (Webbink *et al.*, 1983; Taam, 1983). Their suggestion was supported by the discovery of QPO in Sco X-1 (Middleditch and Priedhorsky, 1985, 1986), and Cyg X-2 (Hasinger *et al.*, 1986) which both have such an evolved companion. We now know that such an evolved companion is not a necessary condition as QPO were detected in 1820 – 30 (Stella *et al.*, 1987b). This system has an 11-min orbital period, and the companion is a degenerate star (Stella *et al.*, 1987a; Rappaport *et al.*, 1987). However, this still leaves open the possibility that the presence of QPO is dictated by the mass-transfer rate, and thus by luminosity. Future observations (e.g. with *Ginga*) of QPO in transient sources (which experience a large decline in luminosity), may be one way to study the possible QPO-luminosity connection.

We do not yet know what causes the QPO. Many interesting ideas have been put forward, but none can cope with the enormous complexity that has been observed. Perhaps more than one mechanism is at work.

There is recent evidence that the magnetic dipole fields of neutron stars do not decay indefinitely, but 'bottom-out' near a field strength of order 10^{9-10} G (Kulkarni, 1986; Van den Heuvel *et al.*, 1986; Bhattacharya and Srinivasan, 1986; Wright and Low,

1986). If this holds in general, the neutron star magnetic fields in the LMXB could be high enough to affect the accretion flow (see Section 1.3.3). It is unclear, however, whether the presence of a magnetosphere is a necessary condition for the QPO.

The discovery of the QPO in the enigmatic LMXB was a welcome surprise. Once understood, the QPO may perhaps become a unique diagnostic tool. We expect that we will learn a great deal from future observations with the Japanese observatory *Ginga*. Particularly studies of the energy-dependent time lags may cast light on the origin of the QPO, and they may also increase our present poor understanding of the origin of X-ray spectra in low-mass X-ray binaries.

Acknowledgements

We thank Günther Hasinger, Fred Lamb, Bill Priedhorsky, Luigi Stella, and Ed van den Heuvel for numerous discussions during the past three years that shaped our thinking about the QPO. We are grateful to Günther Hasinger, Luigi Stella and Jacob Shaham for their valuable comments on this manuscript, and we thank our colleagues who provided us with original copies of their figures. WHGL acknowledges support from the United States National Aeronautics and Space Administration under grants NAG8–571, NAG8–674, and NSG–7643, JvP acknowledges a travel grant from the Leids Kerkhoven Bosscha Fonds.

Note Added in Proofs

The discovery of QPO with a frequency of 0.075 ± 0.001 Hz in the X-ray flux of LMC X-1 was recently reported on the basis of *Ginga* observations by Ebisawa *et al.* of the *Ginga* LAC team (Paper presented at the International Symposium on the Physics of Neutron Stars and Black Holes, February 1–3, 1988, Tokyo). The radial velocity amplitude of the optical companion of LMC X-1 is large, and suggests that the source may be a black hole (Hutchings *et al., Astrophys. J.* **275**, L43, 1983). If LMC X-1 indeed is a black hole, then a magnetospheric origin for the slow QPO detected with *Ginga* can be excluded.

References

Alpar, M.A.: 1986, *Monthly Notices Roy. Astron. Soc.* **223**, 469.
Alpar, M. A.: 1987, in F. Pacini (ed.), *High-Energy Phenomena Around Collapsed Stars*, D. Reidel Publ. Co., Dordrecht, Holland, p. 359.
Alpar, M. A. and Shaham, J.: 1985a, *IAU Circ.*, No. 4046.
Alpar, M. A. and Shaham, J.: 1985b, *Nature* **316**, 239.
Alpar, M. A., Cheng, A. F., Ruderman, M. A., and Shaham, J.: 1982, *Nature* **300**, 728.
Andrews, D.: 1984, *EXOSAT Express* **5**, 31.
Andrews, D. and Parmar, A.: 1985, *EXOSAT Express* **12**, 76.
Andrews, D. and Stella, L.: 1984, *EXOSAT Express* **10**, 35.
Angel, J. R. P., Kestenbaum, H., and Novick, R.: 1971, *Astrophys. J.* **169**, L57.
Argue, A. N., Jauncey, D., Morabito, D. D., and Preston, R. A.: 1984, *Monthly Notices Roy. Astron. Soc.* **211**, 713.

Avni, Y.: 1976, *Astrophys. J.* **210**, 642.
Baan, W. A.: 1977, *Astrophys. J.* **214**, 245.
Baan, W. A.: 1979, *Astrophys. J.* **227**, 987.
Barr, P., White, N. E., Haberl, F., Stella, L., Pollard, G., Gottwald, M., and Parmar, A. N.: 1987, *Astron. Astrophys.* **176**, 69.
Basinska, E. M., Lewin, W. H. G., Sztajno, M., Cominsky, L. R., and Marshall, F. J.: 1984, *Astrophys. J.* **281**, 337.
Bath, G. T.: 1973, *Nature Phys. Sci.* **246**, 84.
Becker, R. H. and Helfand, D. J.: *Nature* **313**, 115.
Berman, N. and Stollman, G.: 1985, *Astron. Astrophys.* **154**, L23.
Beskin, V. S., Gurevitch, A. V., and Istomin, Ya. N.: 1983, *Astrophys. Space Sci.* **102**, 301.
Bhattacharya, D. and Srinivasan, G.: 1986, *Current Sci.* **55**, 327.
Blandford, R. D., Applegate, J. H., and Hernquist, L.: 1983, *Monthly Notices Roy. Astron. Soc.* **204**, 1025.
Blondin, J. M. and Freese, K.: 1986, *Nature* **323**, 786.
Boldt, E. A., Holt, S. S., and Serlemitsos, P. J.: 1971, *Astrophys. J.* **164**, L9.
Bonnet-Bidaud, J. M. and Van der Klis, M.: 1979, *Astron. Astrophys.* **73**, 90.
Boriakoff, V., Buccheri, R., and Fauci, F.: 1983, *Nature* **304**, 417.
Boyle, C. B., Fabian, A. C., and Guilbert, P. W.: 1986, *Nature* **319**, 648.
Bracewell, R., 1965, *The Fourier Transform and its Applications*, McGraw-Hill, New York.
Bradt, H. V., Braes, L. L. E., Forman, W., Hesser, J. E., Hiltner, W. A., Hjellming, R., Kellogg, E., Kunkel, W. E., Miley, G. K., Moore, G., Pel, J. W., Thomas, J., Vanden Bout, P., Wade, C., and Warner, B.: 1975, *Astrophys. J.* **197**, 443.
Bradt, H., Burnett, B., Mayer, W., Rappaport, S., and Schnopper, H.: 1971, *Nature* **229**, 96.
Braes, L. L. E. and Miley, G. K.: 1973, in H. Bradt and R. Giacconi (eds.), 'X- and Gamma-Ray Astronomy', *IAU Symp.* **55**, 86.
Braes, L. L. E., Miley, G. K., and Schoenmakers, A. A.: 1972, *Nature* **236**, 392.
Brainerd, J. and Lamb, F. K.: 1987, *Astrophys. J.* **317**, L33.
Brainerd, J., Lamb, F. K., and Shibazaki, N.: 1986, in M. Ulmer (ed.), *Texas Symposium on Relativistic Astrophysics*, p. 504.
Branduardi, G., Kylafis, N. D., Lamb, D. Q., and Mason, K. O.: 1980, *Astrophys. J.* **235**, L153.
Burbidge, E. M., Lynds, C. R., and Stockton, A. N.: 1967, *Astrophys. J.* **150**, L95.
Bussard, R. W., Weisskopf, M. C., Elsner, R. F., and Shibazaki, N.: 1988, preprint.
Candy, B. N. and Blair, D. G.: 1983, *Monthly Notices Roy. Astron. Soc.* **205**, 281.
Candy, B. N. and Blair, D. G.: 1985, *Astrophys. J.* **307**, 535.
Canizares, C. R., Clark, G. W., Li, F. K., Murthy, G. T., Bardas, D., Sprott, G., Spencer, J. H., Mook, D. E., Hiltner, W. A., Williams, W. L., Moffett, T. J., Grupsmith, G., Vanden Bout, P. A., Golson, J. C., Irving, C., Frohlich, A., and Van Genderen, A.: 1975, *Astrophys. J.* **197**, 457.
Celnikier, L. M.: 1977, *Astron. Astrophys.* **60**, 421.
Charles, P. A., Thorstensen, J. R., Bowyer, S., Clark, G. W., Li, F. K., Van Paradijs, J., Remillard, R., Holt, S. S., Kaluzienski, L. J., Junkkarinen, V. T., Puetter, R. C., Smith, H. E., Pollard, G. S., Sanford, P. W., Tapia, S., and Vrba, F. J.: 1980, *Astrophys. J.* **237**, 154.
Chiappetti, L., Ciapi, A. L., Maraschi, L., Stella, L., Tanzi, E. G., and Treves, A.: 1987, *Astrophys. Space Sci.* **131**, 691.
Clark, G. W., Li, F. K. Canizares, C., Hayakawa, S., Jernigan, G., and Lewin, W. H. G.: 1977, *Monthly Notices Roy. Astron. Soc.* **179**, 651.
Clark, D. H., Parkinson, J. H., and Caswell, J. L.: 1975, *Nature* **254**, 674.
Cordova, F. A. and Mason, K. O.: 1983, in W. H. G. Lewin and E. P. J. van den Heuvel (eds.), *Accretion Driven Stellar X-ray Sources*, Cambridge University Press, Cambridge, p. 147.
Cowley, A. P. and Crampton, D.: 1975, *Astrophys. J.* **201**, L65.
Cowley, A. P., Crampton, D., and Hutchings, J. B.: 1979, *Astrophys. J.* **231**, 539.
Cowley, A. P., Hutchings, J. B., Crampton, D., and Hartwick, F. D. A.: 1987, *Astrophys. J.* **320**, 296.
Crampton, D., Cowley, A. P., Hutchings, J. B., and Kaat, C.: 1976, *Astrophys. J.* **207**, 907.
Davidsen, A., Malina, R., and Bowyer, S.: 1976, *Astrophys. J.* **203**, 448.
Davidson, K. and Ostriker, J. P.: 1973, *Astrophys. J.* **179**, 585.
Deeter, J. E.: 1984, *Astrophys. J.* **281**, 482.
De Groot, T. and Van Nieuwkoop, J.: 1968, *Solar Phys.* **4**, 332.

De Kool, M. and Van den Heuvel, E. P. J.: 1985, *Nature* **317**, 599.
De Kool, M. and Van Paradijs, J.: 1987, *Astron. Astrophys.* **173**, 279.
Dower, R. G., Bradt, H. V., and Morgan, E. H.: 1982, *Astrophys. J.* **261**, 228.
Elsner, R. F., Shibazaki, N., and Weisskopf, M. C.: 1987, *Astrophys. J.* **320**, 527.
Elsner, R. F., Weisskopf, M. C., Darbro, W., Ramsey, B. D., Williams, A. C., Sutherland, P. G., and Grindlay, J. E.: 1986, *Astrophys. J.* **308**, 655.
Ercan, E. N. and Cruise, A. M.: 1984, *Monthly Notices Roy. Astron. Soc.* **209**, 271.
Fahlman, G. C. and Gregory, P. C.: 1983, in J. Danziger and P. Gorenstein (eds.), 'Supernova Remnants and their X-ray Emission', *IAU Symp.* **101**, 445.
Flowers, E. and Ruderman, M. A.: 1977, *Astrophys. J.* **215**, 302.
Forman, W., Jones, C., Cominsky, L., Julien, P., Murray, S., Peters, G., Tananbaum, H., and Giacconi, R.: 1978, *Astrophys. J. Suppl.* **38**, 357.
Forman, W., Jones, C., and Tananbaum, H.: 1976, *Astrophys. J.* **208**, 849.
Friedman, H., Fritz, G., Henry, R. C., Hollinger, J. P., Meekins, J. F., and Sadeh, D.: 1969, *Nature* **221**, 345.
Fuerst, E., Reich, W., Reich, P., Sofue, Y., and Handa, T.: 1985, *Nature* **314**, 720.
Geldzahler, B. J.: 1983, *Astrophys. J.* **264**, L49.
Geldzahler, B. J. and Fomalont, E. B.: 1986, *Astrophys. J.* **311**, 805.
Ghosh, P. and Lamb, F. K.: 1979, *Astrophys. J.* **234**, 296.
Giacconi, R., Gorenstein, P., Gursky, H., and Waters, J. R.: 1967a, *Astrophys. J.* **148**, L119.
Giacconi, R., Gorenstein, P., Gursky, H., Usher, P. D., Waters, J. R., Sandage, A., Osmer, P., and Peach, J. V.: 1967b, *Astrophys. J.* **148**, L129.
Giacconi, R., Gursky, H., Paolini, F., and Rossi, B.: 1962, *Phys. Rev. Letters* **9**, 439.
Giacconi, R., Murray, S., Gursky, H., Kellogg, E., Schreier, E., Matilsky, T., Koch, D., and Tananbaum, H.: 1974, *Astrophys. J. Suppl.* **27**, 37.
Glass, I. S.: 1978, *Monthly Notices Roy. Astron. Soc.* **183**, 335.
Gorenstein, P.: 1975, *Astrophys. J.* **198**, 95.
Goss, W. M. and Mebold, U.: 1977, *Monthly Notices Roy. Astron. Soc.* **181**, 255.
Gottlieb, E. W., Wright, E. L., and Liller, W.: 1975, *Astrophys. J.* **195**, L33.
Gottwald, M., Stella, L., White, N. E., and Barr, P.: 1987, *Monthly Notices Roy. Astron. Soc.* **229**, 395.
Grindlay, J. E. and Gursky, H.: 1977, *Astrophys. J.* **218**, L117.
Grindlay, J. E., Gursky, H., Schnopper, H., Parsignault, D. R., Heise, J., Brinkman, A. C., and Schrijver, J.: 1976, *Astrophys. J.* **205**, L127.
Grindlay, J. E., Hertz, P., Steiner, J. L., Murray, S. S., and Lightman, A. P.: 1984, *Astrophys. J.* **282**, L13.
Grindlay, J. E. and Seaquist, E. R.: 1986, *Astrophys. J.* **310**, 172.
Haberl, F., Stella, L., White, N. E., Priedhorsky, W. C., and Gottwald, M.: 1987, *Astrophys. J.* **314**, 266.
Hameury, J. M., King, A. R., and Lasota, J. P.: 1985, *Nature* **317**, 597.
Harvey, J. A., Ruderman, M. A., and Shaham, J.: 1986, *Phys. Rev.* **D33**, 2084.
Hasinger, G.: 1987a, in D. J. Helfand and J.-H. Huang (eds.), 'The Origin and Evolution of Neutron Stars', *IAU Symp.* **125**, 333.
Hasinger, G.: 1987b, *Astron. Astrophys.* **186**, 153.
Hasinger, G.: 1988, in L. Filipov and N. E. White (eds.), 'The Physics of Compact Objects: Theory Versus Observations', *COSPAR/IAU Symp., Sofia, July 1987*, Pergamon (in press).
Hasinger, G. and Van der Klis, M.: 1987, *IAU Circ.*, No. 4489.
Hasinger, G., Langmeier, A., Sztajno, M., Pietsch, W., and Gottwald, M.: 1988a, in preparation.
Hasinger, G., Priedhorsky, W., and Middleditch, J.: 1988b, *Astrophys. J.* (in press).
Hasinger, G., Langmeier, A., Pietsch, W., and Sztajno, M.: 1985, *Space Sci. Rev.* **40**, 233.
Hasinger, G., Langmeier, A., Sztajno, M., Trümper, J., Lewin, W. H. G., and White, N. E.: 1986, *Nature* **319**, 469.
Haynes, R. F., Komesaroff, M. M., Little, A. G., Jauncey, D. L., Caswell, J. L., Milne, D. K., Kesteven, M. J., Wellington, K. J., and Preston, R. A.: 1986, *Nature* **324**, 233.
Helfand, D. J. and Becker, R. H.: 1985, *Nature* **313**, 118.
Helfand, D. J., Ruderman, M. A., and Shaham, J.: 1983, *Nature* **304**, 423.
Henrichs, H. F.: 1983, in W. H. G. Lewin and E. P. J. van den Heuvel (eds.), *Accretion Driven Stellar X-ray Sources*, Cambridge University Press, Cambridge, p. 393.
Hertz, P. and Grindlay, J. E.: 1984, *Astrophys. J.* **282**, 118.

Hertz, P. and Wood, K. S.: 1986, in A. Treves (ed.), *Variability of Galactic and Extragalactic X-ray Sources*, Associazone per l'Avanzamento dell'Astronomia, Milano–Bologna, p. 221.
Hirano, T., Hayakawa, S., Kunieda, H., Makino, F., Masai, K., Nagase, F., and Yamashita, K.: 1984, *Publ. Astron. Soc. Japan.* **36**, 769.
Hjellming, R. M.: 1978, *Astrophys. J.* **221**, 225.
Hjellming, R. M. and Blankenship, L. C.: 1973, *Nature Phys. Sci.* **243**, 81.
Hjellming, R. M. and Wade, C. M.: 1971a, *Astrophys. J.* **164**, L1.
Hjellming, R. M. and Wade, C. M.: 1971b, *Astrophys. J.* **168**, L21.
Hoffman, J. A., Marshall, H. L., and Lewin, W. H. G.: 1978, *Nature* **271**, 630.
Holt, S. S.: 1980, in R. Giacconi and G. Setti (eds.), *X-ray Astronomy*, D. Reidel Publ. Co., Dordrecht, Holland, p. 89.
Holt, S. S.: 1987, *Astrophys. J.* **312**, 743.
Holt, S. S., Boldt, E. A., Serlemitsos, P. J., and Kaluzienski, L. J.: 1976, *Astrophys. J.* **205**, L27.
Holt, S. S., Kaluzienski, L. J., Boldt, E. A., and Serlemitsos, P. J.: 1979, *Astrophys. J.* **233**, 344.
Hulse, R. A. and Taylor, J. H.: 1975, *Astrophys. J.* **195**, L51.
Ilovaisky, S. A., Chevalier, C., Motch, C., and Janot-Pacheco, E.: 1979, *IAU Circ.*, No. 3325.
Ilovaisky, S. A., Chevalier, C., White, N. E., Mason, K. O., Sanford, P. W., Delvaille, J. P., and Schnopper, H. W.: 1980, *Monthly Notices Roy. Astron. Soc.* **191**, 81.
Inoue, H., Koyama, K., Makishima, K., Matsuoka, M., Murakami, T., Oda, M., Ogawara, Y., Ohashi, T., Shibazaki, N., Tanaka, Y., Kondo, I., Hayakawa, S., Kunieda, H., Makino, F., Masai, K., Nagase, F., Tawara, Y., Miyamoto, S., Tsunemi, H., and Yamashita, K.: 1981, *Astrophys. J.* **250**, L71.
Isern, J., Hernanz, M., Canal, R., Labay, J., and Mochkovitch, R.: 1987, *Astron. Astrophys.* **172**, L23.
Jernigan, J. G. and Clark, G. W.: 1979, *Astrophys. J.* **231**, L125.
Jones, C.: 1977, *Astrophys. J.* **214**, 856.
Jones, C., Giacconi, R., Forman, W., and Tananbaum, H.: 1974, *Astrophys. J.* **191**, L71.
Jones, P. B.: 1987, *Monthly Notices Roy. Astron. Soc.* **228**, 513.
Joss, P. C.: 1978, *Astrophys. J.* **225**, L123.
Joss, P. C. and Rappaport, S. A.: 1983, *Nature* **304**, 419.
Joss, P. C., Avni, Y., and Rappaport, S.: 1978, *Astrophys. J.* **221**, 645.
Kahn, S. M. and Grindlay, J. E.: 1984, *Astrophys. J.* **281**, 826.
Kaluzienski, L. J., Holt, S. S., Boldt, E. A., and Serlemitsos, P. J.: 1976, *Astrophys. J.* **208**, L71.
Kerr, F. J. and Lynden-Bell, D.: 1986, *Monthly Notices Roy. Astron. Soc.* **221**, 1023.
Kleinmann, D. E., Kleinmann, S. G., and Wright, E. L.: 1976, *Astrophys. J.* **210**, L83.
Kraft, R. and Miller, J. S.: 1968, *Astrophys. J.* **155**, L159.
Kristian, J., Sandage, A., and Westphal, J. A.: 1967, *Astrophys. J.* **150**, L99.
Kulkarni, S.: 1986, *Astrophys. J.* **306**, L85.
Kundt, W.: 1981, *Astron. Astrophys.* **98**, 207.
Kylafis, N. D. and Klimis, G. S.: 1988, preprint.
Lamb, F. K.: 1986, in J. Trümper, W. H. G. Lewin, and W. Brinkmann (eds.), *The Evolution of Galactic X-ray Binaries*, NATO ASI Series, Series C: Mathematical and Physical Sciences, Vol. 167, p. 151.
Lamb, F. K., Fabian, A. C., Pringle, J. E., and Lamb, D. Q.: 1977, *Astrophys. J.* **217**, 197.
Lamb, F. K., Pethick, C. J., and Pines, D.: 1973, *Astrophys. J.* **184**, 271.
Lamb, F. K., Shibazaki, N., Shaham, J., and Alpar, M. A.: 1985, *Nature* **317**, 681.
Lampton, M., Margon, B., and Bowyer, S.: 1976, *Astrophys. J.* **208**, 177.
Langmeier, A.: 1988, Thesis, private communication.
Langmeier, A., Hasinger, G., Sztajno, M., Trümper, J., and Pietsch, W.: 1985, *IAU Circ.*, No. 4147.
Langmeier, A., Sztajno, M., Vacca, . D., Trümper, J., and Pietsch, W.: 1986, in: J. Trümper, W. H. G. Lewin, and W. Brinkmann (eds.), *The Evolution of Galactic X-ray Binaries*, NATO ASI Series, Series C: Mathematical and Physical Sciences, Vol. 167, p. 253.
La Sala, J. and Thorstensen, J. R.: 1985, *Astron. J.* **90**, 2077.
Leahy, D. A., Darbro, W., Elsner, R. F., Weisskopf, M. C., Sutherland, P. G., Kahn, S., and Grindlay, J. E.: 1983, *Astrophys. J.* **266**, 160.
Leahy, D. A.: 1987, *IAU Circ.*, No. 4485.
Lewin, W. H. G.: 1977, *Am. Sci.* **65**, 605.
Lewin, W. H. G.: 1985, in Y. Tanaka and W. H. G. Lewin (eds.), *Galactic and Extragalactic Compact X-ray Sources*, Inst. of Space and Aeronautical Sciences, Tokyo, p. 89.

Lewin, W. H. G.: 1986, in K. O. Mason, M. G. Watson, and N. E. White (eds.), 'The Physics of Accretion onto Compact Objects', *Lecture Notes in Physics*, Springer Verlag, Berlin, Vol. 266, p. 177.
Lewin, W. H. G.: 1987, in D. J. Helfand and J.-H. Huang (eds.), 'The Origin and Evolution of Neutron Stars', *IAU Symp.* **125**, 363.
Lewin, W. H. G. and Joss, P. C.: 1981, *Space Sci. Rev.* **28**, 3.
Lewin, W. H. G. and Joss, P. C.: 1983, in W. H. G. Lewin and E. P. J. van den Heuvel (eds.), *Accretion-driven Stellar X-ray Sources*, Cambridge University Press, Cambridge, p. 41.
Lewin, W. H G. and Van Paradijs, J.: 1985a, *Astron. Astrophys.* **142**, 361.
Lewin, W. H G. and Van Paradijs, J.: 1985b, *Astron. Astrophys.* **149**, L27.
Lewin, W. H. G. and Van Paradijs, J.: 1986, *Comm. Astrophys.* **11**, No. 3, 127.
Lewin, W. H. G., Clark, G. W., and Smith, W. B.: 1968, *Astrophys. J.* **152**, L55.
Lewin, W. H. G., Doty, J., Clark, G. W., Rappaport, S. A., Bradt, H. V. D., Doxsey, R., Hearn, D. R., Hoffman, J. A., Jernigan, J. G., Li, F. K., Mayer, W., McClintock, J., Primini, F., and Richardson, J.: 1976, *Astrophys. J.* **207**, L95.
Lewin, W. H. G., Ricker, G. R. and McClintock, J. E.: 1971, *Astrophys. J.* **169**, L71.
Lewin, W. H. G., Van Paradijs, J., Van der Klis, M., Jansen, F., Basinska, E. M., Langmeier, A., Sztajno, M., and Trümper, J.: 1986, *Monthly Notices Roy. Astron. Soc.* (submitted).
Lewin, W. H. G., Van Paradijs, J., Hasinger, G., Penninx, W. H., Langmeier, A., Van der Klis, M., Jansen, F., Basinska, E. M., Sztajno, M., and Trümper, J.: 1987, *Monthly Notices Roy. Astron. Soc.* **226**, 383.
Li, F. K., Joss, P. C., McClintock, J. E., Rappaport, S., and Wright, E. L.: 1980, *Astrophys. J.* **240**, 628.
Liller, W.: 1977: *Astrophys. J.* **213**, L21.
Lynds, C. R.: 1967, *Astrophys. J.* **149**, L41.
Lyne, A. G., Manchester, R. N., and Taylor, J. H.: 1983, *Monthly Notices Roy. Astron. Soc.* **213**, 613.
Maejima, Y., Makishima, K., Matsuoka, M., Ogawara, Y., Oda, M., Tawara, Y., and Doi, K.: 1984, *Astrophys. J.* **285**, 712.
Makishima, K., Mitsuda, K., Inoue, H., Koyama, K., Matsuoka, M., Murakami, T., Oda, M., Ogawara, Y., Ohashi, T., Shibazaki, N., Tanaka, Y., Marshall, F. J., Hayakawa, S., Kunieda, H., Makino, F., Nagase, F., Tawara, Y., Miyamoto, S., Tsunemi, H., Tsuno, K., Yamasjhita, K., and Kondo, I.: 1983, *Astrophys. J.* **267**, 310.
Maraschi, L. and Cavaliere, A.: 1977, in E. A. Mueller (ed.), *Highlights of Astronomy*, D. Reidel Publ. Co., Dordrecht, Holland, Vol. 4, part I, p. 127.
Maraschi, L., Treves, A., and Van den Heuvel, E. P. J.: 1976, *Nature* **259**, 292.
Markert, T. H., Winkler, P. F., Laird, F. N., Clark, G. W., Hearn, D. R., Sprott, G. F., Li, F. K., Bradt, H. V., Lewin, W. H. G., and Schnopper, H. W.: 1979, *Astrophys. J. Suppl.* **39**, 573.
Marshall, N. and Watson, M. G.: 1979, *IAU Circ.*, No. 3318.
Mason, K. O.: 1986, in K. O. Mason, M. G. Watson, and N. E. White (eds.), 'The Physics of Accretion onto Compact Objects' *Lecture Notes in Physics*, Springer-Verlag, Berlin, Vol. 266, p. 29.
Mason, K. O., Charles, P. A., White, N. E., Culhane, J. L., Sanford, P. W., and Strong, K. T.: 1976, *Monthly Notices Roy. Astron. Soc.* **177**, 513.
Matsuoka, M.: 1985, in D. Q. Lamb, and J. Patterson (eds.), *Cataclysmic Variables and Low-Mass X-ray Binaries*, D. Reidel Publ. Co., Dordrecht, Holland, p. 139.
McClintock, J. E.: 1986, in K. O. Mason, M. G. Watson, and N. E. White (eds.), 'The Physics of Accretion onto Compact Objects', *Lecture Notes in Physics*, Springer-Verlag, Berlin, Vol. 266, p. 211.
McClintock, J. E., Petro, L. D., Hammerschlag-Hensberge, G. H., Proffitt, C. R., and Remillard, R. A.: 1984, *Astrophys. J.* **283**, 794.
McDermott, P. N., and Taam, R. E.: 1987, *Astrophys. J.* **318**, 278.
Mereghetti, S. and Grindlay, J. E.: 1987, *Astrophys. J.* **312**, 727.
Mészáros, P., Riffert, H., and Berthiaume, G.: 1988, *Astrophys. J.* (in press).
Michel, F. C.: 1977, *Astrophys. J.* **216**, 838.
Middleditch, J. and Priedhorsky, W.: 1985, *IAU Circ.*, No. 4060.
Middleditch, J. and Priedhorsky, W.: 1986, *Astrophys. J.* **306**, 230.
Milgrom, M.: 1987, *Astron. Astrophys.* **172**, L1.
Mitsuda, K., Inoue, H., Koyama, K., Makishima, K., Matsuoka, M., Ogawara, Y., Shibazaki, N., Suzuki, K., Tanaka, Y., and Hirano, T.: 1984, *Publ. Astron. Soc. Japan* **36**, 741.
Mitsuda, K., and Ginga Team: 1988, in L. Filipov and N. E. White (eds.), *The Physics of Compact Objects: Theory Versus Observations*, Pergamon, London (in press).

Miyamoto, S. and Matsuoka, M.: 1977, *Space Sci. Rev.* **20**, 687.
Morfill, G. E. and Trümper, J.: 1986, in J. Trümper, W. H. G. Lewin, and W. Brinkmann (eds.), *The Evolution of Galactic X-ray Binaries*, NATO ASI Series, Series C: Mathematical and Physical Sciences, Vol. 167, p. 173.
Morgan, E. H. and Remillard, R. A.: 1988, *Astrophys. J.* (in press).
Morgan, E. H., Remillard, R. A., Priedhorsky, W., Stella, L., White, N. E., and Garcia, M.: 1986, *IAU Circ.*, No. 4261.
Muchotrzeb, B.: 1983, *Acta Astron.* **33**, 79.
Norris, J. P. and Wood, K. S.: 1987, *Astrophys. J.* **312**, 732.
Oda, M.: 1980, *IAU Circ.*, No. 3506.
Oda, M., Wada, M., Matsuoka, M., Miyamoto, S., Muranaka, N., and Ogawara, Y.: 1972, *Astrophys. J.* **172**, L13.
Ostriker, J. E.: 1977, *Ann. N.Y. Acad. Sci.* **302**, 229.
Paczynski, B.: 1983, *Nature* **304**, 421.
Paczynski, B.: 1987, *Nature* **327**, 303.
Page, C. G.: 1985, *Space Sci. Rev.* **40**, 387.
Parsignault, D. and Grindlay, J. E.: 1978, *Astrophys. J.* **225**, 970.
Patterson, J.: 1981, *Astrophys. J. Suppl.* **45**, 517.
Payne, D. G.: 1980, *Astrophys. J.* **237**, 951.
Peacock, A., Andresen, R. D., Manzo, G., Taylor, B. G., Villa, G., Re, S., Ives, J. C., and Kellock, S.: 1981, *Space Sci. Rev.* **30**, 525.
Penninx, W., Hasinger, G., Lewin, W. H. G., Van Paradijs, J., Van der Klis, M.: 1988, *Monthly Notices Roy. Astron. Soc.* (in press).
Petro, L. D., Bradt, H. V., Kelley, R. L., Horne, K., and Gomer, R., 1981, *Astrophys. J.* **251**, L7.
Ponman, T.: 1982a, *Monthly Notices Roy. Astron. Soc.* **200**, 351.
Ponman, T.: 1982b, *Monthly Notices Roy. Astron. Soc.* **201**, 769.
Ponman, T. J., Cooke, B. A., and Stella, L.: 1988, *Monthly Notices Roy. Astron. Soc.* (in press).
Pozdnyakov, L. A., Sobol, I. M., and Sunyaev, R. A.: 1983, *Astrophys. Space Phys. Rev.* **2**, 189.
Press, W. H., Flannery, B. P., Teukolsky, S. A., and Vetterling, W. T.: 1986, *Numerical Recipes, The Art of Scientific Computing*, Cambridge University Press, Cambridge, p. 381.
Priedhorsky, W.: 1986a, *Astrophys. J.* **306**, L97.
Priedhorsky, W.: 1986b, *Astrophys. Space Sci.* **126**, 89.
Priedhorsky, W. and Terrell, J.: 1984, *Astrophys. J.* **284**, L17.
Priedhorsky, W., Garmire, G. P., Rothschild, R., Boldt, E., Serlemitsos, P., and Holt, S.: 1979, *Astrophys. J.* **233**, 350.
Priedhorsky, W., Hasinger, G., Lewin, W. H. G., Middleditch, J., Parmar, A., Stella, L., and White, N. E.: 1986, *Astrophys. J.* **306**, L91.
Pringle, J. E.: 1981, *Ann. Rev. Astron. Astrophys.* **19**, 137.
Pringle, J. E. and Rees, M. J.: 1972, *Astron. Astrophys.* **21**, 1.
Radhakrishnan, V.: 1981, in B. Hidayat (ed.), *Proceedings of the IAU Asian-Pacific Regional Meeting*, Bandung.
Radhakrishnan, V. and Srinivasan, G. M.: 1982, *Current Sci.* **51**, 1096.
Rappaport, S. A. and Joss, P. C.: 1983, in W. H. G. Lewin and E. P. J. van den Heuvel (eds.), *Accretion-driven Stellar X-ray Sources*, Cambridge University Press, Cambridge, p. 1.
Rappaport, S. A. and Joss, P. C.: 1984, *Ann. Rev. Astron. Astrophys.* **22**, 537.
Rappaport, S., Nelson, L. A., Ma, P. C., and Joss, P. C.: 1987, *Astrophys. J.* **322**, 842.
Rappaport, S., Zaumen, W., Doxsey, R., and Mayer, W.: 1971, *Astrophys. J.* **169**, L93.
Robinson, E. L. and Nather, R. E.: 1979, *Astrophys. J. Suppl.* **39**, 461.
Ryter, C., Cesarsky, C. J., and Audouze, J.: 1975, *Astrophys. J.* **198**, 103.
Sandage, A., Osmer, P., Giacconi, R., Gorenstein, P., Gursky, H., Waters, J., Bradt, H., Garmire, G., Sreekantan, B. V., Oda, M., Osawa, K., and Jugaku, J.: 1966, *Astrophys. J.* **146**, 316.
Sang, Y. and Chanmugan, G.: 1987, *Astrophys. J.* **323**, L61.
Savonije, G. J.: 1983a, *Nature* **304**, 422.
Savonije, G. J.: 1983b, in W. H. G. Lewin and E. P. J. van den Heuvel (eds.), *Accretion driven Stellar X-ray Sources*, Cambridge University Press, Cambridge, p. 343.
Shaham, J.: 1987, in D. J. Helfand and J.-H. Huang (eds.), 'The Origin and Evolution of Neutron Stars', *IAU Symp.* **125**, 347.

Shapiro, S. L., Lightman, A. P., and Eardley, D. M.: 1976, *Astrophys. J.* **204**, 187.
Shaver, P. A., Salter, C. J., Patniack, A. R., Van Gorkom, J. H., and Hunt, G. C.: 1985, *Nature* **313**, 113.
Shibazaki, N. and Lamb, F. K.: 1987, *Astrophys. J.* **318**, 767.
Shibazaki, N., and Mitsuda, K.: 1984, in S. E. Woosley (ed.), *High Energy Transients in Astrophysics*, AIP Conference Proc. 115, New York, AIP, p. 63.
Shibazaki, N., Elsner, R. F., Bussard, R. W., Ebisuzaki, T., and Weisskopf, M. C.: 1988a, *Astrophys. J.* (in press).
Shibazaki, N., Elsner, R. F., and Weisskopf, M. C.: 1988b, *Astrophys. J.* (in press).
Slettebak, A.: 1987, in: A. Slettebak and T. P. Snow (eds.), *Physics of Be Stars*, Cambridge University Press, Cambridge, p. 24.
Smarr, L. L. and Blandford, R. D.: 1976, *Astrophys. J.* **207**, 574.
Srinivasan, G. and Van den Heuvel, E. P. J.: 1982, *Astron. Astrophys.* **108**, 143.
Stella, L.: 1986, in: N. Kylafis, J. Papamastorakis, and J. Ventura (eds.), *Plasma Penetration into Magnetospheres*, Crete Univ. Press, p. 199.
Stella, L., 1988, in L. Filipov and N. E. White (eds.), 'The Physics of Compact Objects: Theory Versus Observations', *COSPAR/IAU Symp.*, Sofia, July 1987, Pergamon, London (in press).
Stella, L., Chiappetti, L., Ciapi, A. L., Maraschi, L., Tanzi, E. Q., and Treves, A.: 1986, in R. Ruffini (ed.), *Proc. 4th Marcel Grossmann Meeting on General Relativity*, Elsevier Science Publishers, Amsterdam, p. 86.
Stella, L., Haberl, F., Lewin, W., Parmar, A., White, N., and Van Paradijs, J.: 1988a, *Astrophys. J.* **324**, 379.
Stella, L., Haberl, F., Lewin, W. H. G., Parmar, A. N., Van der Klis, M., and Van Paradijs, J.: 1988b, *Astrophys. J. Letters* (in press).
Stella, L., Parmar, A. N., and White, N. E.: 1988c, *Astrophys. J.* (in press).
Stella, L., Kahn, S. M., and Grindlay, J. E.: 1984, *Astrophys. J.* **282**, 713.
Stella, L., Priedhorsky, W., an White, N. E.: 1987a, *Astrophys. J.* **312**, L17.
Stella, L., White, N. E., and Priedhorsky, W.: 1987b, *Astrophys. J.* **315**, L49.
Stella, L., White, N. E., Davelaar, J., Parmar, A. N., Blissett, R. J., and Van der Klis, M.: 1985, *Astrophys. J.* **288**, L45.
Stella, L., White, N. E., and Rosner, R.: 1986, *Astrophys. J.* **308**, 669.
Stollman, G. M., Hasinger, G., Lewin, W. H. G., Van der Klis, M., and Van Paradijs, J.: 1987, *Monthly Notices. Roy. Astron. Soc.* **227**, 7P.
Sztajno, M., Basinka, E. M., Cominsky, L. R., Marshall, F. J., and Lewin, W. H. G.: 1983, *Astrophys. J.* **267**, 713.
Sztajno, M., Van Paradijs, J., Lewin, W. H. G., Langmeier, A., Trümper, J., and Pietsch, W.: 1986, *Monthly Notices Roy. Astron. Soc.* **222**, 499.
Taam, R. E.: 1983, *Astrophys. J.* **270**, 694.
Taam, R. E. and Lin, D. N. C.: 1984, *Astrophys. J.* **287**, 761.
Taam, R. E. and Van den Heuvel, E. P. J.: 1986, *Astrophys. J.* **305**, 235.
Tarenghi, M. and Reina, C.: 1972, *Nature Phys. Sci.* **240**, 53.
Tawara, Y., Hayakawa, S., Kunieda, H., Makino, F., and Nagase, F.: 1982, *Nature* **299**, 38.
Tawara, Y., Hirano, T., Kii, T., Matsuoka, M., and Murakami, T.: 1984, *Publ. Astron. Soc. Japan* **36**, 861.
Taylor, B. G., Andresen, R. D., Peacock, A., and Zobl, A.: 1981, *Space Sci. Rev.* **30**, 479.
Tennant, A. F.: 1987a, *Monthly Notices Roy. Astron. Soc.* **226**, 963.
Tennant, A. F.: 1987b, *Monthly Notices Roy. Astron. Soc.* **226**, 971.
Tennant, A. F.: 1988a, *Monthly Notices Roy. Astron. Soc.* **230**, 403.
Tennant, A. F.: 1988b, in L. Filipov and N. E. White (eds.), 'The Physics of Compact Objects: Theory Versus Observations', *COSPAR/IAU Symp.*, Sofia, July 1987, Pergamon, London (in press).
Tennant, A. F., Fabian, A. C., and Shafer, R. A.: 1987a, *Monthly Notices Roy. Astron. Soc.* **219**, 871.
Tennant, A. F., Fabian, A. C., and Shafer, R. A.: 1987b, *Monthly Notices Roy. Astron. Soc.* **221**, 27P.
Tjemkes, S. A., Zuiderwijk, E. J., and Van Paradijs, J.: 1986, *Astron. Astrophys.* **154**, 77.
Toor, A.: 1977, *Astrophys. J.* **215**, L57.
Turner, M. J. L., Smith, A., and Zimmermann, H. U.: 1981, *Space Sci. Rev.* **30**, 513.
Vacca, W. D., Lewin, W. H. G., and Van Paradijs, J.: 1986, *Monthly Notices Roy. Astron. Soc.* **220**, 339.
Van den Heuvel, E. P. J.: 1975, *Astrophys. J.* **198**, L109.
Van den Heuvel, E. P. J.: 1981, in W. Sieber and R. Wielebinski (eds.), 'Pulsars – 13 Years of Research on Neutron Stars', *IAU Symp.* **95**, 379.
Van den Heuvel, E. P. J.: 1983, in W. H. G. Lewin and E. P. J. van den Heuvel (eds.), *Accretion-driven Stellar X-ray Sources*, Cambridge University Press, Cambridge, p. 303.

Van den Heuvel, E. P. J., and Rappaport, S.: 1987, in A. Slettebak and T. P. Snow (eds.), *Physics of Be Stars*, Cambridge University Press, Cambridge, p. 291.
Van den Heuvel, E. P. J., Van Paradijs, J. and Taam, R. E.: 1986, *Nature* **322**, 153.
Van den Heuvel, E. P. J., and Verbunt, F.: 1988, *Rev. Mod. Phys.* (in preparation).
Van der Klis, M.: 1986a, in K. O. Mason, M. G. Watson, and N. E. White (eds.), 'The Physics of Accretion onto Compact Objects', *Lecture Notes in Physics*, Springer-Verlag, Berlin, Vol. 266, p. 157.
Van der Klis, M.: 1986b, in A. Treves (ed.), *Variability of Galactic and Extragalactic X-ray Sources*, Associazone per l'Avanzamento dell' Astronomia, Milano–Bologna, p. 185.
Van der Klis, M.: 1987, in D. J. Helfand and J.-H. Huang (eds.), 'The Origin and Evolution of Neutron Stars', *IAU Symp.* **125**, 321.
Van der Klis, M.: 1988, in L. Filipov and N. E. White (eds.), 'The Physics of Compact Objects: Theory Versus Observations', *COSPAR/IAU Symp.*, Sofia, July 1987, Pergamon, London (in press).
Van der Klis, M. and Jansen, F. A.: 1985, *Nature* **313**, 768.
Van der Klis, M. and Jansen, F.: 1986, in: J. Trümper, W. H. G. Lewin and W. Brinkmann (eds.), *The Evolution of Galactic X-ray Binaries*, NATO ASI Series, Vol. 167, p. 129.
Van der Klis, M. and Rappaport, S.: 1983, *Astron. Astrophys.* **121**, 119.
Van der Klis, M., Jansen, F., Van Paradijs, J., Lewin, W. H. G., Trümper, J., and Sztajno, M.: 1985a, *IAU Circ.*, No. 4043.
Van der Klis, M., Jansen, F., Van Paradijs, J., Lewin, W. H. G., Van den Heuvel, E. P. J., Trümper, J. E., and Sztajno, M.: 1985b, *Nature* **316**, 225.
Van der Klis, M., Jansen, F., White, N. E., Stella, L., and Peacock, A.: 1985c, *IAU Circ.*, No. 4068.
Van der Klis, M., Jansen, F., Van Paradijs, J., Lewin, W. H. G., Sztajno, M., and Trümper, J.: 1987a, *Astrophys. J.* **313**, L19.
Van der Klis, M., Stella, L., White, N. E., Jansen, F., and Parmar, A. N.: 1987b, *Astrophys. J.* **316**, 517.
Van der Klis, M., Hasinger, G., Stella, L., Langmeier, A., Van Paradijs, J., and Lewin, W. H. G.: 1987c, *Astrophys. J.* (in press).
Van Paradijs, J.: 1983, in W. H. G. Lewin and E. P. J. van den Heuvel (eds.), *Accretion-driven Stellar X-ray Sources*, Cambridge University Press, Cambridge, p. 189.
Van Paradijs, J., and Verbunt, F.: 1984, in S. E. Woosley (ed.), *High Energy Transients in Astrophysics*, AIP Conference Proceedings, Vol. 115, p. 49.
Van Paradijs, J., Cominsky, L., and Lewin, W. H. G.: 1979, *Monthly Notices Roy. Astron. Soc.* **189**, 387.
Van Paradijs, J., Hasinger, G., Lewin, W. H. G., Van der Klis, M., Sztajno, M., Schulz, N., and Jansen, F.: 1988a, *Monthly Notices Roy. Astron. Soc.* (in press).
Van Paradijs, J., Penninx, W., and Lewin, W. H. G.: 1988b, *Monthly Notices Roy. Astron. Soc.* (in press).
Van Paradijs, J., Joss, P. C., Cominsky, L., and Lewin, W. H. G.: 1979, *Nature* **280**, 375.
Van Paradijs, J., and Lewin, W. H. G.: 1986, in: J. Trümper, W. H. G. Lewin, and W. Brinkmann (eds), *The Evolution of Galactic X-ray Binaries*, NATO ASI Series, Series C: Mathematical and Physical Sciences, Vol. 167, p. 187.
Verbunt, F.: 1987, *Astrophys. J.* **312**, L23.
Vrtilek, S. D., Swank, J. H., and Kallman, T. R.: 1988, *Astrophys. J.* (in press).
Wang, Y.-M. and Schlickheiser, R.: 1987, *Astrophys. J.* **313**, 200.
Warner, B.: 1983, in: M. Livio and G. Shaviv (eds.), *Cataclysmic Variables and Related Objects*, D. Reidel Publ. Co., Dordrecht, Holland, p. 155.
Warwick, R. S., Marshall, N., Fraser, G. W., Watson, M. G., Lawrence, A., Page, C. G., Pounds, K. A., Ricketts, M. J., Sims, M. R., and Smith, A.: 1981, *Monthly Notices Roy. Astron. Soc.* **197**, 865.
Webbink, R. F., Rappaport, S. A., and Savonije, G. J.: 1983, *Astrophys. J.* **270**, 678.
Wesselink, T.: 1987, Ph.D. thesis, University of Nijmegen.
Whelan, J. A. J., Mayo, S. K., Wickramasinghe, D. T., Murdin, P. G., Peterson, B. A., Hawarden, T. G., Longmore, A. J., Haynes, R. F., Goss, W. M., Simons, L. W., Caswell, J. L., Little, A. G., and McAdam, W. B.: 1977, *Monthly Notices Roy. Astron. Soc.* **181**, 259.
White, N. E., Charles, P. A., and Thorstensen, J. R.: 1980, *Monthly Notices Roy. Astron. Soc.* **193**, 731.
White, N. E., Kaluzienski, J. L., and Swank, J. H.: 1984, in: S. E. Woosley (ed.), *High Energy Transients in Astrophysics*, AIP Conference Proceedings, Vol. 115, p. 31.
White, N. E., Mason, K. O., Sanford, P. W., Ilovaisky, S. A., and Chevalier, C.: 1976a, *Monthly Notices Roy. Astron. Soc.* **176**, 91.
White, N. E., Mason, K. O., Huckle, H. E., Charles, P. A., and Sanford, P. W.: 1976b, *Astrophys. J.* **209**, L119.

White, N. E., Mason, K. O., Sanford, P. W., Johnson, H. M., and Catura, R. C.: 1978, *Astrophys. J.* **220**, 600.
White, N. E., Peacock, A., Hasinger, G., Mason, K. O., Manzo, G., Taylor, B. G., Branduardi-Raymont, G. A.: 1986, *Monthly Notices Roy. Astron. Soc.* **218**, 129.
White, N. E., Peacock, A., and Taylor, B. G.: 1985, *Astrophys. J.* **296**, 475.
White, N. E. and Stella, L.: 1988, *Monthly Notices Roy. Astron. Soc.* (in press).
White, N. E., Stella, L., and Parmar, A. N.: 1988, *Astrophys. J.* **234**, 363.
White, N. E., Swank, J. H., and Holt, S. S.: 1983, *Astrophys. J.* **270**, 711.
Wijers, R. A. M. J., Van Paradijs, J., and Lewin, W. H. G.: 1987, *Monthly Notices Roy. Astron. Soc.* **228**, 17P.
Wood, K. S., Meekins, J. F., Yentis, D. J., Smathers, H. W., McNutt, D. P., Bleach, R. D., Byram, E. T., Chubb, T. A., Friedman, H., and Meidav, M.: 1984, *Astrophys. J. Suppl.* **56**, 507.
Woosley, S. E. and Taam, R. E.: 1976, *Nature* **263**, 101.
Wright, G. A. and Low, E. D.: 1986, *Nature* **324**, 127.